Bio-based adhesives for wet environments inspired by the natural mussel adhesive

Kang, Junjie

Publication date:
2023

Document Version
Publisher's PDF, also known as Version of record

DTU Chemistry
June 2023

Bio-based adhesives for wet environments inspired by the natural mussel adhesive

Junjie Kang

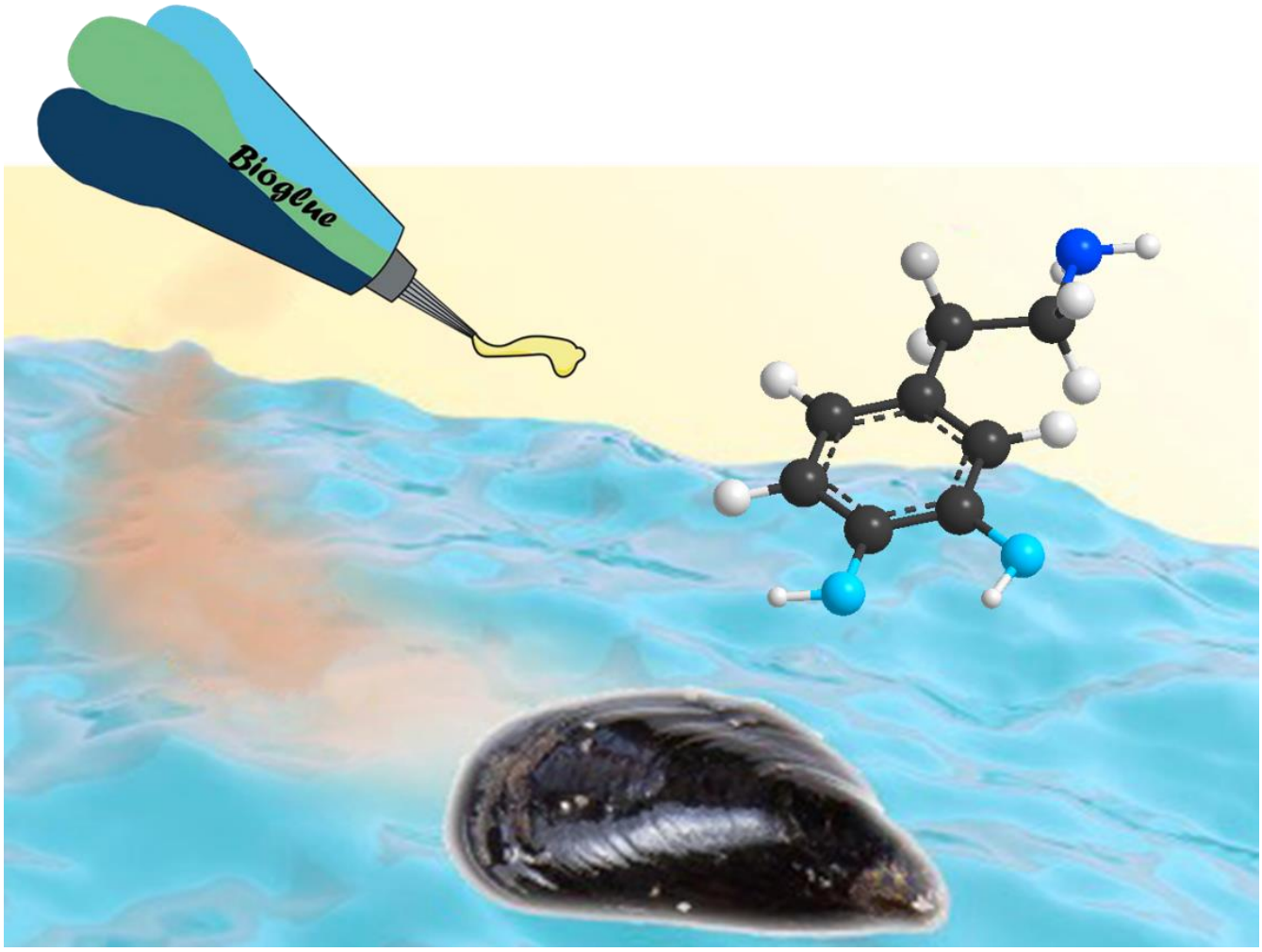

Bio-based adhesives for wet environments inspired by the natural mussel adhesive

Junjie Kang

PhD Dissertation

Technical University of Denmark

June 2023

Supervisors:

Prof. Esben Thormann

Dr. Saeed Zajforoushan Moghaddam

Assoc. Prof. René Wugt Larsen

Technical university of Denmark

Department of chemistry

Kemitorvet, Building 206

2800 Kgs. Lyngby, Denmark

Abstract

Due to the environmental issues associated with synthetic adhesives, considerable research efforts are dedicated to developing bio-based alternatives. While bio-based adhesives are generally more eco-friendly, their performance, particularly in terms of wet adhesion, is often relatively poor. This limitation makes them ineffective under outdoor conditions, highlighting the need for new design ideas.

Mussels offer an inspiration for designing new bio-based adhesives with better wet performance, as they can adhere to various surfaces, even underwater, using a complex protein-based adhesive. It thus suggests that bio-based adhesives have the potential to work effectively in wet environments. As such, researchers have focused on understanding the mechanisms behind mussel adhesion, which are believed to play a key role in their robust adhesion behaviors.

The objective of this PhD thesis is to explore mussel-inspired adhesion mechanisms as a means to design new bio-based adhesives with improved wet adhesion. To achieve this objective, various bio-based ingredients were selected to mimic the basic chemistry of mussel adhesive. Subsequently, these ingredients were combined under optimized conditions to achieve physical properties similar to those of mussel adhesive. The adhesion properties of these mussel-inspired materials were then investigated under wet conditions. The findings of this PhD study suggest that certain bio-based materials, with proper modification, can exhibit effective adhesion in wet environments.

Resumè

På grund af miljøproblemer forbundet med syntetiske klæbemidler er der betydelige forskningsindsatser dedikeret til udvikling af bio-baserede alternativer. Selvom bio-baserede klæbemidler kan være mere miljøvenlige, viser de generelt relativt dårlige præstationer, især når det kommer til våd vedhæftning. Denne begrænsning gør dem ineffektive under udendørs forhold, hvilket indikerer behovet for nye designidéer.

Mussel er en inspirationskilde til design af nye bio-baserede klæbemidler med bedre vådvedhæftning, da de kan hæfte til forskellige overflader, selv under vand, ved hjælp af et komplekst proteinbaseret klæbemiddel. Det antyder derfor, at bio-baserede klæbemidler har potentialet til at fungere effektivt i våde miljøer. Som sådan har forskere fokuseret på at forstå mekanismerne bag musselhæftning, som antages at spille en nøglerolle i deres robuste hæfteegenskaber.

Dette ph.d.-projekt sigter mod at udforske mussel-inspirerede hæftemekanismer som et middel til at designe nye bio-baserede klæbemidler med forbedret vådvedhæftning. For at opnå dette mål blev forskellige bio-baserede ingredienser valgt til at efterligne den grundlæggende kemi i musselklæbemidlet. Derefter blev disse ingredienser kombineret under optimaliserede betingelser for at opnå fysiske egenskaber, der ligner dem for musselklæbemidlet. Vedhæftningsegenskaberne for disse mussel-inspirerede materialer blev derefter undersøgt under våde forhold. Resultaterne af denne ph.d.-undersøgelse antyder, at visse bio-baserede materialer, med passende modificering, kan udvise effektiv vedhæftning i våde miljøer.

Acknowledgment

As I look back on my four-year PhD journey, I realize it as an adventure filled with both challenges and rewards. This is the perfect moment for me to express my sincere gratitude and deepest appreciation to all those who have supported and encouraged me along the way. I am genuinely grateful for each and every one of you.

I am deeply grateful to my principle supervisor, Prof. ***Esben Thormann***, for his invaluable suggestions and extraordinary guidance. It has been an honor to work under your mentorship. Your positive attitude and great enthusiasm for excellent have been a tremendous inspiration for my future career. I am truly thankful for everything you have done. I would also like to express my gratitude to my co-supervisor, Dr. ***Saeed Zajforoushan Moghaddam***, for his brilliant ideas, patient training, and vast knowledge. During the difficult times, you were there to provide comfort, advice, and strength, helping me overcome challenges and persevere. Your contributions have been invaluable, and I am forever thankful. Additionally, I extend my thanks to my co-supervisor, Assoc. Prof. ***René Wugt Larsen***, for his assistance with experiment facilities and data interpretation. Lastly, I am grateful for the support provided by the ***China Scholarship Council (CSC)***, which has afforded me the opportunity to study at DTU.

Additionally, I would like to express my sincere appreciation to **OpenAI** (ChatGPT, version 4) for its invaluable assistance in translating the abstract into Danish, language proofreading, grammar correction, and wordiness checking, which greatly improved the readability of my thesis.

The other one is from the workplace, it has the best workshop in the world, great technician teams, as well as the most wonderful colleagues. They help me a lot in both my research and my personal life since I landed in Denmark, particularly within the Group of Polymers and Functional Interfaces (GPFI). We embrace diverse cultures, share captivating stories, and engage in laughter-filled

conversations with ease and grace in this special and enchanting environment. I feel incredibly blessed to be a part of this group and cherish every moment we have spent together.

On a personal note, I would like to express my gratitude to all the clubs and communities I joined (Biking, Frisbee, Dancing, and Gym). These experiences have provided me with incredible memories, infused me with passionate energy, and helped forge close friendships. I am truly grateful to have such amazing friends, who have always been there to lend a listening ear and extend kind gestures. Your presence in my life will be forever cherished. Thank you all so much!

Finally, I would like to express my deepest appreciation to my parents, Mrs. Han and Mr. Kang, my elder brother Junpeng, sister-in-law Huihui, and all my friends in China. Your unwavering love and support have been instrumental in motivating me to pursue my goals. I cherish you all dearly!

Junjie Kang

Lyngby, June, 2023

List of Abbreviations

3, 4-dihydroxy phenyl-L-alanine	DOPA
3, 4-Dihydroxybenzaldehyde	DHBA
3-glycidoxypropyltrimethoxysilan	GOPS
Alginate	Alg
Alginate-catechol	AlgC
Alginate-dopamine	Alg-DA
Attenuated total reflection	ATR
Chitosan	Chi
Chitosan-catechol	ChiC
Chitosan and alginate complex	Chi-Alg
Chitosan-catechol and alginate complex	ChiC-Alg
Chitosan and alginate-catechol complex	Chi-AlgC
Chitosan-catechol and alginate-catechol	ChiC-AlgC
Dopamine	DA
Dynamic light scattering	DLS
Double distilled water	DDW
ε-polylysine	ε-PL
ε-polylysine and tannic acid complex	ε-PL–TA
Fourier-transform infrared spectroscopy	FTIR

Glycerol diglycidyl ether	GDE
High substitution	HS
Horseradish peroxidase	HRP
Hydrogen peroxide	H_2O_2
Low substitution	LS
Layer-by-layer	LbL
Moderate substitution	MS
Mussel foot proteins	Mfps
Poly(ethyleneimine)	PEI
Polyamidoamine-epichlorohydrin	PAE
Poly(vinyl alcohol)	PVA
Proton nuclear magnetic resonance	^{1}H-NMR
Quartz crystal microbalance with dissipation	QCM-D
Soybean protein-TA-PEI	STP

List of Publications

1. Self-cross-linkable Chitosan-Alginate Complexes Inspired by the Mussel Glue Chemistry. Junjie Kang, Saeed Zajforoushan Moghaddam, Esben Thormann* (Submitted)

2. A Biomimetic Water-resistant Adhesive Based on ε-polylysine/Tannic Acid Complexation. Junjie Kang, Saeed Zajforoushan Moghaddam, René Wugt Larsen, Esben Thormann* (Submitted)

3. Self-coacervation of catechol-modified chitosan for biomaterial mimicking mussel adhesive properties. Junjie Kang, Saeed Zajforoushan Moghaddam, Esben Thormann* (In submission)

Contents

1. INTRODUCTION

1. Introduction

In my PhD research, I aim to explore mussel-inspired adhesion mechanisms as a strategy for designing new bio-based adhesives that perform well in wet conditions. It is suggested that the key factors contributing to the underwater adhesion of mussels include: i) the presence of catechol groups, ii) the synergy between catechol and amine functionalities, and iii) the coacervation of the adhesive proteins. Building upon these aspects, each study focuses on selecting a bio-based candidate and investigating its wet performance.

In study **I**, the chitosan-alginate (Chi-Alg) complex has been chosen as a candidate due to its amine groups and complexation properties. To achieve catechol functionality, Chi-Alg complexes with catechol on one or both polymers were modified, expecting to demonstrate an enhanced wet performance.

In Study **II,** polylysine (ε-PL) and tannic acid (TA) are considered as potential candidates due to their combination of catechol and amine moieties. With complexation achievement in an optimized condition, the ε-PL–TA candidates are expected to exhibit strong water resistance.

In study **III**, the chitosan-catechol (ChiC) polymer is investigated as an ideal candidate, given its combination of catechol and amine moieties. By studying its self-complexation, the ChiC candidates are anticipated to be coacervates, serving as underwater adhesives suitable for engineering applications.

The overall structure of this PhD thesis is as follows: Chapter 2 provides a brief introduction to mussel adhesion mechanisms and reviews mussel-inspired adhesives. Chapter 3 focuses on the experimental methods employed in this PhD study, including information on polymers functionality, adhesives preparation, and characterization techniques. In chapter 4, I present the

ideas and outlines of each study, discuss the results, and highlight the main findings. Finally, chapter 5 offers valuable insights and potential avenues for future research.

2. BACKGROUND

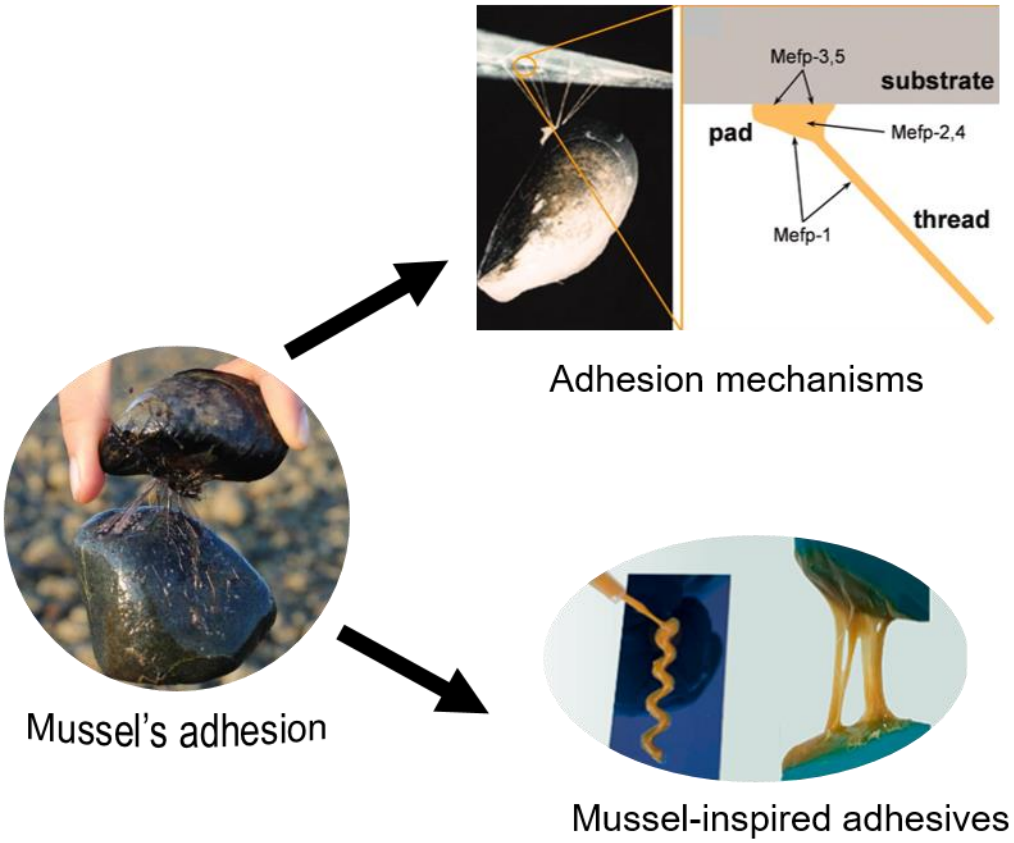

*The schematic illustration describes the adhesion system of mussels and the mussel-inspired adhesives. Reprinted with permission from[1,2]

2. Background

Mussels are known for their superb wet adhesion. Inspired by this natural system, extensive research has been dedicated to developing mussel-inspired adhesives. This chapter of my PhD thesis aims to provide an overview of the literature on mussel adhesion and mussel-inspired adhesives. Firstly, I will briefly introduce the suggested adhesion mechanisms of mussels. Next, I will summarize recent studies on mussel-inspired adhesives, with a focus on bio-based materials.

2.1 Biological inspiration: mussel adhesion

Figure 2.1 illustrates the general anatomy of a mussel. As depicted in Figure 2.1A, mussel uses a group of threads, called byssus, to attach itself to surfaces.[3] Among the different sections of the byssus, the plaque is mainly responsible for the mussel adhesion,[4] which will be briefly introduced in the following sections.

2.1.1 Adhesive plaque

The adhesive (byssal) plaque is composed of a mixture of several proteins and is formed through a complex multi-step process. This section will introduce two aspects of the plaque: its protein composition (Section 2.1.1.1) and plaque formation (Section 2.1.1.2).

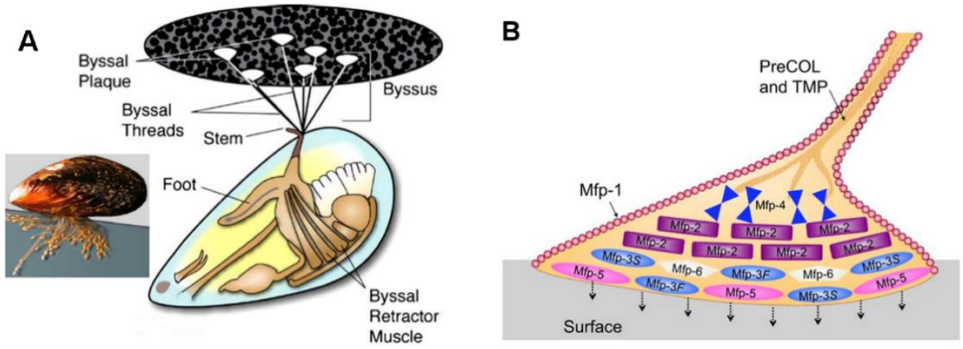

Figure 2.1. Illustration of mussel's anatomy, and distribution of proteins inside the plaque. A) An adult *M. edulis* mussel displaying an extensive byssus attached to a mica surface, as well as its anatomy. B) Schematic illustration of the mussel foot proteins distribution in the plaque. Reprinted with permission[3,4].

2.1.1.1 Plaque compositions

As shown in Figure 2.1B, the plaque contains six different kinds of proteins, Mfp-1, -2, -3, -4, -5, and -6. These proteins are secreted in a sequential order, with surface-targeted proteins (Mfp-3, and -5) secreted first, followed by the proteins of Mfp-2, -4, and -6, and then Mfp-1 comes last as a protective coating.[5–7] These proteins have different molecular weights and amino acid compositions as studied in the literature.[3–7]

Each of these proteins is suggested to contribute to the mussel adhesion in a unique way. Mfp-3 and -5 contain a large number of surface-active groups such as catechol and amine (which will be discussed in Section 2.1.2),which enable strong adhesion to various materials.[4,8,9] On the other hand, Mfp-2, -4, and -6 are considered important for adjusting the cohesive properties of the plaque through various covalent and non-covalent interactions. For instance, Mfp-2 is suggested to form coordination interactions with iron or calcium ions, acting as an ion bridge to cross-link with Mfp-5.[10–12] Lastly, Mfp-6, rich in thiolate groups, is considered responsible for the redox adjustment[13] or functions as a cross-linker to bind with Mfp-3.[12,14]

2.1.1.2 Plaque formation

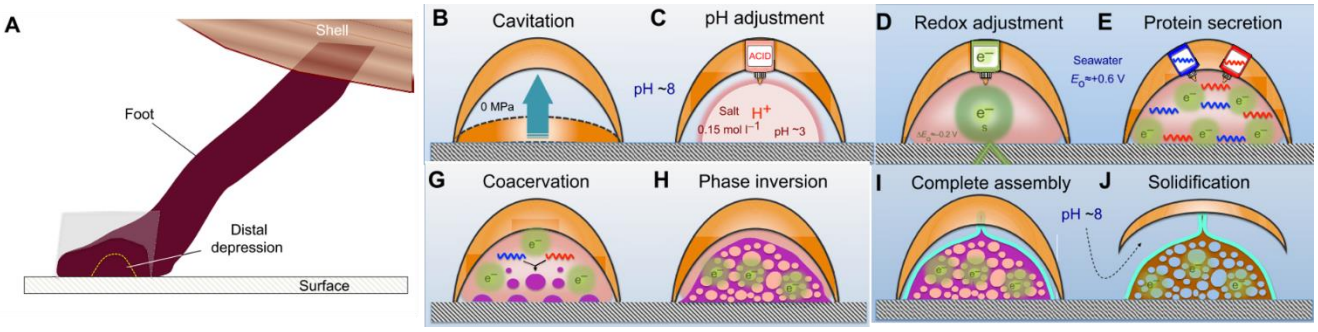

Figure 2.2 Schematic illustration of mussel adhesive plaque formation. Reprinted with permission[4]

Figure 2.2 illustrates the multiple steps involved in the formation of the mussel adhesive plaque.[4] Initially, the mussel foot is pressed against the target surface to create contact (Figure 2.2A). Next, a negative pressure is created to form a cavity underneath the foot (Figure 2.2B). This suction is believed to serve two purposes: firstly, to provide an initial attachment to the surface, and secondly, to draw the adhesive proteins onto the target surface. Subsequently, it is suggested that the pH within the cavity is adjusted to ~3-5, and the ionic strength to ~0.15 M (Figure 2.2C).[4] The acidity and low salt concentration are considered to prevent oxidative reactions of catechol groups (will be discussed in Section 2.1.2.1) and control proteins fluidity. Furthermore, a redox adjustment occurs (Figure 2.2D), which is believed to be influenced by the contrasting conditions between seawater (with high pH and O_2 concentration) and the plaque (with low pH and an abundance of electron donors). This redox adjustment is considered to play a crucial role in regulating the surface adhesion and cohesion properties of the plaque. Following this, the Mfps are secreted in a sequential order (Figure 2.2E). When these proteins are mixed at a specific pH and concentration, they tend to undergo a liquid-liquid phase separation, which is known as coacervation (Figure 2.2G, see Section 2.1.2.3 for more discussion on coacervation).[15] Next, it is suggested that such coacervates may undergo phase inversion, transforming into a structured fluid (Figure 2.2H).[16,17] This is followed by an assembly process that completes the formation of an ordered coacervate system within the plaque (Figure 2.3I). Finally, solidification occurs in the plaque upon exposure to external seawater (Figure 2.2J, see Section 2.1.2.4 for discussion on curing reactions).

2.1.2 Adhesion mechanisms

The ability of mussels to robustly adhere to wet surfaces is suggested to be a result of several unique mechanisms, which will be discussed in this section.

2.1.2.1 Catechol chemistry

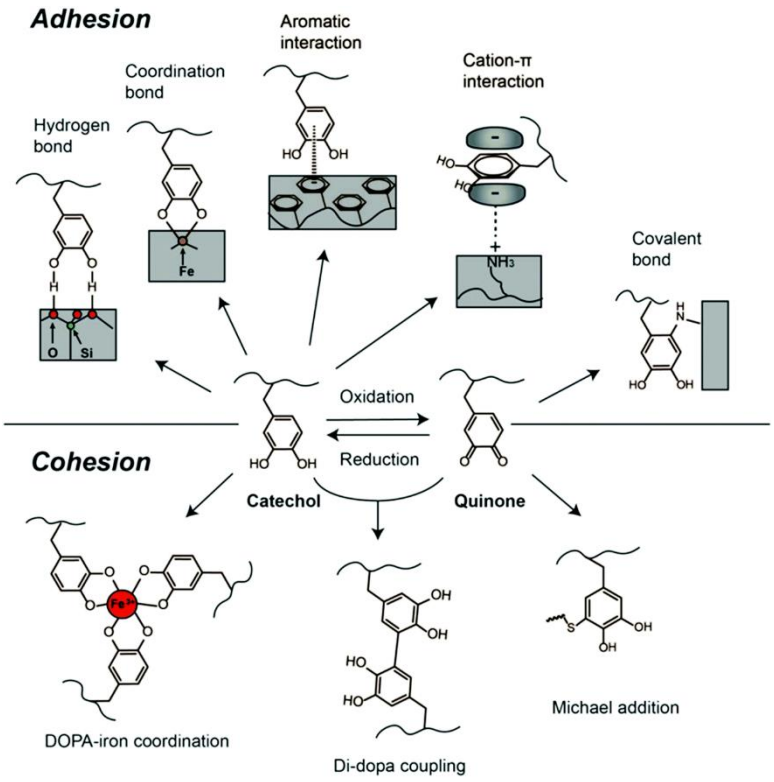

Figure 2.3 Catechol-related interactions regarding the surface adhesion and cohesion of the plaque. Reprinted with permission[18,19].

All Mfps contain 3,4-dihydroxyphenylalanine (DOPA), and its catechol groups are believed to be crucial for mussel adhesion.[20] Catechol has been reported to exhibit versatile chemistry, enabling it to form numerous interactions.[21,22] This versatility is suggested to enable Mfps to establish strong interactions with various surfaces (interfacial adhesion) as well as with other Mfps (cohesion).

Figure 2.3 illustrates the versatile chemistry of catechol moieties in their two chemical forms: the reduced catechol and the oxidized quinone. It is widely believed that these two forms play a crucial role in the regulation of both interfacial adhesion and cohesion of the plaque.[20]

i) Catechol interactions

Hydrogen bond: Catechol exhibits the ability to interact with various inorganic substrates, such as silicon, mica, glass, through non-covalent hydrogen bonding.[23,24] Despite not being a covalent bond, the connection between catechol and inorganic substrates commonly takes the forms of bidentate bonding, leading to a robust surface attachment.[25,26]

Coordination bond: Catechol can interact with metal ions or metal oxide surfaces, forming strong yet reversible coordination bonds. Within the adhesive plaque, it is suggested that this coordination capability is utilized to promote protein crosslinking and improve cohesiveness. However, this ability has been reported to be pH-dependent.[27,28] At low pH, mono- complexes are formed, whereas at higher pH levels, the ligand affinity is enhanced, resulting in the formation of stable bis- and tris- complexes.

Hydrophobic interaction: π-π stacking is considered the primary hydrophobic interaction involved in catechol interactions. For example, studies have reported that catechol moieties can engage in π-π stacking with polystyrene substrates.[19,29,30] While this interaction is sensitive and reversible, it provides support for surface attachment and cohesion.[31–33]

Cation-π interaction: The catechol-NH_3^+ interaction is recognized as the primary cation-π interaction in the adhesive plaque. Despite being a non-covalent bond, cation-π interactions play a significant role in surface adhesion and cohesion in mussels.[34,35] For example, catechol can bond to a surface by incorporating with amine moieties. Additionally, the catechol-NH_3^+ interaction can also occur between proteins, contributing to their cohesion property.[28-30]

According to reports, catechol-related interactions appear to be dynamic and are suggested to be influenced by various external factors, including pH and ionic strength. In contrast to the reduced catechol, the oxidized quinone moieties can form more stable covalent bonds through various chemical reactions.

ii) Quinone interactions

The formation of quinones in mussel's system is suggested to occur as describes. After the creation of the byssus plaque, the mussel's foot tends to lift off, exposing the plaque to seawater. When the pH increases to ~ 8, catechol moieties undergo oxidation, leading to the production of quinones. It is believed that these oxidized quinone moieties react with other functional groups in the Mfps, such as catechols, amines, and thiols.[39] These reactions are considered to promote proteins' cross-linking, resulting in enhanced cohesion and water resistance of the adhesive.[40] Two primary reactions are involved:

Michael addition: Quinone can react with amine and thiol groups through Michael addition reaction. This reaction leads to the formation of a permanent covalent bond, ensuring the strong and long-lasting underwater adhesion in mussels' plaque.[41]

Schiff base formation: On the other hand, quinone can also react with amine groups through Schiff base formation.[42] Unlike the Michael addition reaction, this reaction results in the formation of a dynamic imine bond, which is sensitive in nature. Therefore, it is believed to contribute only slightly to the wet adhesion of the plaque.[43,44]

2.1.2.2 Catechol-amine synergy

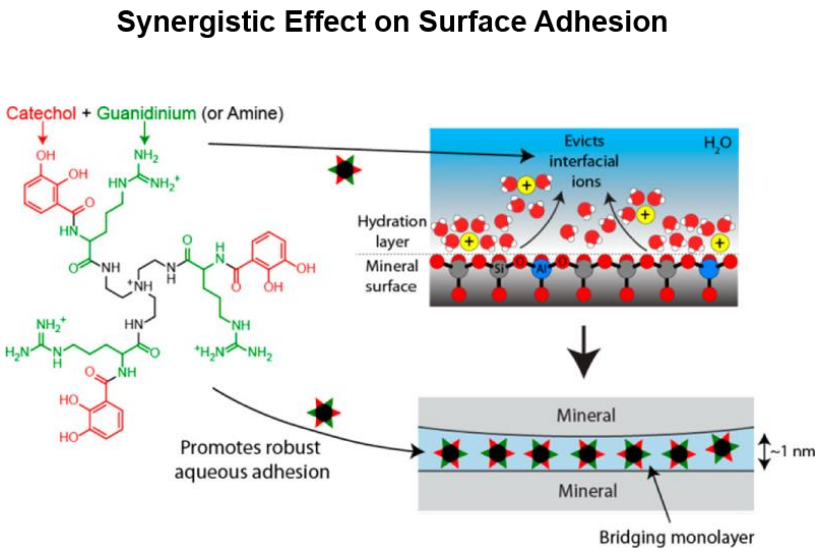

Figure 2.4. Scheme description of catechol-amine synergistic effect on surface adhesion based on surface forces apparatus technique. Reprinted with permission[45].

Recent studies suggest that catechol functionality is not the sole factor contributing to mussel's wet adhesion. The synergy of catechol and amine groups is believed to be another important factor influencing both surface adhesion and cohesive strength of the plaque.[36,43,46–50]

Maier et al. conducted a study to investigate the impact of catechol-amine synergy on surface adhesion of the plaque, as depicted in Figure 2.4. They synthesized three types of polymers with varying catechol and amine functionalities: i) polymer I contained both catechol and amine groups, ii) polymer II had amine moieties without catechol, iii) polymer III had catechol moieties but lacked amine. Surface forces apparatus (SFA) experiments were conducted to characterize surface adhesion. In this method, a probe coated with a specific polymer was brought into contact with mica surfaces. Force-distance profiles were collected, and the maximal force during retraction was used to determine the wet adhesion. The polymer with both catechol and amine moieties exhibited

largest adhesion compared to the two other polymers. Based on these findings, it was concluded that the synergy between catechol and amine groups plays a crucial role in enhancing the adhesive properties. This study also proposed a hypothesis that a hydrated layer forms as a molecular barrier at the liquid-substrate interface, hindering the connection of catechol moieties with the substrates.[51,52] However, the introduction of amine moieties displaced the hydrated layer, creating a single monolayer "molecular bridge" that increased adhesion.[48]

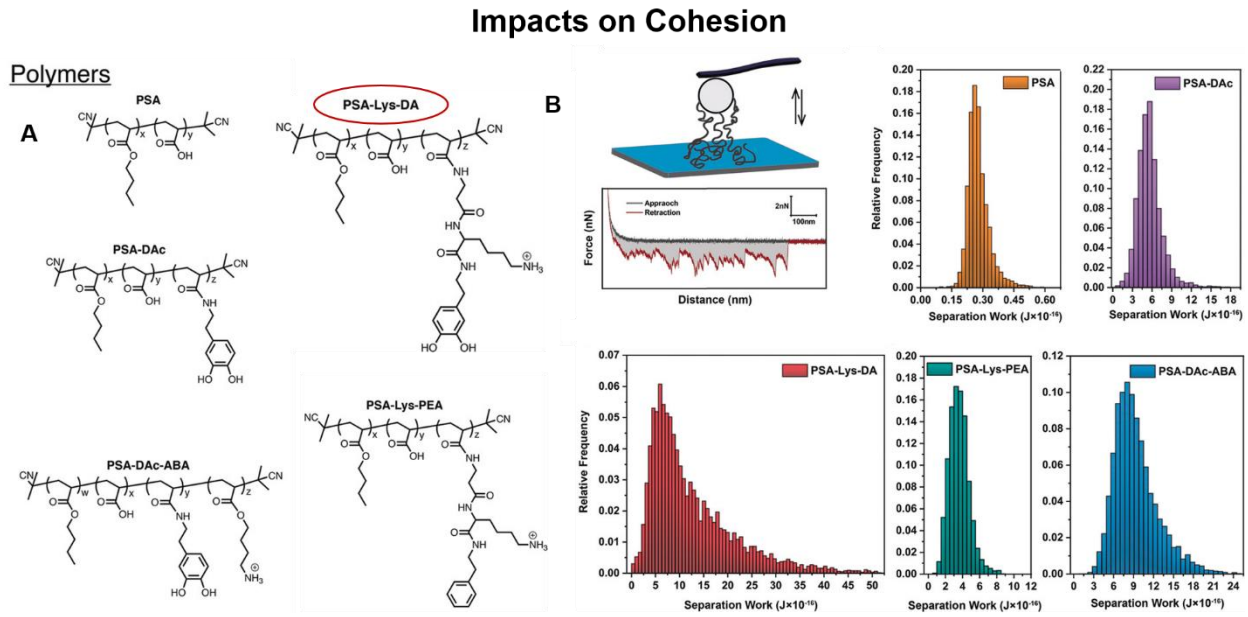

Figure 2.5. Cooperativity of catechol-amine moieties on mussel's cohesion. A) Structure of synthetic polymers with varying catechol and amine functionalities. B) Experimental schematic diagram and a representative Force-Distance curve for PSA-based polymers using colloidal probe spectroscopy characterization. Reprinted with permission[36]

Tiu et al. employed colloidal probe spectroscopy (CPS) to investigate the influence of catechol and amine moieties on mussel cohesion, as depicted in Figure 2.5A.[36] They synthesized various polymers with varying catechol and amine functionalities, such as PSA (no catechol and amine groups), PSA-DAc (catechol only), PSA-Lys-PEA (amine only), PSA-DAc-ABA (having catechol and amine located randomly along the backbone), and PSA-Lys-DA (having catechol and amine

located adjacent along the backbone). Adhesive forces were measured between a colloidal particle and a mica substrate, both coated with these polymers. Cohesion was estimated by integrating the area under the retraction trace in the force-distance curves, representing the separation work (Figure 2.5B). The results demonstrated that the polymer (PSA-Lys-DA), incorporating both catechol and amine moieties, exhibited higher separation work or cohesion energies compared to the others.

2.1.2.3 Coacervation

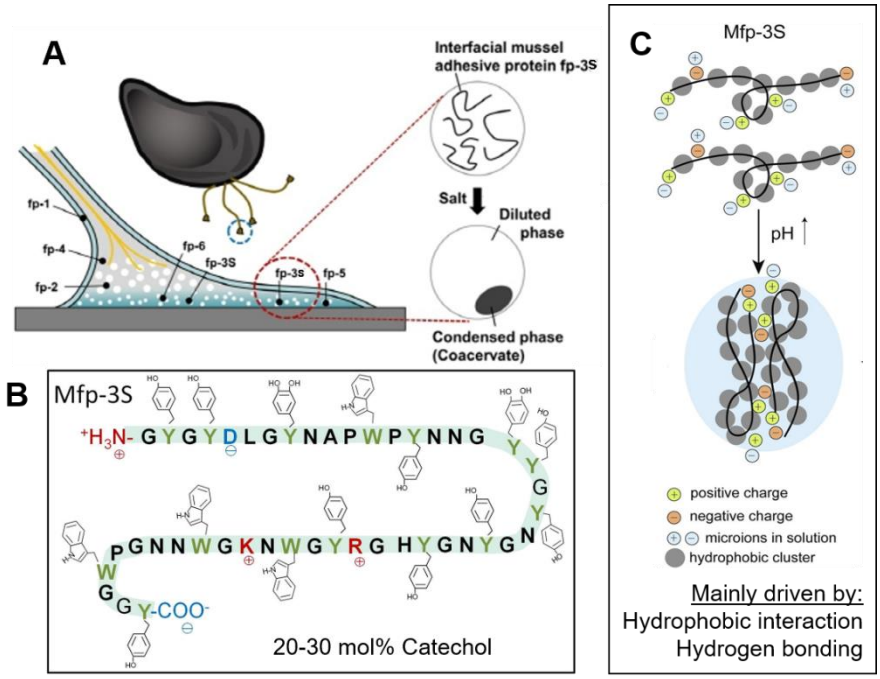

Figure 2.6 Mfp-3s coacervation in mussel adhesive plaque. A) Formation of Mfp-3s self-coacervates. B) Representative sequence of Mfp-3s. C) Interactions involved in Mfp-3s coacervation. Reprinted with permission.[15,53]

The chemistry and interactions involved in mussel glue are not the only factors contributing to its adhesive properties. The physical properties of the glue, such as viscosity and surface tension, are also considered significant for wet adhesion. As discussed in the section on plaque formation,

mussel glue is more than just proteins dissolved in water. The proteins undergo complex phase transitions, including coacervation.

There are different types of coacervation, with complex coacervation being the common one where oppositely charged molecules bind and neutralize each other. However, this is not typically observed in mussels. In the adhesive plaque of mussels, it is suggested that proteins undergo self-coacervation. For example, Mfp-3, a cationic protein, is believed to undergo self-coacervation induced by changes in ionic strength or pH values.[54–56] This process involves complex interactions, resulting in the formation of two phases: a diluted phase and a condensed phase, known as the coacervate phase (Figure 2.6A).[57,58]

Coacervation offer advantages to adhesion as it is hyphothesized that coacervate phase has lower viscosity and interfacial energy compared to the dispersed protein solution (uncondensed). This allows for better spreadability without dispersion in seawater. The physical properties of the secreted glue have been suggested to significantly impact mussel adhesion.[6]

As shown in Figure 2.6B, Mfp-3s have a low charge density and contain 20-30% of catechol moieties.[46–49] In a study by Wei et al., it has been suggested that the phase separation of Mfp-3s is primarily driven by hydrophobic interactions and hydrogen bonding (Figure 2.7C).[15] The physical properties of Mfp-3s coacervates were characterized using SFA and microscopy.[15,63] It was found that Mfp-3s coacervate demonstrates significantly low interfacial energy in the range of 0.5-3.7 mJ m^{-2} compared to the Mfp-3s solution. This facilitates easy surface wetting with large contact areas. Other studies have also reported that coacervate phase contains high protein concentrations and exhibits good fluidity, reduced viscosity, and low interfacial energy.[54,64,65] These properties

enable the spontaneous spreading of mussel glue over wet surfaces, thus resulting in robust wet adhesion of the plaque.[28,66,67]

2.1.2.4 Underwater curing

Curability is considered a crucial factor in the creation of durable and long-last underwater adhesives in mussel's system.[1,46,68] Once the byssus plaque is created, the mussel's foot tends to lift off, exposing the adhesive plaque to seawater with a pH of ~ 8. This exposure triggers the curing process, which is believed to involve the formation of coordination bonds and covalent bonds.[69] Mussel glue curing is thought to occur through two chemical routes:

i) Coordination chemistry

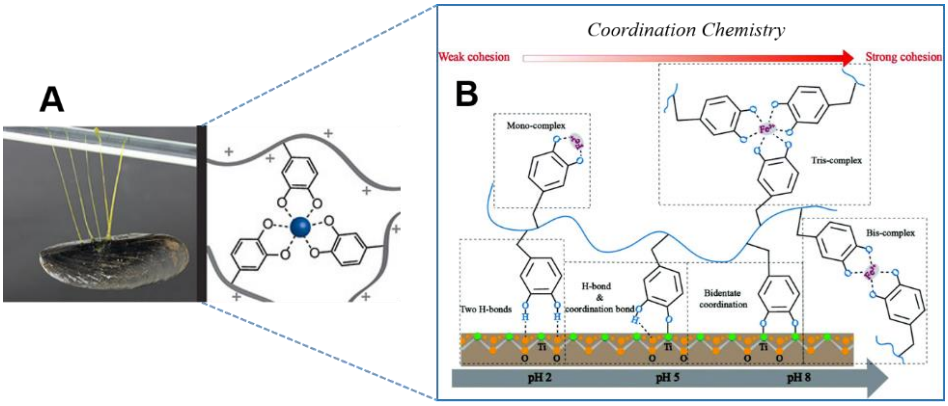

Figure 2.7 Coordination chemistry in the adhesive plaque. (A) Abilities of mussels bind to the surface by coordination crosslinking. (B) Crosslinking variations as a function of pH value. Reprinted with permission[38,66]

The plaque, besides proteins, contains inorganic elements such as Fe^{3+}, which play a crucial role in creating the coordination crosslinking through DOPA-Fe^{3+} complexes.[71] It is suggested that coordination interactions are dynamic and pH sensitive. During initial protein deposition in the plaque, the foot appears to significantly acidify the interface (pH ~ 2-4). At this point, it is believed that there is no coordination crosslinking or appeared in a state of the mono- complex. Upon pH

increasing, the coordination interactions between DOPA and Fe^{3+} are suggested to be occurred in the forms of bis-, and tris- complexes.[72] The increased protein crosslinking is believed to have a significant impact on the transition of physical properties from a liquid to a solid state, leading to the enhanced mechanical properties.

In a study conducted by Holten-Andersen, the impact of pH on the physical behavior was investigated.[73] The study involves the reaction of a DOPA-modified polyethylene glycol polymer with $FeCl_3$ in a fixed molar ratio. Mixtures were characterized by rheometry at different pH levels: 5 (representing the proposed pH in the adhesive plaque), 8 (seawater pH), and 12 (complete tris-DOPA-Fe^{3+} cross-linking) to understand the transitions. The results revealed distinct responses in the mixtures depending on the pH. At pH 5, the mixtures exhibited a viscous response in dynamic oscillatory rheology. However, as the pH was raised to 8, a transformation into a sticky gel occurred. Furthermore, at pH 12, an increasing elastic behavior was observed. These findings suggest that the increased crosslinking of DOPA-Fe^{3+} complexes may play a crucial role in enhancing the extensibility of mussel adhesives.[74] Additionally, the pH responsiveness of coordination bonds allow the byssus plaque to exhibit "self-heal" capabilities.[40]

The presence of DOPA-Fe^{3+} coordination moieties were found in Mfp-1. To further understand the impact of coordination chemistry on cohesive properties, Zeng et al. conducted a study using SFA.[75] Specifically, they employed Mfp-1 coated mica surfaces to investigate the interactions of DOPA-Fe^{3+}, both in the absence and presence of Fe^{3+} ions (~10 μM, pH 5.5). When two Mfp-1 layers were brought into contact and immediately separated, a significant and reversible adhesion (F_{ad}/R: ~−6 mN/m) was observed in the presence of Fe^{3+} ions. The results suggest that Fe^{3+} plays a significant role in establishing cohesive bridges between Mfp-1 molecules.

ii) Oxidative covalent crosslinking

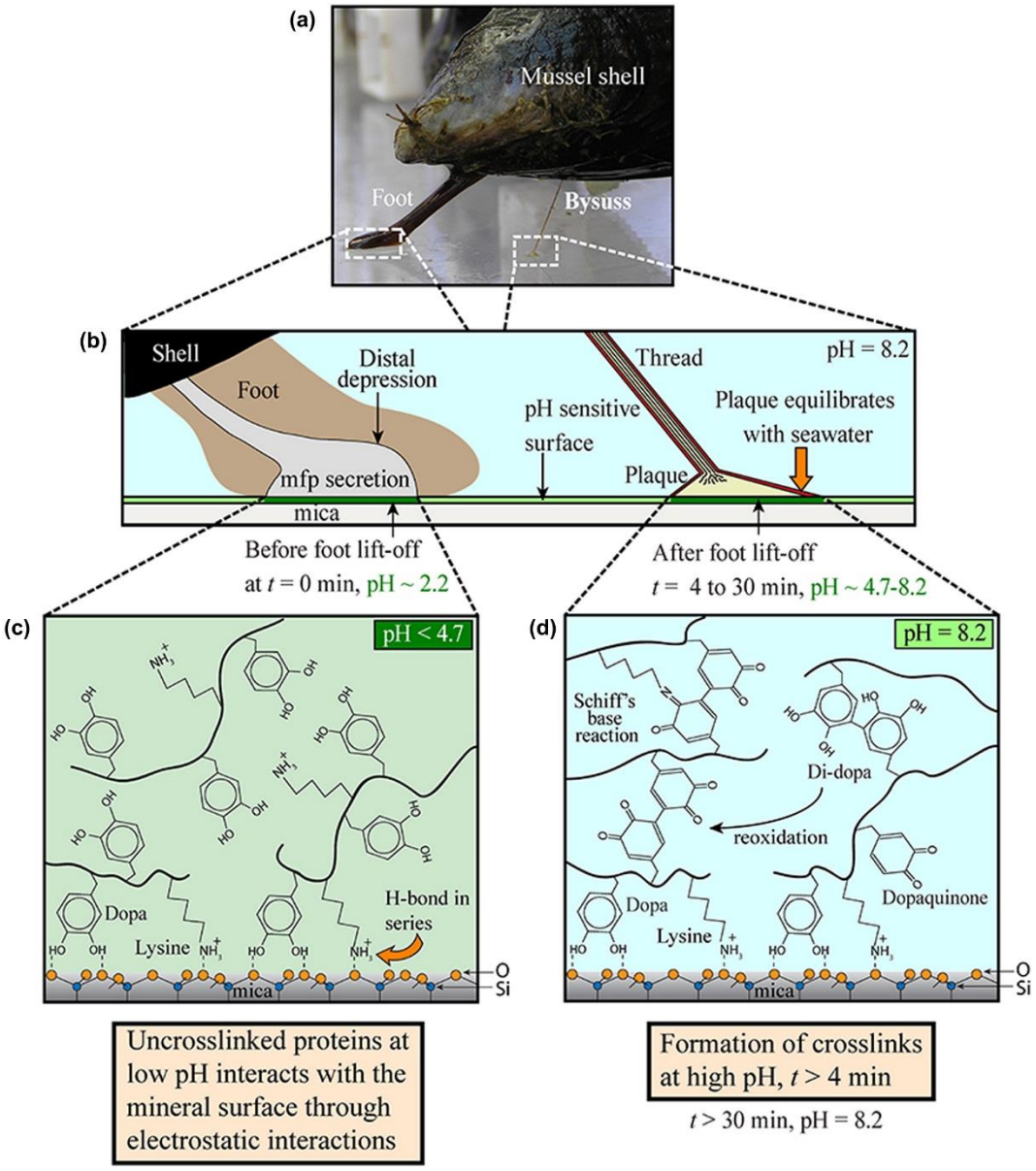

Figure 2.8 Oxidative crosslinking mechanisms in the adhesive plaque with the pH value increasing from acid to alkaline. Reprinted with permission[76]

In addition to coordination interactions, oxidative covalent crosslinking is another mechanism involved in adhesive curability.[76] Figure 2.8 illustrates the chemical reactions that occur during the formation of the mussel adhesive plaque under reducing conditions (acidic pH) and oxidizing

conditions (neutral to slightly alkaline pH). As the pH increases, oxidative crosslinking begins to take place. Tyrosinase, acting as a catalyst, plays a key role in accelerating the reaction kinetics for rapid oxidative crosslinking.[7] During this process, catechol moieties from DOPA are oxidized to quinones, which then react with the amines, leading to crosslink formation within the proteins.[75] These oxidative crosslinking reactions, including phenol coupling, Micheal addition, and Schiff base formation, are considered essential for enhancing cohesive strength.[77–79]

In a study by Seo et al, the impact of oxidation crosslinking on cohesion properties was investigated using SFA.[80] The SFA measurements involved obtaining force-distance curves between two mica surfaces coated with copolyampholyte under pH 3, 4, and 7. Cohesion was estimated by integrating the area under the retraction trace in the force-distance curves. It was found that the cohesion force between the polymer films disappeared at pH 3, whereas it increased to 32.9 ± 3.5 mJ/m^2 at pH 7. The stronger cohesion at the higher pH is believed to be attributed to the oxidative crosslinking.

2.2 Engineered bio-based adhesives

Adhesives play a significant role in our daily lives, with billions of pounds being consumed globally every year.[81] However, many of these adhesives are made from petroleum-derived polymers such as polyurethane,[82] epoxy,[83,84] silicone,[85] cyanoacrylates,[86] and acrylic[87]. Although these synthetic adhesives are effective in bonding various materials, they raise significant environmental concerns.[88,89] Thus, bio-based adhesives from renewable biomaterials, as an alternative to petro-derived adhesives, have attracted great attention in recent years.[90–92]

Efforts have been focused on developing bio-based adhesives using entirely or partially bio-based raw materials.[91–95] Animal and plant sources, such as proteins, polysaccharides, and vegetable oils,

have been utilized as feedstocks for such adhesives.[90] Despite rather dry adhesion, bio-based adhesives when applied to wet surfaces or exposed to outdoor environments show poor adhesoin.[2,96]

2.2.1 Mussel-inspired bio-based adhesives

Therefore, there is a need to enhance their wet adhesion, and that's where the inspiration from mussels becomes valuable. In this section, I will briefly discuss the relevant literature on mussel-inspired bio-based adhesives.

2.2.1.1 Bio-based adhesives containing catechol or catechol-amine

As discussed in Section 2.1.2.1 and 2.1.2.2, mussel adhesives contain both catechol and amine moieties. Some studies aim to mimic this composition by achieving either catechol or both catechol and amine functionalities.

To mimic the functionality of catechol, two commonly used approaches are:

i) grafting bio-based polymers with catechol moieties;

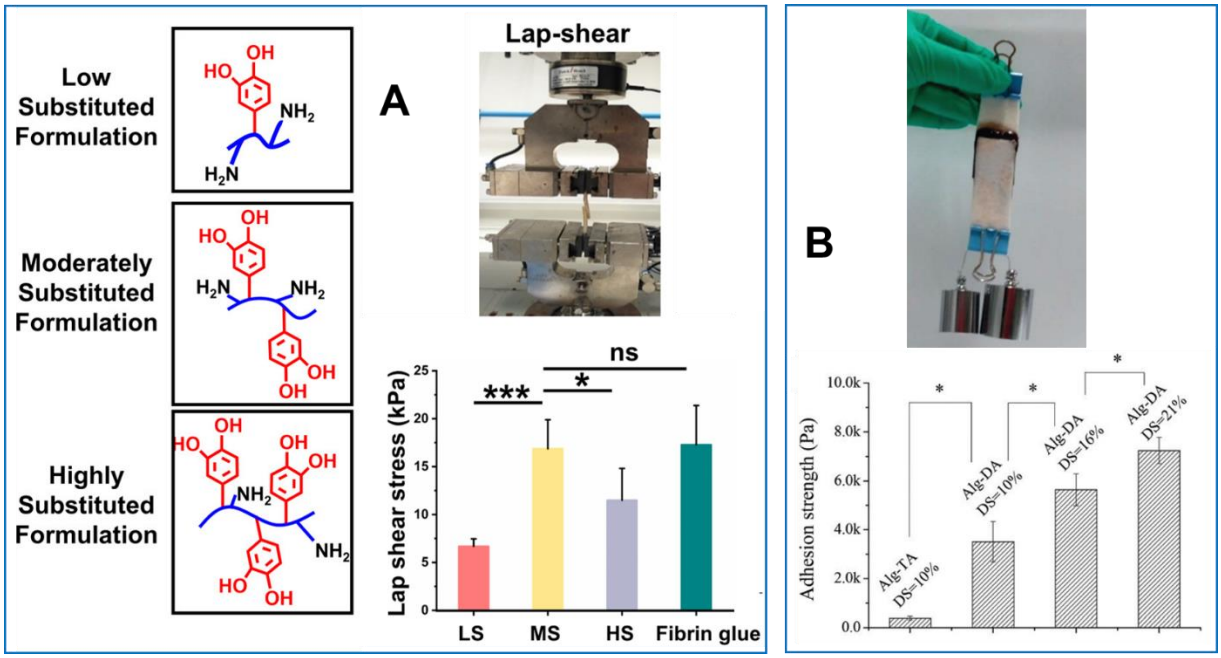

Figure 2.9 Catechol modification impacted on adhesion strength of bio-based adhesives. A) Gelatin-based adhesives with different catechol substitutions. B) Dopamine-functionalized alginate (Alg-DA) adhesives effected by catechol modification. All samples were applied onto wet porcine skin. Reprinted with permission.[97,98]

Catechol is often conjugated onto biopolymers through different chemical reactions, including Schiff base formation and carbodiimide chemistry.[99–103] In a study by Gowda et al., gelatin was modified with catechols using carbodiimide chemistry.[104] The degree of conjugation was controlled by adjusting the ratio of dopamine (DA) to gelatin. As shown in Figure 2.9A, it was observed that catechol-modified gelatin exhibited comparable wet adhesion to commercial fibrin glue following appropriate modification. In another study, Hou et al. examined the impact of catechol on wet performance using lap shear adhesion test on porcine skin (Figure 2.9B). It was found that only 10% catechol group (DA) modification onto Alg led to the increase of wet adhesion strength from 0.5 kPa to 3.5 kPa.[98] Both studies suggest that the modification of catechol can be a promising strategy in improving the wet adhesion of bio-based materials. While this approach has

proven to be effective, the synthetic routes and controls for catechol grafting adds the complexity to the process.

ii) mixing plant phenolics with bio-based polymers;

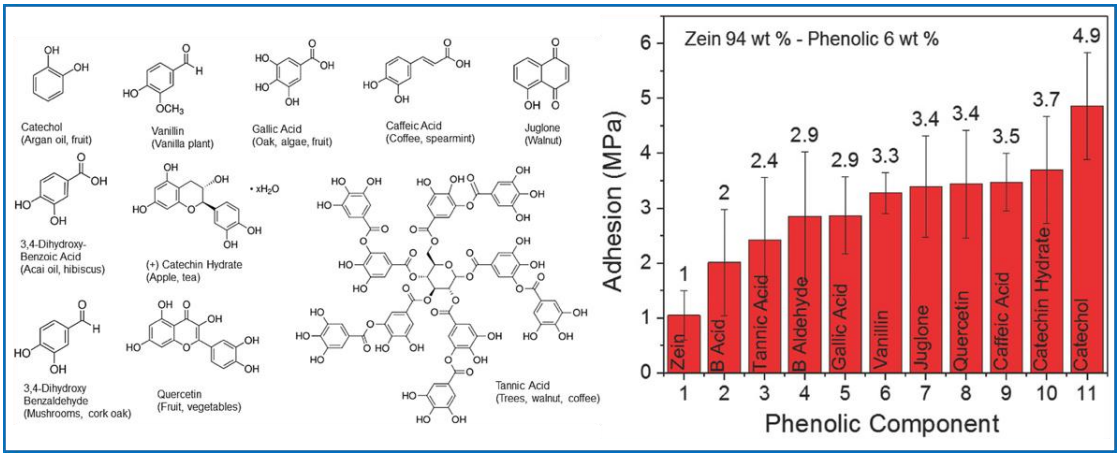

Figure 2.10 Catechol functionalized by adding "catechol-like" plant phenols to zein-based adhesives. Adhesion strength performed in wet conditions. Reprinted with permission[105].

Another alternative method is to use a mixing approach instead of grafting. This method is simpler but offers less control over the degree of grafting.

Schmidt et al. conducted a study combining zein with phenolic components from plants, including catechol, tannic acid, caffeic acid, gallic acid and others.[105] The bonding performance was tested on wet aluminum substrates using lap shear configurations. Figure 2.10 illustrates the structures of plant phenols and the preparation of zein-based adhesives by combining these components in an optimized weight ratio. The addition of plant phenols led to a significant increase in wet adhesion strength, ranging from ~ 2 MPa to ~ 4.9 MPa, compared to pure zein adhesives with ~ 1 MPa. This suggests that incorporating plant phenols is an effective approach to enhance the wet performance of bio-based adhesives.

As a comparison, there have been limited reports on bio-based adhesives with both catechol and amine functionalities by a mixing manner. To mimic the amine functionalities, researchers have introduced polymers with amine moieties into their adhesive formulations, following the established approach of utilizing catechol functionality.

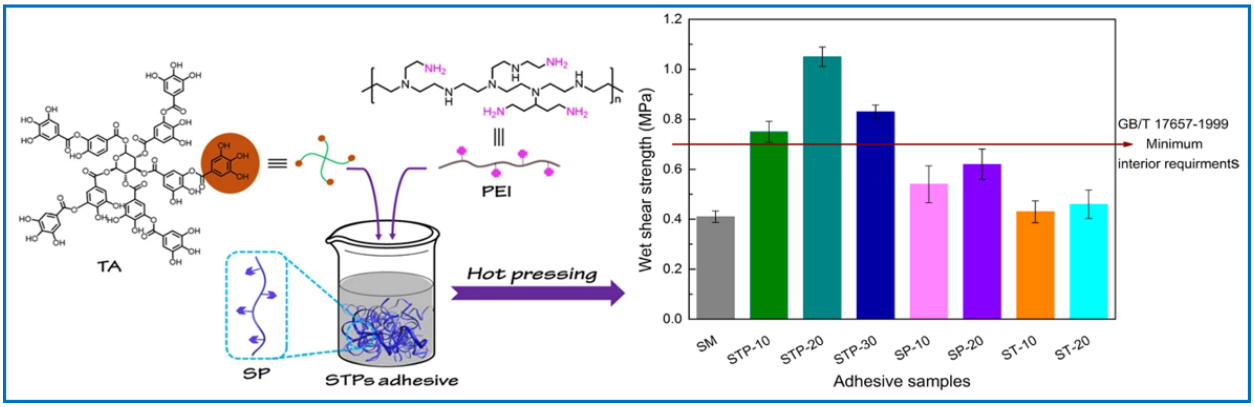

Figure 2.11 Bio-based adhesives prepared by mixing soybean proteins, TA, and PEI. Graph B reprinted with permission[106].

In a study by Wang et al., a soybean meal-based adhesive was prepared by combining tannic acid (TA) and polyethyleneimine (PEI) with soybean protein to achieve both functionalities.[106] Wet adhesion strength were measured underwater after 3 hours. Figure 2.11 illustrates the preparation of soybean-based adhesives and the effect of one or both functionalities on adhesion properties. It was found that both TA and PEI co-crosslinking systems exhibited improved wet adhesion strength, exceeding ~ 0.7 MPa. On the other hand, adding TA or PEI alone to pure soybean did not lead to a significant enhancement in wet adhesion strength. These findings suggest that, both catechol and amine functionality are crucial in the design of bio-based adhesives.[107–109]

2.2.1.2 Mussel-inspired bio-based adhesives based on coacervation

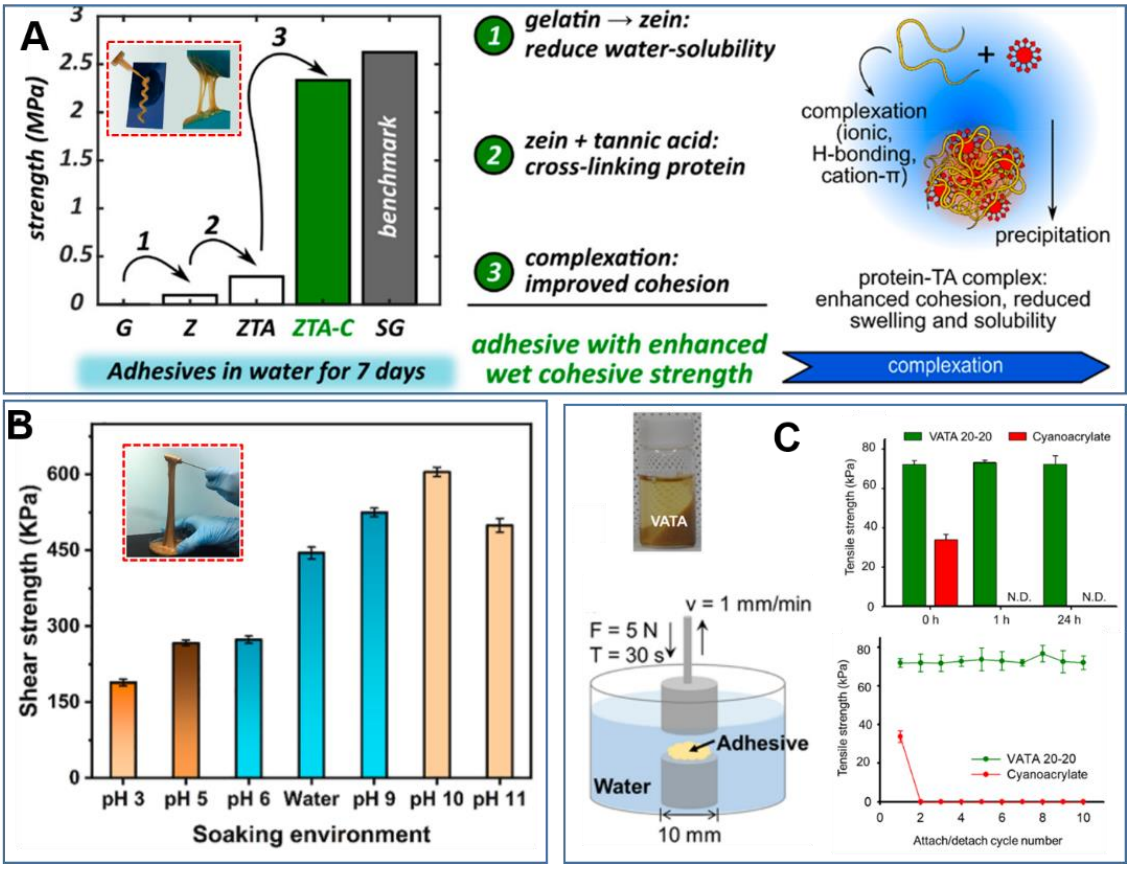

Figure 2.12 Preparation of bio-based adhesives in a coacervation and their wet adhesion measurements. A) Water resistance properties of zein-base adhesives after immersion underwater for 7 days. The underwater adhesion strength of B) polyamidoamine-epichlorohydrin (PAE)-base adhesives after soaking at different pH values for one day; and C) poly(vinyl alcohol) (PVA)-based adhesives as a function of soaking time and the recycling tests. Graph A reprinted with permission[2]. Graph B reprinted with permission[110]. Graph C reprinted with permission[111]

Coacervation is an aspect of mussels that has been mimicked to enhance the wet adhesion of bio-based adhesives. For instance, Moghaddam et al. investigated the impact of coacervation on the water resistance of zein-based adhesives.[2] Three types of systems were prepared to compare the effect of coacervation on adhesion behaviors: pure zein, zein mixed with tannic acid in a solution without coacervation, and zein and tannic acid in a coacervation state. The formation of zein-TA coacervate was achieved by adding TA into a zein solution under optimized conditions, where

exhibiting properties similar to mussel glue (as shown in the insert photo of Figure 2.11A). To assess water resistance, a lap shear adhesion test was conducted after 7 days of underwater immersion. The results showed that pure zein polymers exhibited no water resistance, while the addition of TA to the zein solution led to a slight improvement of ~ 0.2 MPa. In contrast, the zein-TA coacervate demonstrated a significant improvement in water resistance, reaching ~ 2.5 MPa. This improvement can be attributed to the unique properties of coacervates, such as reduced solubility, decreased swelling, and enhanced crosslinking.

In another study by Wang et al., a polyelectrolyte-based adhesive was reported by combining TA and polyamidoamine-epichlorohydrin (PAE) polycation.[110] In this approach, an aqueous TA solution was added to the PAE solution in an optimized ratio and mixed manually. The resulting mixture underwent precipitation, leading to the formation of fluidic condensates. Over time, these condensates transformed into a solid-like water-immiscible coacervate phase (as shown in the inserted photo of Figure 2.11B). To evaluate the underwater adhesion properties, the specimens were immersed in an aqueous solution for 24 hours and then subjected them to a lap shear adhesion test. The results suggested that adhesives in a coacervate state exhibited a strong underwater adhesive strength up to ~ 600 kPa.

Furthermore, Lee et al. developed an underwater adhesive with reusable properties by simply mixing poly(vinyl alcohol) (PVA) and TA solutions.[111] During the mixing process, a turbid precipitation was observed, and the sticky part was collected as the adhesive (see Figure 2.11C). The resulting coacervates were applied onto an aluminum plate in water, then the other plate was pressed on top with a fixed contact force of 50 N. After 24 hours, a tensile adhesion test was performed on the specimen. The attaching and detaching cycle was repeated up to 10 times without

exchanging the adhesive. This result demonstrated that the PVA-TA coacervate maintained nearly 100% of its initial adhesion strength, even after 10 repetitions of attach-detach cycles.

To summarize, these studies emphasize the potential of coacervation as a valuable strategy to enhance the water resistance, adhesive strength, and reusability of bio-based adhesives. They offer valuable insights for the development of innovative bio-based adhesive designs.

2.2.1.3 Bio-based adhesives with mussel-inspired curing chemistry

As discussed in Section 2.1.2.4, mussel glue undergoes a series of coordination chemistry and oxidative covalent crosslinking among the proteins. These mechanisms have been employed in the development of curable bio-based wet adhesives.

In mussel's system, it has reported that adhesive curability is primarily triggered by pH values. However, other factors such as UV, chemical oxidants, and enzymes have also been suggested to promote curability. Here are examples of each stimulus:

A study conducted by Levkin's group, it reported a photo-cross-linking reaction involved the oxidation of dopamine[112] and plant polyphenols, [113] using UV irradiation. For example, with UV treatment, catechol moieties generated various radical compounds, leading to the production of quinones.[114–116] The quinones could crosslink with catechol or other quinones, forming complex intermolecular netweorks.[117] As a result, this method led to the formation of a coating with enhanced stability. In a related study, Hong et al. developed a methacrylated gelatin-based adhesive that exhibited strong binding to wet tissue surfaces after UV activation (Figure 2.13A).[118] The gels formed within seconds, and their adhesion was evaluated by testing the hemostatic performance. It was observed that the adhesives treated with UV exhibited reduced bleeding and

enhanced mechanical property. This result suggested that adhesives after UV treatment can be curable with an enhanced adhesion strength, possibly due to the increased molecular crosslinking.

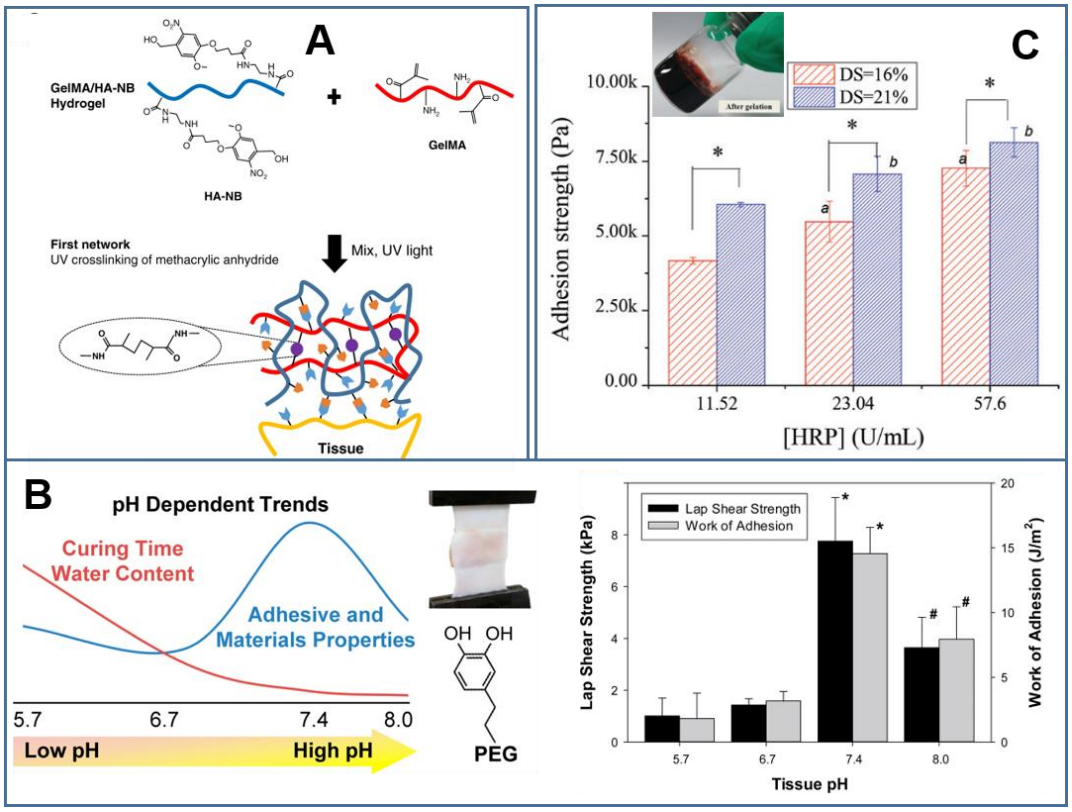

Figure 2.13. Mussel-inspired curability in different ways. A) Methacrylated gelatin-based adhesives treated by UV light; B) poly(ethylene glycol)-DA adhesives cured by different pH values; C) Alg-DA cured and gelled by horseradish peroxidase (HRP) treatment. Graph A reprinted with permission.[118] Graph B reprinted with permission.[119] Graph C reprinted with permission.[98]

The addition of chemical oxidants is proposed as another way to induce adhesives curability, which can be achieved by controlling the concentrations of oxidants, the ratios of oxidants to catechol, and the reaction time.[44,98,120] Four chemical oxidant agents including NaOH,[121,122] metal ions,[123,124] $NaIO_4$,[125–127] and H_2O_2,[120,128,129] have been widely used for adhesive curability.

Morgan et al. conducted a study on the curing of poly(ethylene glycol)-DA adhesives under different pH values controlled by NaOH concnetrations.[119] The impact of the cured adhesives on wet adhesion was investigated using lap shear test on porcine skin. As shown in Figure 2.13B, with pH increasing, adhesives exhibited the largest lap adhesion strength ~ 8 kPa at pH 7.4, which was four times stronger than those at other pH levels.

Another example involves the use of metal ions to achieve adhesive curability through coordination crosslinking. Li et al. conducted a study on a metal-crosslinked ε-poly-L-lysine tissue adhesive by introducing a low Fe^{3+} content at pH 7.4.[124] The wet adhesion properties were envaluated using a lap shear test on collagen substrates. The results demonstrated that the adhesive strength reached ~105 kPa, which was about eight times higher than that of fibrin glues.

In addition to metal ions, chemical oxidants such as $NaIO_4$ have also been utilized to promote curability of bio-based adhesives. Lee et al. reported that the addition of $NaIO_4$ to DOPA-modified poly (ethylene glycol) resulted in rapid gelation with an improved crosslinking network.[130] This approach showed promise in adhesive's curability; however, it is important to consider that these chemical oxidants are generally cytotoxic and have limitations in biological science due to their potential adverse effects.

Alternatively, enzyme-mediated approaches offer a promising way to achieve curability. Enzymes like horseradish peroxidase (HRP),[131] laccases,[132] and tyrosinase,[133,134] have been used in the curability of bio-based adhesives for tissue engineering applications. Hou et al. developed an alginate-based adhesive cured by HRP for adhesion strength improvement.[98] In this system, catechol oxidative cross-linking was achieved in the presence of HRP and H_2O_2. The adhesion strength was determined by lap shear adhesion tests on porcine skin. Figure 2.13C illustrates that

the alginate-based adhesives were cured in a gel state and exhibited improved adhesion strength of ~ 8 kPa.

These methods have been suggested as effective tools for achieving curability in bio-based adhesives. Additional examples or methods for adhesives curability are summarized in Table 2.1. Compared to adhesives without any curing treatment, the use of mussel-inspired curing chemistry has shown promise in enhancing the wet performance of bio-based adhesives.

Table 2.1. The determination of wet adhesion from bio-based adhesives with different cured methods.

Curing methods		**Bio-based adhesives**	**Treat time**	**Adhesion in wet condition**		**Ref.**
				[kPa]	substrates	
Stimuli-induced	UV	Gelatin-based	60 s	120	Collagen films	[135]
	Heat	Zein-TA	24 h	400	Aluminum	[136]
Oxidant agents	$NaIO_4$	Gelatin-TA	108 s	36.31	Bovine leather	[137]
	H_2O_2	TA-Polyamine	0.5 h	1060	Plywood	[138]
	pH	PEG-DA	12 h	8	Porcine skin	[119]
Enzyme-mediated	HRP	EPL-based	3 s	147	Porcine skin	[131]
	Laccase	Soy protein	24 h	3600	Wood	[132]
	Tyrosinase	Chi-based	24 h	400	Glass	[139]

3. EXPERIMENTAL METHODS

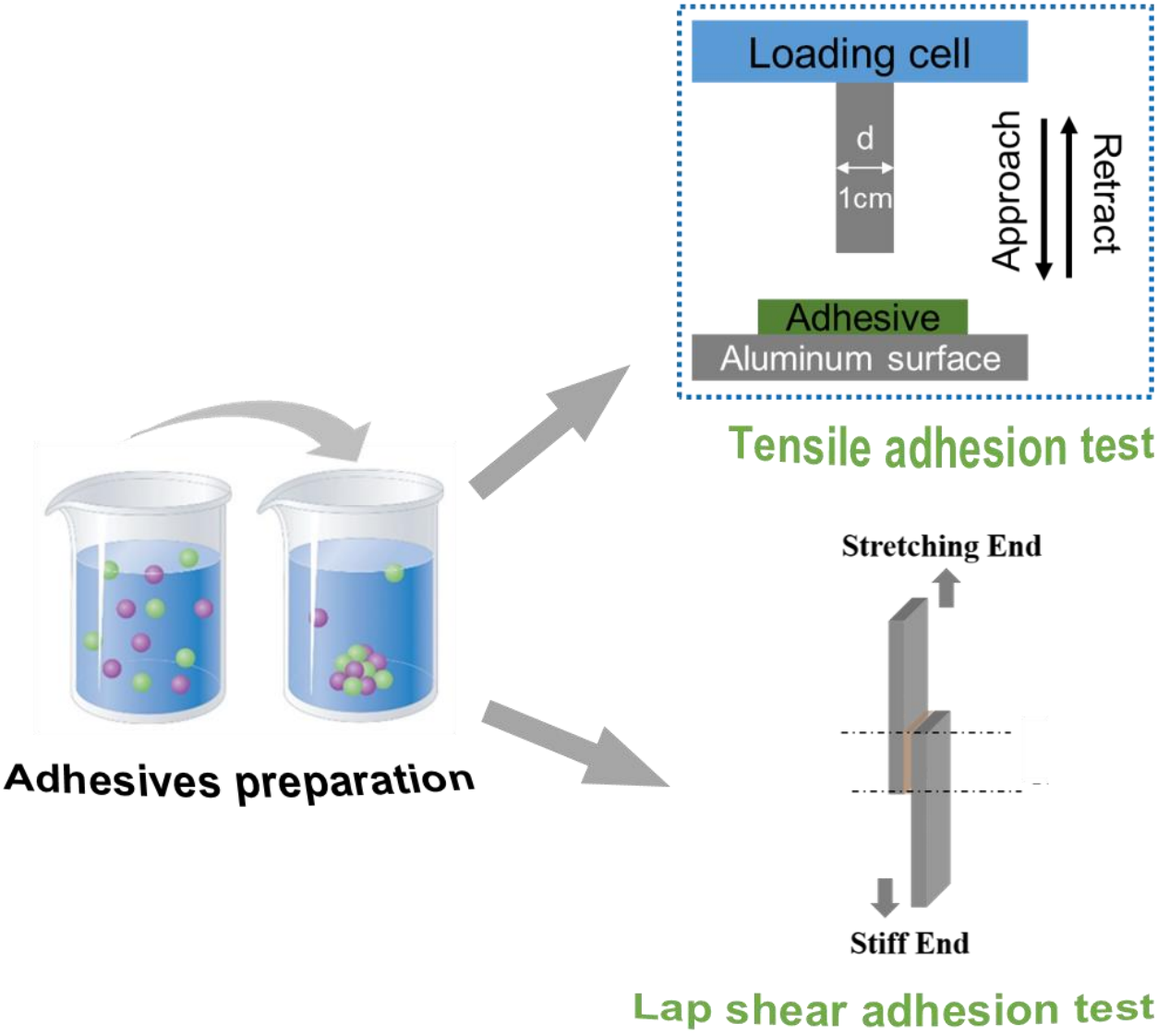

3 Experimental methods

In this chapter, I will present the experimental methods used in my PhD research. First, I will provide a brief introduction to the synthetic methods used for substituting catechol onto the biopolymers. Next, I will describe the preparation process for each bio-based adhesive, along with an overview of the employed characterization methods.

3.1 Catechol-functionalized biopolymers: Synthesis

In papers I and paper III, biopolymers were functionalized with catechol moieties. In paper I, Chi and Alg were each substituted with ~ 20% catechol. This substitution was accomplished through two different reactions: Schiff base formation and Carbodiimide coupling, respectively. In paper III, Chi was synthesized using the same method, but with varying levels of catechol substitution ranging from 10% to 50%. The specific procedures for each method are described below:

3.1.1 Chitosan-catechol

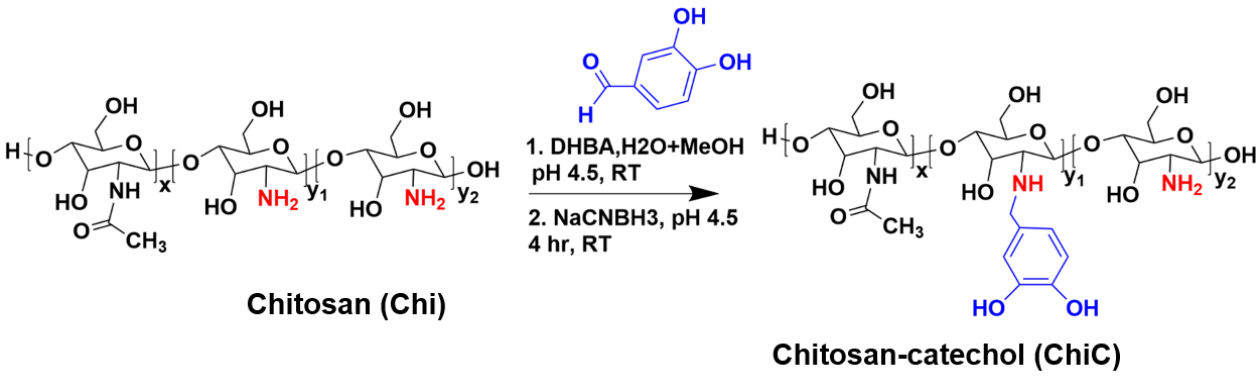

Figure 3.1 Synthetic reaction and structure of ChiC.

Figure 3.1 depicts the synthesis of Chitosan-catechol (ChiC) through a Schiff base reaction. The catechol moiety is introduced onto Chi by nucleophilic addition between amine groups (-NH_2) from Chi and aldehyde groups (-CHO) from 3, 4-Dihydroxybenzaldehyde (DHBA), followed by a reductive amination reaction.[140–142] The synthesis steps and reagent ratios were adopted from a

previous study.[126] Briefly, 2 g of Chi (~13 mmol glucosamine repeat units) were added into 140 ml of 1 wt% glacial acetic acid solution and stirred overnight. The pH was adjusted to 4.5 using 1 M HCl, and then a DHBA solution (60 ml, methanol: water = 2: 4) was added to the reaction mixture. The pH was monitored and readjusted to around 4.5 throughout the synthesis process. The degree of catechol conjugation can be controlled by adjusting the mass of DHBA and reaction time, as shown in Table 3.1. For the reductive amination step, $NaCNBH_3$ (2 g, dissolved into 50 ml of water at pH 4.5) was added gradually over 15 minutes, and the mixture was kept stirring for 4 h. Subsequently, the pH was adjusted to 6.5 by dropwise addition of 1 M NaOH under vigorous stirring to precipitate the polymers. The precipitates were collected via centrifugation (6.5 K rpm/min, 5 min) and re-dissolved in ~ 50 ml of 1 M HCl. The resulting solution was dialyzed for 48 h against an HCl solution (pH 3.0-3.5) using a regenerated cellulose dialysis membrane with a molecular weight cutoff of 3.5 KDa. During the first 8 h, the HCl solution was exchanged every 2 h. After 48 h, dialysis was continued in Mili-Q water for an additional 4 h to remove excess HCl. The ChiC products, with a yield of ~ 75%, were finally obtained via freeze-drying.

Table 3.1 Summary of the conditions for substituting catechol onto Chi from 10% to 50%

Target Samples	Mass of DHBA added (g)	Reaction time (hours)	Reducing time (hours)	Reducing agent	pH Values	
					For reaction	For precipitation
ChiC10%	0.16	1	4	$NaCNBH_3$	4.5	6.5
ChiC20%	0.5	1				
ChiC25%	0.65	1				
ChiC34%	1.0	1				
ChiC43%	1.5	1				
ChiC54%	2.5	2				

3.1.2 Alginate-catechol

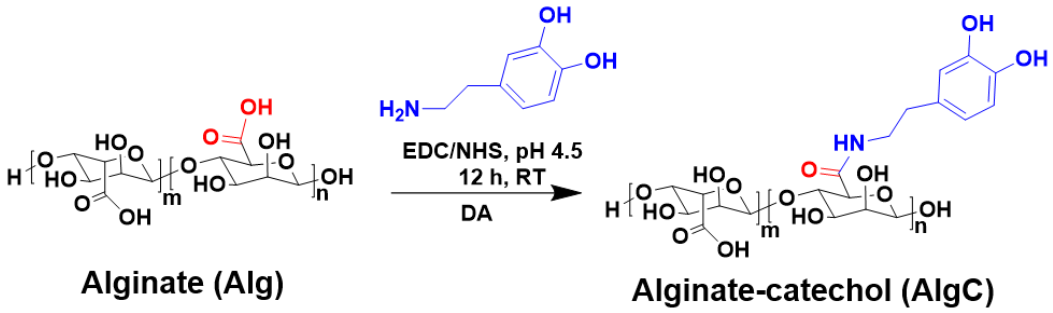

Figure 3.2 One-step conjugation of catechol onto Alg.

Figure 3.2 illustrates the synthesis of alginate-catechol (AlgC) by coupling carboxylic groups (-COOH) from Alg with the amine groups ($-NH_2$) from DA, using 1-ethyl-3-(3-dimethylaminopropyl)-carbodiimide hydrochloride (EDC) and N-hydroxysulfosuccinimide (NHS) as catalysts.[98,143–145] Briefly, 2 g Alg (~10 mmol in terms of repeating unit) was dissolved in 200 ml of water and stirred overnight, followed by pH adjustment to 4.5 using 1 M HCl. Subsequently, 1.2 g of EDC and 2.0 g of NHS (both 10 mmol) were gradually added to the solution. After 30

minutes, 2.0 g DA•HCl was added to the solution in a 1: 1 molar ratio with Alg. The reaction was then conducted at room temperature overnight while maintaining a pH of ~ 4.5. The solution was then dialyzed for 2 days using acidic water (pH 4.5), followed by dialysis with water for 4 hours, and finally freeze-dried. This process yielded ~ 90% dry solids.

During the synthesis and dialysis procedures of both ChiC and AlgC, tin foil papers were used to prevent the production of light-induced adducts. The resulting ChiC and AlgC products were stored at -20℃ in a desiccator for future use.

3.2 Preparation of adhesives

This section provides a detailed description of the preparation process for each adhesive.

3.2.1 Preparation of Chi-Alg-based adhesives

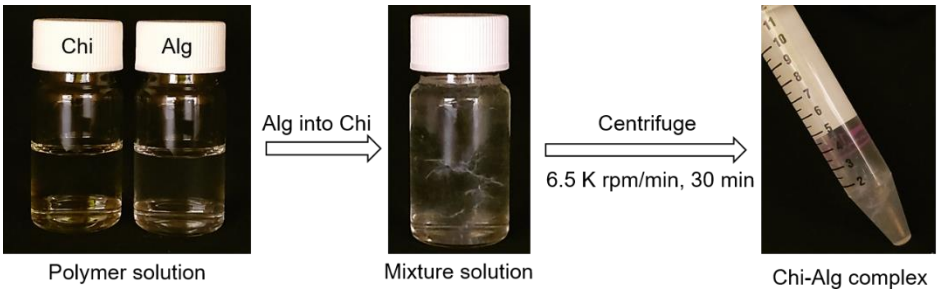

Figure 3.3 Procedures of Chi-Alg complex preparation.

In this study, I prepared four different types of polyelectrolyte complexes using a simple method: Chi-Alg, ChiC-Alg, Chi-AlgC, and ChiC-AlgC. Initially, the biopolymers were dissolved in a solution containing 15 mM NaCl at pH 3.0 overnight. The pH was then readjusted to 3.0 by adding 1 M HCl dropwise. Next, 10 ml of Alg/AlgC (5 mg/ml) solutions were added suddenly to Chi/ChiC (10 mg/ml) solutions in a 1:1 volumetric ratio under continuous magnetic stirring (450 rpm/min). Upon mixing, the solutions instantly turned cloudy. After 15 minutes, the precipitates were

collected by centrifugation (6.5 K rpm, 30 min), as shown in Figure 3.3. The collected precipitates were then used directly for adhesion tests and other characterizations.

3.2.2 Preparation of ε-PL–TA adhesives

The preparation of ε-PL–TA adhesives involved two steps: first, obtaining the ε-PL–TA complexes, followed by the preparation of the adhesives with different formulations.

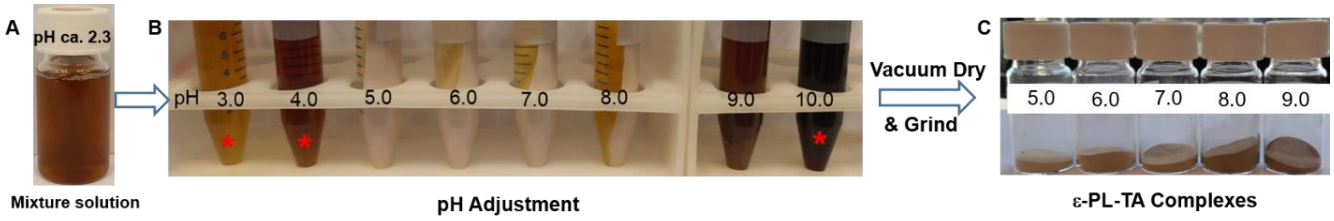

Figure 3.4 Formation of ε-PL–TA complexes. (A) Mixture solution of ε-PL (40 wt%) and TA (20 wt%) in a 1:1 weight ratio without pH adjustment. (B) Mixture solution with pH adjustment ranging from 3.0 to 10.0. (C) The collected precipitates (ε-PL–TA complexes) were vacuum dried and ground for further adhesives preparation and characterization. (Red asterisk indicates no complexes)

Figure 3.4 illustrates the formation of ε-PL–TA complexes through several steps. Initially, TA (20 wt%) and ε-PL (40 wt%) solutions were prepared in water. Then, 5 g of TA (20 wt%) solution was suddenly added to the ε-PL (40 wt%) solution in a 1: 1weight ratio under continuous magnetic stirring at 450 rpm/min. Initially, no precipitation was observed in this mixture (Figure 3.4A), and the pH was measured to be ~ 2.3. Subsequently, the pH was adjusted from 3.0 to 10.0 by adding 10 M NaOH dropwise while stirring. Precipitation occurred at certain pH values (Figure 3.4B), and the resulting precipitates were collected by centrifugation at 6.5 K rpm/min for 5 minutes. They were then dried in a vacuum oven for two days and finally crushed into powders for further adhesive preparation (Figure 3.4C).

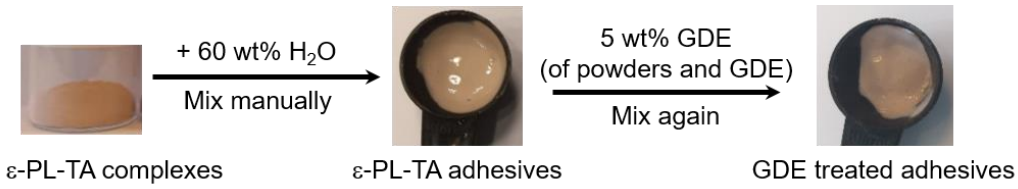

Figure 3.5 Preparation of ε-PL–TA adhesives.

Dried powder complexes were then used to prepare water-based adhesives, as shown in Figure 3.5. Briefly, 1.2 g water was added into the dried complexes in a 6: 4 weight ratio and manually mixed until a uniform phase was obtained. In a separate set of adhesives, glycerol diglycidyl ether (GDE) was included as an additional component. The hybrid adhesives, with various GDE concentrations, are summarized in Table 3.2. For all adhesives, the weight ratio of water content was fixed at 60%.

Table 3.2 Formulations of ε-PL–TA adhesives with various GDE concentrations

Adhesives	Mass of dry complex (g)	Mass of GDE (g)	Mass of water (g)
0% GDE	0.8	-	1.2
2.5% GDE	0.78	0.02	
5% GDE	0.76	0.04	
10% GDE	0.72	0.08	
20% GDE	0.64	0.16	

3.2.3 Preparation of ChiC adhesives

Figure 3.6 Phase separation of one typical ChiC solution.

In study III, ChiC adhesives were prepared following these steps. First, ChiC conjugates with varying catechol contents (10%, 20%, 25%, 34% 43%, and 54%) were synthesized as described

in Section 3.1.1. Then, 1.5 g of ChiC products were dissolved in a 150 ml solution containing 1 mM NaCl at pH 3.0 overnight. The pH value was then readjusted back to 3.0 from the initial solution (with a pH range of ~ 4-5). For each ChiC solution, the final ionic strength was varied from 0.1 to 2.0 M, as illustrated in Figure 3.6. This variations was achieved by preparing various NaCl solutions with pH 3.0 and ionic strengths ranging from 0.2 to 4.0 M. Subsequently, 5 ml of these solutions were rapidly added to the ChiC solutions in a 1: 1 volume ratio under continuous magnetic stirring at 450 rpm/min. Upon mixing, phase separation occurred, with the observations depending on the catechol content and ionic strength. Finally, for samples where precipitation occurred, the precipitates were collected through centrifugation at 6500 rpm for 5 minutes and further examined for adhesion measurements.

Horseradish peroxidase (HRP) and hydrogen peroxide (H_2O_2) were employed to facilitate the curing of ChiC coacervates. Specifically, ChiC coacervates with a catechol content of 25% and prepared at an ionic strength of 1.2 M were selected for this experimental study. The preparation process consisted of two equal parts: one containing ChiC and HRP, and the other containing ChiC and H_2O_2 (see Table 3.3 for specific details). In the first part, 100 µl of HRP (1 mg/ml) was added to 0.5 g of ChiC coacervates, while in the second part, 100 µl of H_2O_2 (8 mg/ml) was mixed with 0.5 g of ChiC coacervates. The two parts were thoroughly mixed using a spatula. The adhesion properties of the cured ChiC adhesives were further determined underwater.

Table 3.3 Preparation of ChiC adhesives treated by HRP and H_2O_2

Adhesives	ChiC coacervates (g)	HRP (1 mg/ml) (µl)	H_2O_2 (8 mg/ml) (µl)	Weight Ratio	
				ChiC/HRP	ChiC/H_2O_2
Part I	0.5	100	-	1500: 1	-
Part II	0.5	-	100	-	625: 1

3.3 Characterization

3.3.1 Lap shear adhesion testing

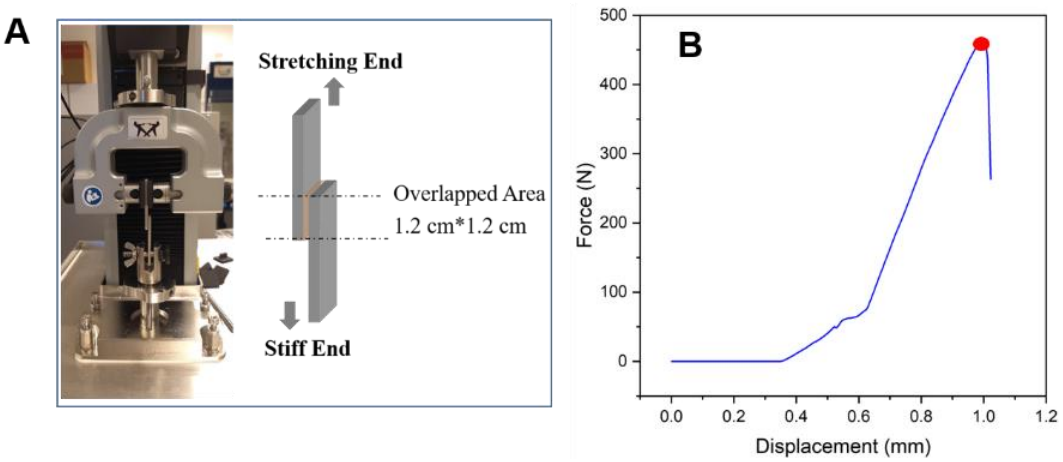

Figure 3.7 Lap shear adhesion measurements for wet adhesion determination. A) Illustration of lap shear configuration and substrates. B) A representative force curve obtained from ε-PL–TA adhesives, with the red spot indicating the maximum force at the point of failure.

Single-lap shear adhesion tests were conducted using the Universal Testing System (Instron 34SC-2, USA) equipped with two different loading cells. For study I, a 50 N loading cell was employed, while a 2 kN loading cell was utilized for study II. Adhesion measurements were performed on aluminum substrates. Prior to testing, pre-cut aluminum substrates with dimensions of 50 mm × 12 mm × 10 mm (L×W×H) were prepared by polishing and cleaning with ethanol and acetone. The adhesive was then applied between the two aluminum substrates, creating an overlap area of 12 mm × 12 mm (Figure 3.7A), and the substrates were clamped together.

Adhesion strength was evaluated by removing the samples from water and subjecting them to a controlling pulling force at a speed of 1.5 mm/min until failure. The maximum force at the point of failure was recorded, as indicated by the red point in Figure 3.7B. The shear adhesion strength (expressed in kPa or MPa) was calculated by dividing the maximum force at joint failure by the

overlapping area, using the force curves obtained from the tests. The data were plotted as mean ± standard deviation based on seven specimens. Statistical evaluation was conducted using a one-way analysis of variance test with OriginPro 2021 software. Adhesion strengths were considered statistically significant with a level of $p < 0.001$.

3.4.2 Underwater tensile adhesion testing

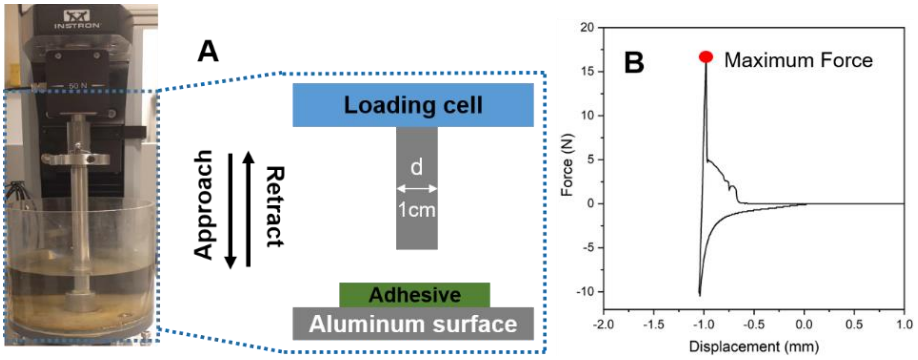

Figure 3.8 Underwater tensile adhesion test. A) Images and schematic illustration of the tensile adhesion test setup. B) A representative force-displacement curve obtained from ChiC adhesives, with the red point indicating the maximum force at the point of failure.

In study III, tensile adhesion testing was performed on a universal testing machine equipped with a 50 N loading cell. The configuration consists of two aluminum cylinders fixed to the machine (Figure 3.8A). To measure the adhesion underwater, a given amount of the adhesive sample was applied to the lower cylinder (diameter: 20 mm). Subsequently it was immersed in a tank container filled with 1 mM NaCl solution. The upper cylinder (diameter: 10 mm) then approached the lower cylinder at a controlled speed of 1 mm/min until a contact made (setpoint force: 10 N; duration time: 60 s). Afterwards, the upper cylinder was retracted until separation, and a force-displacement curve was recorded (Figure 3.8B). The adhesion strength was calculated based on the following equation:

$$Adhesion\ strength\ (Pa) = \frac{Maximum\ Force\ (N)}{Overlapped\ area(pr^2,\ m^2)}$$

The results were expressed as mean ± standard deviation based on ten replica specimens.

3.4.3 Quartz crystal microbalance with dissipation monitoring (QCM-D)

QCM-D (Biolin Scientific Q-SenseE1, Sweden) was utilized to investigate the complexation and stability of Chi-Alg-based complexes. The experimental protocols involved two steps: the multilayers buildup via the layer-by-layer assembly and the pH cycle tests from 3.0 to 9.0.

First, the sensors were cleaned and experienced several treatments, as follows: The silica-coated sensors (QSX 303, Biolin Scientific) were first cleaned with water and acetone, dried with compressed air, and then subjected to a 5-minutes treatment with Plasma (PDC-32G plasma cleaner, Harrick Plasma) at medium intensity under a water atmosphere (vapor pressure of 500 mTorr) to remove organic contaminants. Subsequently, they were immersed in an 18 (v/v)% 3-glycidoxypropyltrimethoxysilan (GOPS)/acetone solution for 24 h, rinsed with acetone three times to remove any unreacted GOPS, and kept at 80 °C for 1 h. The sensors were then rinsed into 200 ppm of Chi solution (pH 3.0) for 20 minutes, followed by rinsing water to remove the unreacted Chi polymers. Having sensors treatment, the entire system was cleaned by flushing 2% hellmanex for 30 minutes and water for 1 h.

The deposition of multilayers was achieved through layer-by-layer (LbL) techniques on the modified sensors. Briefly, a 15 mM of NaCl at pH 3 was injected at a flow rate of 150 µl/min until a stable baseline was reached. The first layer was formed by flushing a 200 ppm Alg solution for 20 minutes, followed by rinsing with a background solution (15 mM of NaCl, pH 3) for an additional 20 minutes. For the second layer, a 200 ppm Chi solution was introduced for 20 minutes,

followed by another 20-minute rinse with the same background solution. This process was repeated seven times to yield a Chi-Alg multilayer (14 layers in total). The same procedure was conducted to create the Chi-AlgC, ChiC-Alg, and ChiC-AlgC multilayers. Each combination was independently measured three times.

After multilayers creation, the pH cycle tests were performed by sequentially loading acidic (NaCl 15 mM, pH 3) and basic (NaCl 15 mM, pH 9) solutions for 20 minutes each, repeated three times. To maintain a stable pH value of the basic solution, the pH 9.0 solution was freshly prepared by adding 15 µl of 0.1 M NaOH to 30 ml of 15 mM NaCl. The shifts in frequency (Δf) and dissipation (ΔD) were monitored and analyzed using the QTools software (Q-Sense, Sweden).

3.4.4 Attenuated Total Reflection (ATR) Infrared Spectroscopy

In study II, ATR spectroscopy was employed to analyze the structural of ε-PL–TA adhesives. All of the samples were fully dried, ground into powder, and stored in a desiccator. The ATR spectra were collected by a VERTEX80v Fourier transform vacuum spectrometer from Bruker Optics GmbH Fourier. The Fourier-transform infrared spectroscopy (FTIR) apparatus was equipped with a Germanium on KBr beam splitter, a liquid N_2-cooled HgCdTe detector, and a thermal globar radiation source. The sample spectra were recorded in blocks of 300 scans within the wavenumber range of 700 to 3800 cm^{-1}, with a resolution of 2 cm^{-1}. Background spectra with a cleaned Ge crystal were collected before and after sample measurements. The spectra data were processed and analyzed using OPUS-7.2 software (Bruker Optik GmbH, Germany). Specifically, the absorption spectra were firstly obtained by averaging the sample and background scans, and further adjustments were made to correct for any residual water vapor absorption occurring in the

atmosphere. Following this, a baseline correction was then performed. Finally, an ATR correction was applied to account for the wavelength-dependent penetration depth of the infrared probe beam.

Curve-fitting process was carried out using OPUS-7.2 software to handle the congested spectra of overlapped peaks in the range of 1250-980 cm^{-1}. The specific procedures involved the following steps [146,147]: (i) selecting the frequency range (two options: 1050-700 cm^{-1} or 1416-700 cm^{-1}) for normalization, (ii) identifying the overlapped peaks (1250-980 cm^{-1}) for analysis, and (iii) fitting the wavelength within the ranges from 1250 cm^{-1} to 980 cm^{-1} for Voigt modeling. For quantitative analysis (step iii), it was employed using OriginPro 2021 software by integrating the peak area within the range of 1150-1050 cm^{-1}. The results were statistically evaluated using the coefficient of determination(R squared), which was considered trustable due to the high accuracy ($R^2 > 0.998$).

3.4.5 Other characterization techniques (UV-Vis, DLS, AF4, and TGA)

In addition to the mentioned techniques, I employed several other methods to characterize my samples, including NMR spectroscopy, Dynamic Light Scattering (DLS), UV-Vis spectroscopy, and Thermogravimetric Analysis (TGA). Standard protocols were followed for all of these techniques.

NMR experiments were carried out on a Bruker Avance, 400 MHz using D2O as a solvent and TMS as the internal reference. The acquired data was processed using Mestrenova 11.0.0 software. This method was utilized to investigate the structure of biopolymers, such as ε-PL, ChiC, and AlgC.

DLS measurements were employed on a Malvern Zetasizer Nano ZS90 instrument to estimate the hydrodynamic size of ChiC and AlgC. Solutions of 2 mg/ml^{-1} Chi/ChiC (in 0.1 M citric acid-Na_2HPO_4 buffer; pH 3.0) and Alg/AlgC (in water; pH 6.0) were prepared and filtered through a 0.45 µm polyether sulfone (PES) membrane.

UV-Vis spectroscopy was employed on a NanoDrop 2000c Spectrophotometer to determine the catechol content of ChiC and AlgC. The spectra were collected in the range of 200 to 800 nm. Samples were measured in a quartz cuvette with a path length of 10 mm, and background absorption was subtracted prior to measurement. To determine the degree of catechol conjugation, biopolymers were dissolved in an aqueous buffer solution at a concentration of 0.1 mg/ml. For the creation of a standard curve, a series of DA solutions with varying concentrations were prepared by diluting the stock solution (1 mg/ml). The standard curve was created by plotting the absorbance at 280 nm, and the degree of conjugation was calculated using the equation derived from the standard curve.

A TGA 5500 analyzer (Mettler Toledo, Guyancourt, France) was used to investigate the thermal stability of ε-PL–TA complexes. Sample weighing 3-5 mg was placed into a platinum pan and heated at a rate of 10 ℃/min under a nitrogen atmosphere with a flow rate of 20 ml/min, within a temperature range from 25 to 800 ℃.

4. SUMMARY OF RESULTS

4. Summary of results

As discussed in the background chapter, recent studies have been dedicated to developing bio-based adhesives with improved functionality in wet environments. Mimicking mussel adhesion mechanisms can be a promising strategy to achieve this goal. While most studies have primarily focused on utilizing mussel-inspired catechol chemistry for designing bio-based adhesives, only a limited number of studies have recognized the importance of incorporating amine functionality and coacervation. In this section, the scope and main findings of my three studies will be discussed. Each study investigated a bio-based candidate that mimics all three mussel adhesion mechanisms:

i) containing catechol or catechol-like groups,

ii) having amine moieties,

iii) undergoing complexation/coacervation.

4.1 Catechol-modified Chi-Alg complexes (Paper I)

Chi and Alg are oppositely charged polysaccharides that can form polyelectrolyte complexes driven by electrostatic forces.[148–150] Additionally, Chi is a polyamine, allowing Chi-Alg complexes to fulfill two out of the three design criteria. Based on this, it was hypothesized that the addition of catechol groups to Chi-Alg complexes would meet all three criteria and expect the enhanced wet performance.

To achieve this, Chi and Alg were each substituted with ~ 20% catechol groups for several reasons. First, it allowed for the retention of a considerable number of charge. Second, it introduced catechol-amine crosslinking. Four complex combinations (Chi-Alg, ChiC-Alg, Chi-AlgC, and ChiC-AlgC) were investigated to determine the impact of having catechol on one or both polymers on the adhesion performance.

First, ChiC and AlgC were synthesized using Schiff base formation and carbodiimide coupling reactions, respectively. The overall synthetic route is summarized in Figure 4.1, and the specific synthesis procedures are described in Section 3.1.1. The successful catechol modification was confirmed using ^{1}H-NMR and UV-Vis spectroscopy (see discussion in paper I). The degree of catechol conjugation was determined to be 20.2% and 18.7% for ChiC and AlgC, respectively, using UV-Vis measurements.

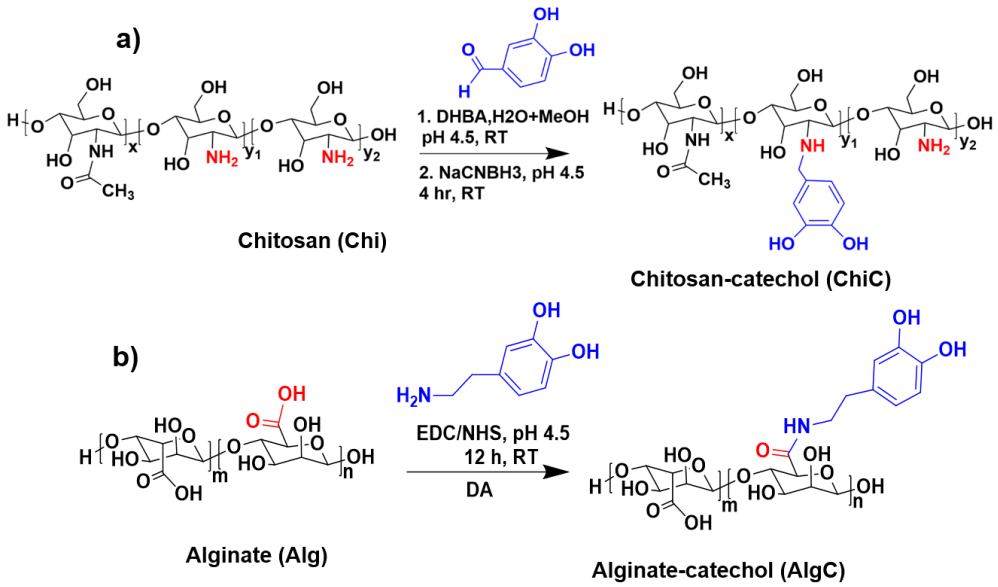

Figure 4.1 Overall synthetic routes and reactions involved in the synthesis of (a) ChiC and (b) AlgC.

A QCM-D investigation was conducted to determine whether the addition of catechol to the polymers affects complexation, i.e., the amount of complex formed. To address this question, an experiment was designed to study the LbL assembly of each complex combination using QCM-D. In this method, the oppositely charged polymers are deposited on the QCM-D sensor in a step-by-step manner to create a multilayer through polymer complexation. QCM-D allows for an estimation of the mass or amount of the deposited multilayer/complex, which provides insight into how the additional catechol introduction impacted the complexation. Figure 4.2 illustrates the

QCM-D data in terms of the shifts in the oscillation frequency (F) and dissipation factor (D). The ΔF correlates to the effective mass (complex plus water content) coupled to the sensor, while the ΔD represents the ability of multilayers to dissipate the oscillatory energy. Both parameters are relevant for determining mass and viscoelastic properties and serve as measures of the amount of adsorbed complexes.[151] As shown, ΔF and ΔD are almost the same for all combinations, indicating that the amount of adsorbed complex is approximately the same. This finding suggests that replacing 20% of ionic units with catechol groups does not significantly impact the complexation process. Thus, in these complexes, biopolymers are formed mainly driven by long-range electrostatics.

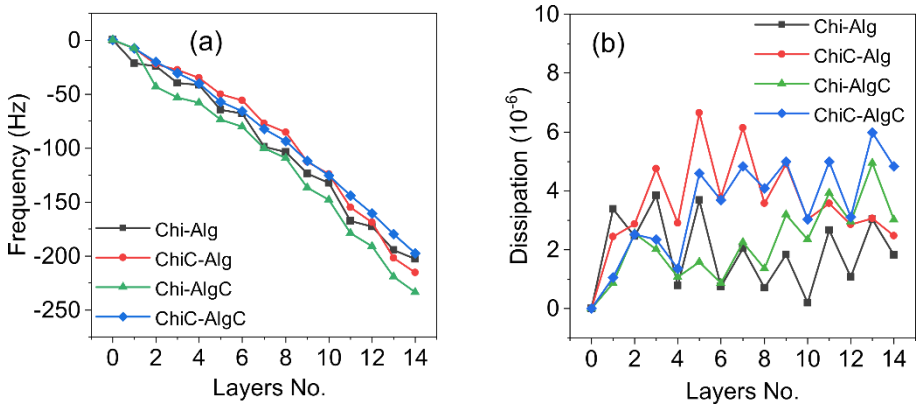

Figure 4.2 Complexes determination via LbL assembly. QCM-D data of a) frequency and b) dissipation shifts for 3rd overtone as a function of layers number (Odd layer: Alg or AlgC polymer, Even layer: Chi or ChiC polymer).

To investigate the impact of catechol on the stability of Chi-Alg complexes, an additional experiment was conducted after complexation. The hypothesis was that the addition of catechol moieties could result in catechol-amine interaction, potentially affecting the intermolecular network.[34,152,153] To answer this question, a pH cycle test at 3 and 9 was performed after the LbL assembly. Upon switching the pH to 9.0, one expected that catechol moieties could oxidize and cross-link with amine groups, creating intermolecular cross-linking networks that may impact pH

stability.[34,152,153] The stability of the complexes was characterized using QCM measurements to investigate their pH responsiveness.

Figure 4.3 illustrates the swelling and shrinking behaviors of the complexes. Overall, it was found that all complexes showed an increased in D and a decreased in F when the pH increased from 3 to 9. This results indicated that all complexes demonstrated a swelling behavior, which could cause by the excess negative charge generated (i.e., reduced charge on Chi and increased charge on Alg). Notably, the changes in D and F varied to different extents depending on the presence of catechol on one or both polymers, indicating their differences in stability.

The reference complex (Chi-Alg), mainly driven by electrostatic forces, exhibited irreversible swelling/collapse with quite large changes in F and D (Figure 4.3a). Additionally, F and D demonstrated an increasing magnitude with each cycle. These observations collectively indicated the absence of stabilizing covalent interactions in the complex. Having catechol modification, one expect the presence of catechol-amine interactions could render reversible swell/collapse cycles with reduced structural changes. Interestingly, the ChiC-Alg multilayer (Figure 4.3b) also displayed quite a similar behavior to Chi-Alg multilayer, suggesting a lack of stable structure despite the presence of catechol groups. In contrast, Chi-AlgC (Figure 4.3c) and ChiC-AlgC (Figure 4.3d) multilayer demonstrated a small shift in F and D with each cycle, indicating a more stable and reversible swelling-collapse behavior. These results demonstrate that having catechol on Alg significantly improves pH stability, which could be attributed to the catechol-amine association. However, having catechol only on Chi did not improve the stability, suggesting that catechol-amine interactions are only possible between Chi units (inter- and intra-chain), thus, leading to Alg excluded from the intermolecular cross-linked network. Nevertheless, having catechol on Alg enables the intermolecular cross-linking of Chi and Alg chains.

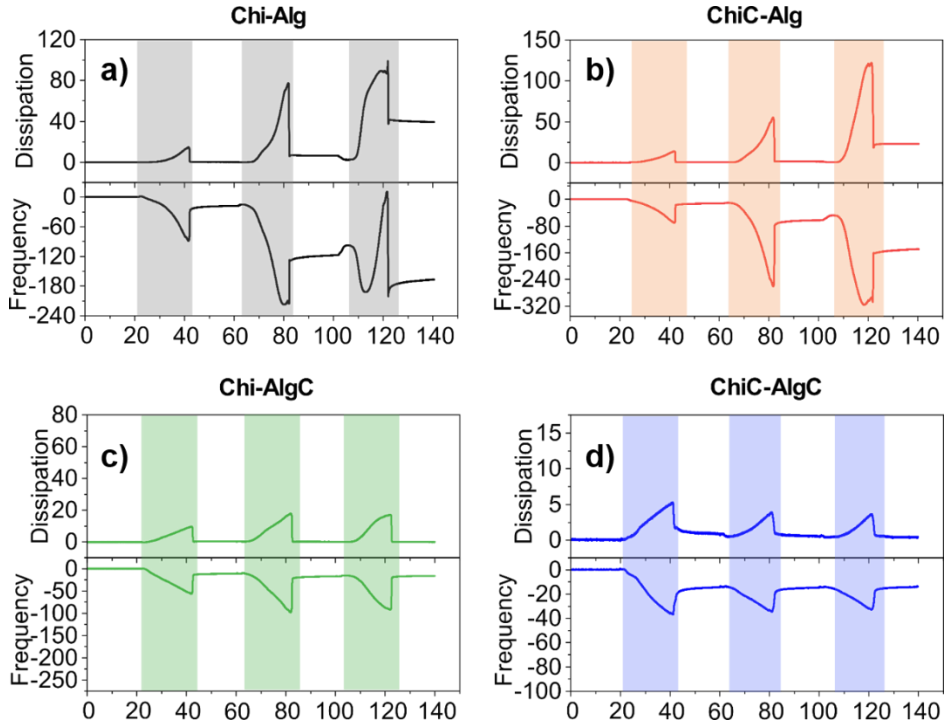

Figure 4.3 pH cycle (3-to-9-to-3) test of four multilayer complexes: a) Chi-Alg, b) ChiC-Alg, c) Chi-AlgC, and d) ChiC-AlgC (note: the highlighted areas indicated the pH at 9). For each pH value, samples were examined 20 minutes.

Additionally, variations in hysteresis provide a way to assess the stability of complexes.[154,155] The hysteresis of each multilayer, calculated by baseline shift after three pH cycles, is summarized in Table 4.1. Specifically, if there is a small change of hysteresis in both F and D, it would suggest a reversible structural changes in the multilayer.[154] As shown in Table 4.1, it was found that Chi-Alg and ChiC-Alg multilayers exhibited a rather large hysteresis in both F and D, suggesting irreversible structural changes in the multilayers. Conversely, Chi-AlgC and ChiC-AlgC multilayers showed relatively smaller hysteresis in F and negligible baseline shift in D, indicating a reversible swelling-collapse cycles that could ascribe to the efficient catechol-amine cross-linking. These findings suggest that having catechol on Alg in Chi-Alg complexes, the wet performance has been improved. One can expect that the improvement is facilitated by the efficient catechol-amine interactions, enabling enhanced self-cross-linking properties.

Table 4.1 Baseline shift (hysteresis = baseline after 3rd cycle – baseline before 1st cycle) as a result of three pH cycles

Sample		D hysteresis after three pH cycle test	D at Mean ± S.D	F hysteresis after three pH cycle test	F at Mean ± S.D
Chi-Alg	1	39.62	18.96±18.00	-169.05	-153.83±19.97
	2	10.52		-161.22	
	3	6.73		-131.21	
ChiC-Alg	1	2.27	13.15±10.46	-54.45	-111.74±50.58
	2	23.13		-150.19	
	3	14.04		-130.59	
Chi-AlgC	1	-0.19	-0.34±0.50	-28.03	-43.76±38.03
	2	0.06		-16.12	
	3	-0.90		-87.13	
ChiC-AlgC	1	0.32	1.00±1.38	-14.55	-16.03±6.12
	2	2.59		-22.75	
	3	0.09		-10.78	

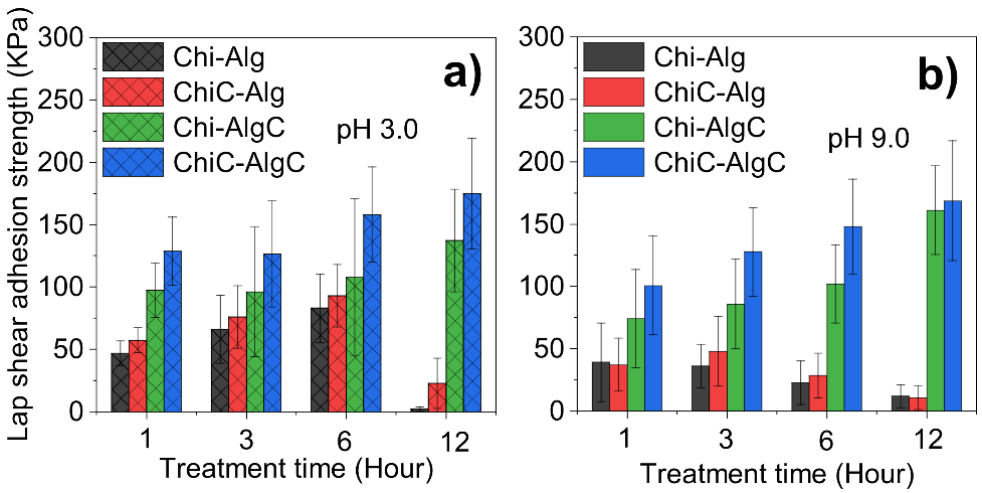

Figure 4.4 Lap shear adhesion determination in wet environments at pH 3.0 a) and pH 9.0 b) as a function of immersion time.

To investigate the impact of catechol modification on the intermolecular cross-linked networks, lap shear wet adhesion tests were conducted to evaluate the cohesive properties. Four complexes

in a bulk state were prepared following specific steps and methods described in Section 3.2.1. The lap shear wet adhesion tests were carried out by applying the complexes onto aluminum substrates and immersing them in solutions with pH 3.0 and 9.0 for different durations (1, 3, 6, and 12 hours).

The adhesion results are illustrated in Figure 4.4a and Figure 4.4b. At pH 3.0, the Chi-Alg and ChiC-Alg complexes displayed a slight increase in adhesion strength until 6 h, followed by a significant decrease, indicating their instability and dissolution over time. In comparison, the complexes with catechol on Alg demonstrated improved adhesion strength, which might be due to the strong bonding strength and complex molecular crosslinking in the presence of catechol-amine interactions. Switching to pH 9, Chi-Alg and ChiC-Alg complexes showed a decaying lap shear strength with time, while Chi-AlgC and ChiC-AlgC complexes demonstrated a growing lap shear strength, indicating weak bonding strength and poor cohesive properties for the former two complexes. Overall, the presence of catechol on Alg resulted in a significant improvement of adhesion strength, which can be attributed to the contribution of catechol-amine interactions.

These results suggest that catechol-modified Chi-Alg complexes exhibit improved wet performance and hold promise for applications in wet adhesives. In summary, this study highlights the following key findings:

- Based on QCM-D measurements, Chi-AlgC and ChiC-AlgC complexes cross-link through possible catechol-amine covalent interaction.
- Adhesion testing shows that both Chi-AlgC and ChiC-AlgC exhibit enhanced wet adhesion strength at pH 9, indicating the contribution from catechol-amine covalent interaction.
- Introducing 20% catechol on Alg provides approximately 60% increased adhesion strength, suggesting an effective strategy for designing wet adhesives.

- However, the improvement in adhesion strength is still insufficient, possibly due to hydration of the materials. Exploring other materials with less hydration may lead potential improvements.

4.2 ε-PL–TA combination (Paper II)

ε-PL, a polycationic compound rich in amine moieties, exhibits high water solubility over a broad pH range, making it suitable for adhesive preparation with fewer limitations. On the other hand, TA, a water-soluble plant phenolic compound containing numerous galloyl moieties, has the ability to mimic catechol groups. By incorporating two out of three mussel-inspired mechanisms, the hypothesis was that the complexation of ε-PL and TA would enable ε-PL–TA combinations to fulfill all three adhesion mechanisms observed in mussels. Guided by these design principles, this study aimed to investigate the potential of ε-PL–TA as a mussel-inspired wet adhesive.

For ε-PL and TA complexation, it was assumed to be pH-dependent. Specifically, ε-PL is a cationic polypeptide that exhibits reduced charge as pH increases (pKa ~ 9.4).[156] TA is a polyphenol that undergoes two possible pathways as pH increases,: i) deprotonation of hydroxyl groups resulting in a negative charge (pKa ~ 6.0),[157] and ii) oxidation into quinone species.

The amine and galloyl groups, along with their respective forms at elevated pH, are expected to form complex through various physical (hydrogen bonding and ionic bonding) and chemical (covalent Michael addition and reversible Schiff base formation) mechanisms.[1,158–160] To answer this question, ε-PL and TA complexation as a function of pH values (ranging from 3.0 to 10.0) was investigated. It was found the ε-PL–TA complexation was pH-dependent (see details in Section 3.2.2). One expected that the pH-driven complexes could hypothetically impact cohesive properties, as well as water resistance performance.

To begin, ε-PL–TA complexes at pH 5.0, 7.0, and 9.0 were selected to prepare ε-PL–TA adhesives by adding 60 wt% water. Lap shear adhesion tests were conducted to determine the water-resistance properties by immersing samples in water for two and seven days. Figure 4.5 illustrates the properties of ε-PL–TA adhesives as a function of pH, regarding to the adhesion and hydrolysis. Overall, it was discovered that adhesives produced at higher pH value result in stronger water resistance (Figure 4.5a). The enhanced adhesion strength might be due to mechanical reinforcement resulting from galloyl–amine covalent cross-linking. After seven days of immersion in water, the adhesive complexes created at pH 5 and 7 de-bonded. Notably, the adhesive complex produced at pH 9 maintained some level of adhesion (0.35 MPa, ~ 15% of dry state). This finding confirms that changes in the chemical structure/interactions of the complex occur depending on the pH of the complex preparation. Comparison with the negative control, i.e., an aqueous solution of ε-PL (20 wt.%) and TA (20 wt.%), indicates that complexation of ε-PL and TA enhances water-resistance. Despite both TA and ε-PL being highly water-soluble, their water resistance is overall improved when they are in a complexed/condensed state.

Further confirmation of the observed trends is obtained through the measurements of insoluble matter content in ε-PL–TA adhesives (Figure 4.5b). Since both ε-PL and TA are highly soluble in water, the presence of insoluble matter content can be attributed to the cross-linked part. The results indicate that the complexes prepared at elevated pH exhibit a higher insoluble content, providing additional evidence for covalent cross-linking between ε-PL and TA complexes formed at elevated pH.

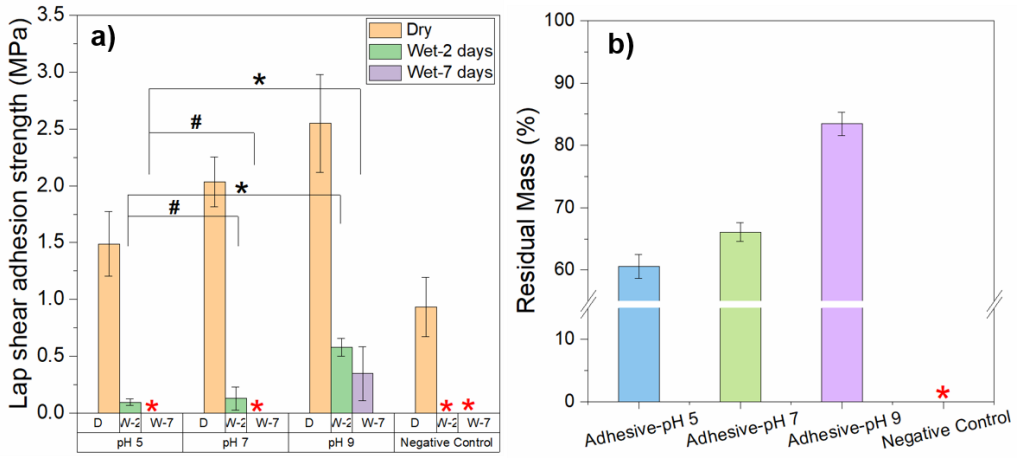

Figure 4.5 Characterizations of the ε-PL–TA adhesives at pH 5, 7, and 9. a) Adhesion strength measured in a dry and wet state for 2 or 7 days. b) Hydrolysis residual test for stability comparison. (Red asterisk means no adhesion strength or specimens separated before testing in panel a, or samples dissolved completely in panel b; * indicates the statistical significance of $p < 0.001$, # indicates no significant difference between two samples)

To understand the wet adhesion properties of the ε-PL–TA complexes, ATR spectroscopy measurements were employed for structural analysis. Figure 4.6 illustrates the molecular cross-linking interactions within the ε-PL–TA complexes at pH 5, 7, and 9. The absorbance of the bands related to C=O (1630-1570 cm^{-1}) and C=N (1700-1630 cm^{-1}) stretching in the range of 1800-1400 cm^{-1} was investigated, exhibiting a significant difference. At pH 9, a higher amount of functional groups was observed compared to the other pH values. The increase in C=O groups suggests greater oxidation of tannic acid moieties and increased cross-linking at pH 9.

Furthermore, the covalent bonding interactions involved in Michael Addition and Schiff base reactions exhibit distinct characteristics. Michael Addition leads to the formation of permanent covalent bonds (-C-N-) (1150-1050 cm^{-1}), while Schiff base reactions involve dynamic covalent bonds (-C=N-) (1700-1630 cm^{-1}). The absorbance of the C=N bond is stronger than that of the C-N bond. This observation suggests that the primary oxidative coupling reaction is responsible for Schiff base formation.

The current findings demonstrate that ε-PL and TA, both highly water-soluble, can be transformed into a partially cross-linked adhesive with water resistance through complexation and pH control. However, it is important to investigate the reasons for the relatively low water resistance (maintaining only 15% of their initial dry state) and explore methods to enhance it further. One potential reason for the relatively poor water resistance could be that the Schiff base bonds are the primary means of forming complex self-cross-links. The produced imine bonds (-C=N-) are considered less stable in nature, which may explain the relatively weak water resistance property of ε-PL–TA adhesives at pH 9.

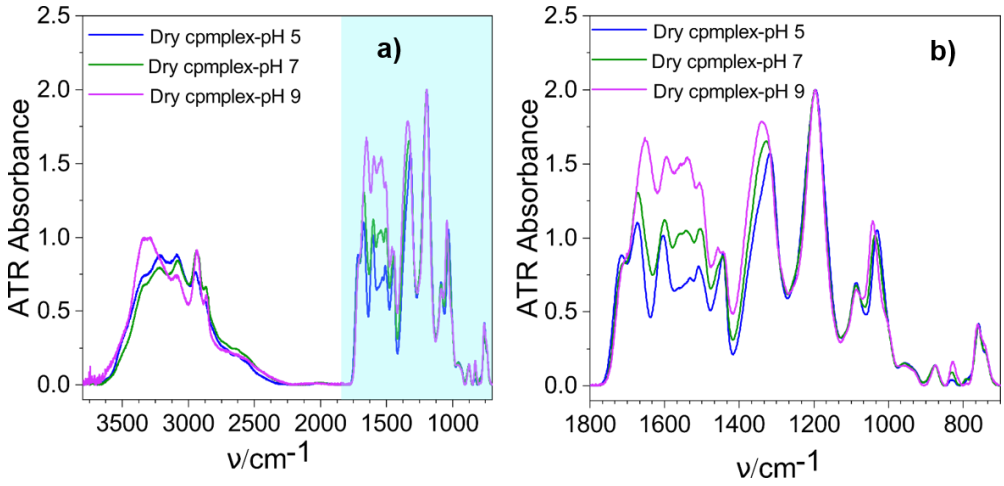

Figure 4.6 ATR spectroscopy of the ε-PL–TA complexes at pH 5, 7, and 9. a) Full spectra ranging from 3800-700 cm^{-1}. b) The region at 1800-700 cm^{-1} was enlarged to precisely distinguish the peaks of three samples.

To enhance the water-resistance of the ε-PL–TA adhesives, an approach was proposed to introduce a secondary source of cross-linking. Glycerol diglycidyl ether (GDE), a cross-linker, was selected for its advantages: i) It is non-toxic and derived from renewable sources; ii) It is water-soluble, allowing for homogenous mixture with the ε-PL–TA adhesive; and iii) It contains epoxide functional group, enabling it to react with ε-PL (amine) and TA (hydroxyl group) to form

permanent covalent bonds (C-N and C-O). The formation of these new covalent bonds was expected to enhance the cohesive properties and improve water resistance.

As depicted in Scheme 4.1, the epoxide groups react with the hydroxyl groups on TA,[49] resulting in the production of stable ether bonds (C-O). It is suggested that the reactivity of this reaction is influenced by the pH values, as the hydroxyl group becomes more active and facilitates the formation of epoxide and hydroxyl groups at higher pH values (pH 5-9).[163] Moreover, the epoxide groups on GDE can react with the amines present in ε-PL, leading to the formation of covalent C-N bonds.[52] This reaction mechanism involves the activation of the epoxy ring through the active hydrogen present in amines. Previous studies have shown that the pH within the range of 5-9 (lower than pKa of ε-PL) does not significantly affect the amine-epoxide reactions.[164,165]

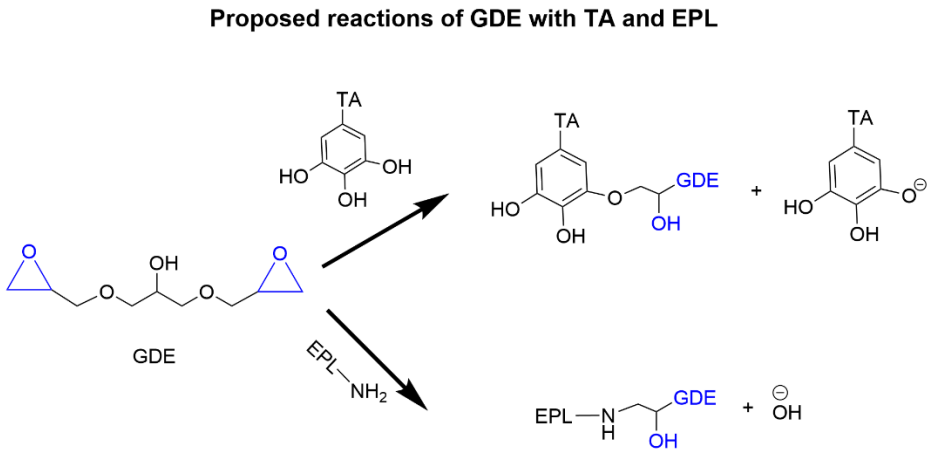

Scheme 4.1 Illustration of proposal reaction mechanisms about GDE reacted with amine and catechol moieties.

To investigate the impact of GDE on the water resistance of ε-PL–TA adhesives, various concentrations of GDE (ranging from 2.5 wt% to 20 wt%) were added to the adhesive formulation. The effect of GDE concentrations on the lap shear adhesion strength was characterized and depicted in Figure 4.7. Upon adding GDE in the range of 2.5 wt% to 5 wt%, the wet adhesion strength showed an increasing trend from 0.5 MPa to 2.0 MPa after a 7-day immersion period.

However, with a further increase in GDE concentration, the wet adhesion strength exhibited a significant decrease. Based on these findings, ε-PL–TA adhesives containing 5 wt% GDE were selected for subsequent adhesion studies.

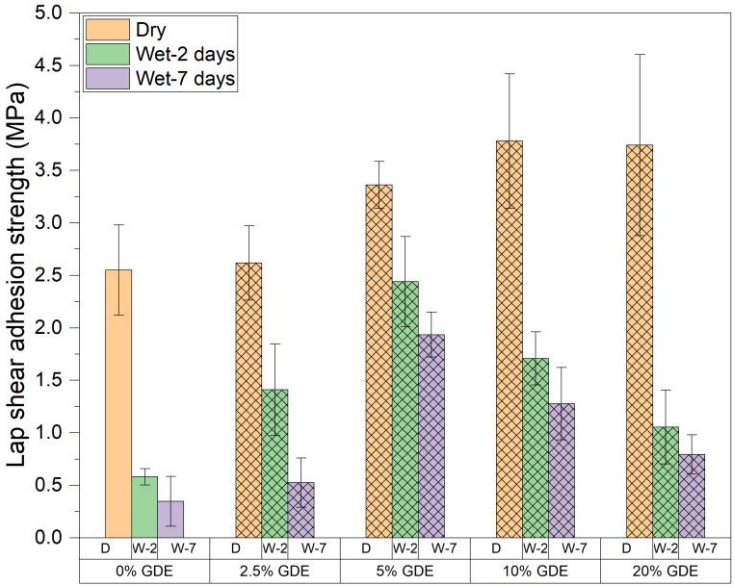

Figure 4.7 GDE concentrations optimized and their effects on adhesion strength in dry and wet conditions.

Figure 4.8 illustrated the water resistance properties of ε-PL–TA adhesives at pH 5, 7, and 9 after GDE treatment. It was observed that ε-PL–TA adhesives at all pH values displayed an improved wet adhesion strength. Notably, at pH 9, the wet adhesion strength exhibited a significantly increase to ~ 2 MPa after 7-day immersion, which still kept ~ 55% of the initial dry state. A consistent result was observed in the hydrolysis testing (Figure 4.8b). It suggests that all ε-PL-TA adhesives showed an improved water stability compared to those without GDE treatment. Once again, an increased trend ε-PL–TA adhesives at pH 9 demonstrated the highest residual mass being ~90%.

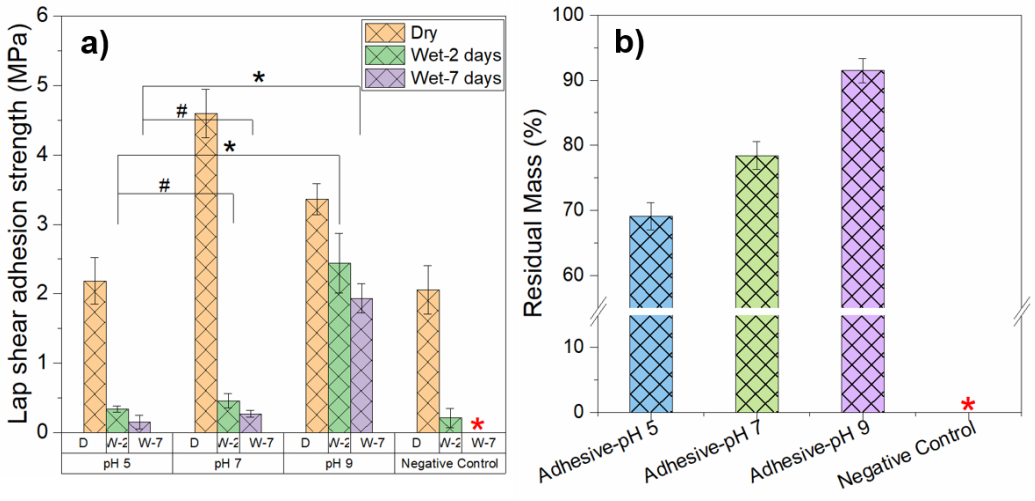

Figure 4.8 GDE treatment (5 wt%) and its effects on a) water-resistance properties; and b) hydrolysis solubility. (Red asterisk means no adhesion strength or specimens separated before testing or dissolved completely; Black asterisk indicates the statistical significance of $p < 0.001$, # indicates no significant difference between two samples)

To investigate the impact of GDE on cross-linking interactions, FT-IR analysis was performed. The anticipated epoxy-hydroxyl and epoxy-amine reactions were expected to show absorption band within the range of 1150-1050 cm^{-1}. The quantification of C-O (or C-N) groups, severing as an indicator of cross-linking, was carried out using curve-fitting technique (See details in Section 3.4.4) for ε-PL-TA adhesives with and without GDE at each pH value (Figure 4.9).

Without GDE treatment, the integrated area of C-O (or C-N) was observed to be approximately 15.5±0.8, 12.5±0.9, and 5.7±0.6 for ε-PL–TA adhesives at pH 5, 7, and 9, respectively. The decrease in integrated area with increasing pH can be attributed to the reduction in hydroxyl groups caused by catechol oxidation. Upon GDE treatment, a slight increase (20-40%) in the integrated area of C-O/C-N was observed for adhesives at pH 5, a moderate increase (40-70%) at pH 7, and a significant increase (100-120%) at pH 9. The larger increase in the integrated area at higher pH values suggests a higher number of newly formed C-O (or C-N) bonds, indicating enhanced cross-linking between GDE and ε-PL–TA adhesives.

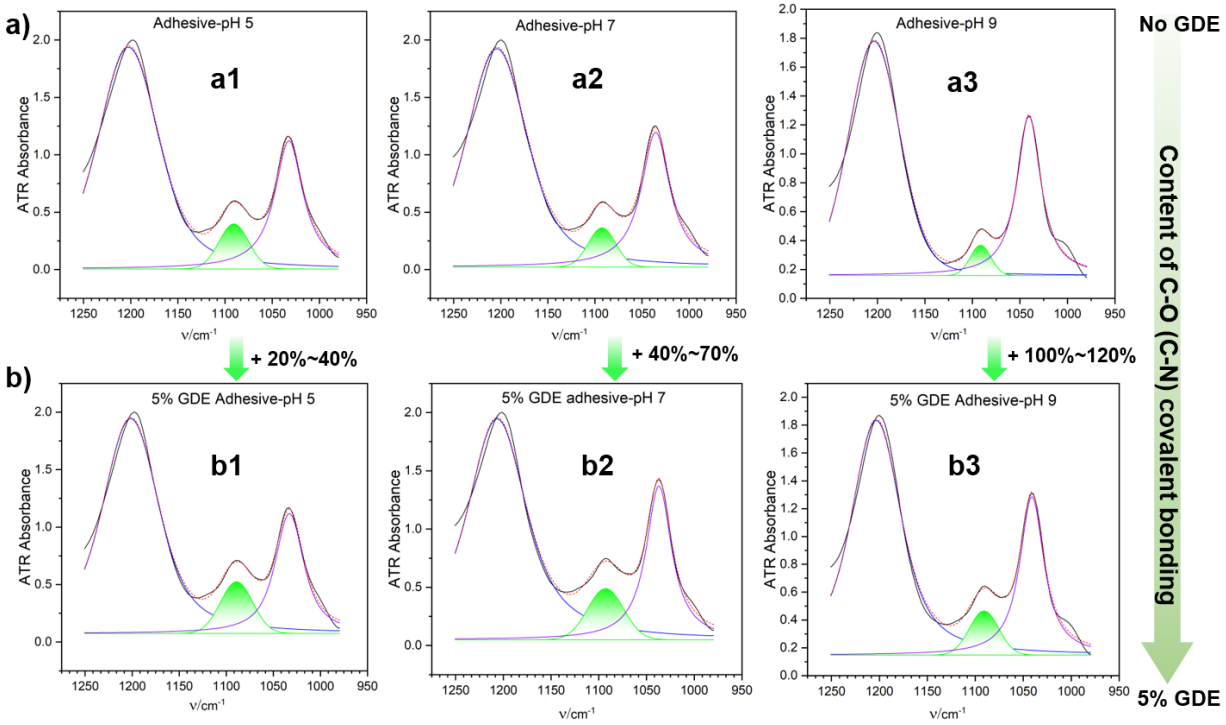

Figure 4.9 Quantification of C-O or C-N functional groups of the ε-PL–TA adhesives a) with GDE treatment and b) without GDE treatment. Normalization performed within the range of 1800-700 cm^{-1}; the highlight green area at 1150-1050 cm^{-1} indicated the C-O (or C-N) groups.

These findings suggest that the ε-PL–TA combination holds promise as a bio-based wet adhesive for commercial use, particularly due to its enhanced water resistance properties facilitated by the addition of a cross-linker. To summarize, the key conclusions of this study are as follows:

- Due to the impact of catechol oxidative coupling reactions, ε-PL–TA adhesives at higher pH exhibit a stronger wet adhesion.
- ε-PL–TA adhesives at pH 9 remain the adhesion strength only ~ 15% after 7-day immersion periods, which is probably attributed to the newly formed dynamic bonds (C=N).
- By introducing GDE, the double cross-linking through epoxide chemistry promotes the adhesion strength to significantly increase by ~55%.

4.3 Single-component ChiC candidate (Paper III)

ChiC polymers contain both catechol and amine functional groups, making them excellent candidate that fulfills two out of three desired requirements. If self-coacervation process occurs in ChiC, it is expected to form a single-component mussel-inspired coacervate, resembling Mfp-3 observed in mussels. The objective of this study was to investigate the properties of a phase-separated condensed material formed during ChiC complexation and explore its potential as an effective adhesive in wet environments.

To reach out ChiC complexation, two parameters were systematically studied: ionic strength and catechol content. The ionic strength of the ChiC solution ranged from 0.1 M to 2 M, while maintaining a pH value of 3.0. This design was chosen to mimic the conditions found in mussel adhesive plaques (pH ~ 3) and seawater (ionic strength of ~ 0.7 M). ChiC polymers with catechol contents ranging from 10% to 50% were synthesized, ensuring the water solubility and examining the impact of catechol contents.

Figure 4.10 provides insight into the phase behavior of ChiC as a function of NaCl concentration and catechol content. At low levels of salt and catechol, the ChiC solution remained homogeneous without phase separation. However, as the salt concentration and catechol content increased, phase separation took place. The initiation of phase separation required a minimum level of catechol in the presence of salt, with the exact amount of salt needed depending on the catechol content. Notably, ChiC materials with higher catechol contents and greater ionic strength exhibited increased hardness. These findings highlight the importance of both salt concentration and catechol content in determining the phase behavior of ChiC solutions, as well as influencing the properties of ChiC materials.

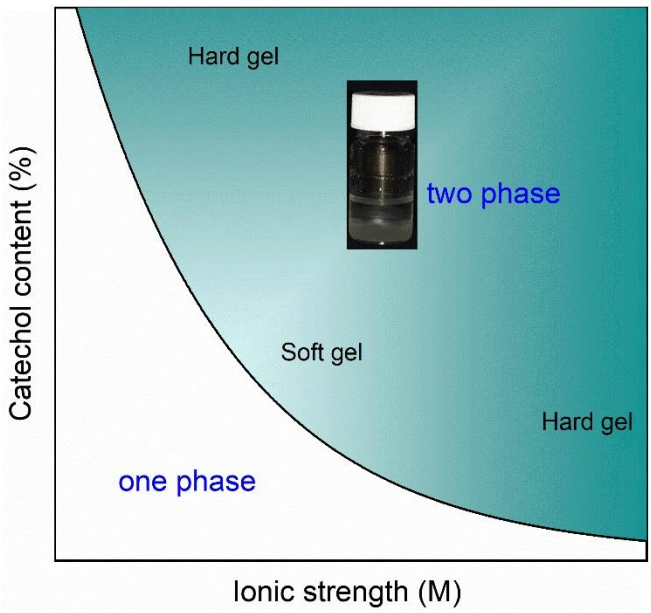

Figure 4.10 Phase behaviors of ChiC solutions as a function of salt and catechol.

The next step was to examine the adhesion properties of ChiC precipitates. The aim was to investigate how variations in salt and catechol content influenced the properties of the precipitates. Given the design of ChiC was inspired by mussel adhesives, the underwater adhesion performance was determined using tensile tack test (see experimental details in Section 3.4.2). Figure 4.11 illustrates the adhesion strength of ChiC precipitates with different catechol contents prepared using varying salt concentrations. These results demonstrated that the physical properties of the precipitates significantly impact their adhesion strength. The gel-like material represented by the blue bars exhibited higher adhesion properties, likely due to its ability to flow and establish good contact between the substrates. Conversely, the solid rubbery material represented by the pink bars had limited flow and contact area, resulting in reduced adhesion.

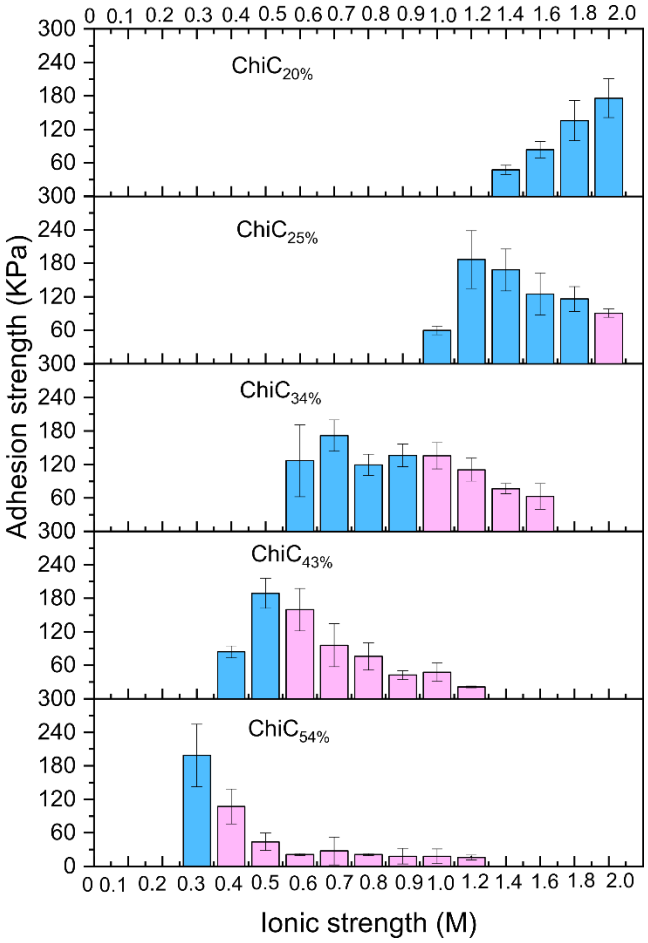

Figure 4.11 Underwater adhesion strength measured through a tack test, showcasing the influence of ionic strength and catechol content. The blue bars represent an injectable soft gel sample, while the pink bar represents a solid rubbery material. Data are presented as the average ± standard deviations based on 10 replicas.

So far, it has been demonstrated that controlling the catechol content and salt concentration enables ChiC precipitates to function as underwater adhesives. However, it is important to investigate the reasons behind the relatively low underwater adhesion and explore ways to enhance it further. One possible explanation for the relatively poor wet adhesion could be attributed to the presence of only the non-covalent molecular crosslinking among ChiC polymers. It is suggested that these non-covalent interactions are reversible in nature, they may not provide strong support for effective wet performance. Therefore, introducing covalent crosslinking interactions is expected to significantly reinforce the underwater adhesion strength.

Taking inspiration from mussel adhesion, the cross-linking approach involving catechol-amine coupling holds great potential. Previous reports have shown that catechol moieties can undergoing oxidative crosslinking in the presence of HRP and H_2O_2 when amine moieties are present. It is anticipated that ChiC adhesives can undergo oxidative crosslinking with HRP and H_2O_2 treatment under specific optimal conditions. For this purpose, $ChiC_{25\%}$ material prepared at 1.2 M ionic strength, chosen due to its favorable physical properties and maximal underwater adhesion strength, was used as a representative for further curing study.

Firstly, the curability of ChiC coacervate with and without HRP/H_2O_2 treatment was investigated using rheological techniques. The viscoelastic properties were measured in a strain-controlled oscillatory mode with a fixed frequency at 10 Hz. The storage modulus (G') and loss modulus (G") were recorded within a 2-minute time frame during the measurement, reflecting the elastic and viscous characteristics, respectively. G' was used to evaluate the gel strength of ChiC coacervate and its resistance to deformation. For example, the higher G' suggests the better gel strength. Typically, linear viscoelastic region (LVR) is used for elastic properties evaluation, as stress changes occur within this region without structural damage.[166]

Figure 4.12a-b illustrates the gel evolution of ChiC coacervates influenced by HRP/H_2O_2 treatment. To begin, ChiC coacervate with and without HRP/H_2O_2 treatment was placed onto the rheometer and then examined immediately. It was observed that G' and G" values were rather similar in the LVR (strain: 0.01%-1%), with G' being higher than G". These results suggest that ChiC coacervate treated by HRP/H_2O_2 exhibits a gel-like behavior similar to its original state. As the strain increased from 1% to 100%, the G' and G" values of ChiC coacervate without HRP/H_2O_2 treatment significantly decreased. In contrast, the G' and G" values of ChiC coacervate with HRP/H_2O_2 treatment followed a similar trend. One possible reason for this could be that the

measurement took ~ 2 minutes, allowing curability to initiate during the testing period. Thus, ChiC coacervate with HRP/H_2O_2 treatment exhibited slightly stronger resistance to deformation compared to its original state.

To further confirm the occurrence of curability, Figure 3b demonstrates the viscoelastic properties of ChiC coacervates with 15-minutes HRP/H_2O_2 treatment. It was observed that ChiC coacervate without HRP/H_2O_2 did not exhibit significant changes in G' and G" values. However, with HRP/H_2O_2 treatment, ChiC coacervate showed at least two times higher G' values, indicating that HRP/H_2O_2 can accelerate crosslinking and significantly improve the mechanical strength of the hydrogels.[167] Furthermore, with increasing strain from 10%-100%, a slight decrease in G' and G" values was noticed for ChiC coacervate with HRP/H_2O_2 treatment. This suggests that prolonged curing time may lead to a decrease in gel strength and reduced resistance to deformation.

Next, the resistance to deformation of ChiC coacervate with and without HRP/H_2O_2 treatment was investigated using a compression-release vision test. As depicted in Figure 4.12c, a visible color change from white to brown was observed in the HRP/H_2O_2-treated ChiC, indicating the occurrence of catechol oxidative crosslinking. It was also observed that the introduction of HRP/H_2O_2 enhanced the rigidity of ChiC coacervate, resulting in higher compression strength and improved resilience. These findings suggest that HRP/H_2O_2 curability can endow ChiC coacervate with a robust crosslinking network, potentially leading to an enhanced wet performance.

Figure 4.12d displays the wet adhesion strength of ChiC coacervates with and without HRP/H_2O_2 curing underwater. For a given curing time (15 minutes), it was observed that HRP/H_2O_2 curability significantly improved adhesion strength to ~ 550 kPa, nearly doubling the strength compared to ChiC coacervate without HRP/H_2O_2. Once again, it was found that curing time is also crucial in

wet adhesion strength. For example, ChiC coacervate without HRP/H_2O_2 did not exhibit significant changes in adhesion strength after only one-minute curing. All results suggest that ChiC coacervate with HRP/H_2O_2 treatment can facilitate catechol oxidative crosslinking and significantly enhance its wet adhesion strength after 15 minutes of curability.

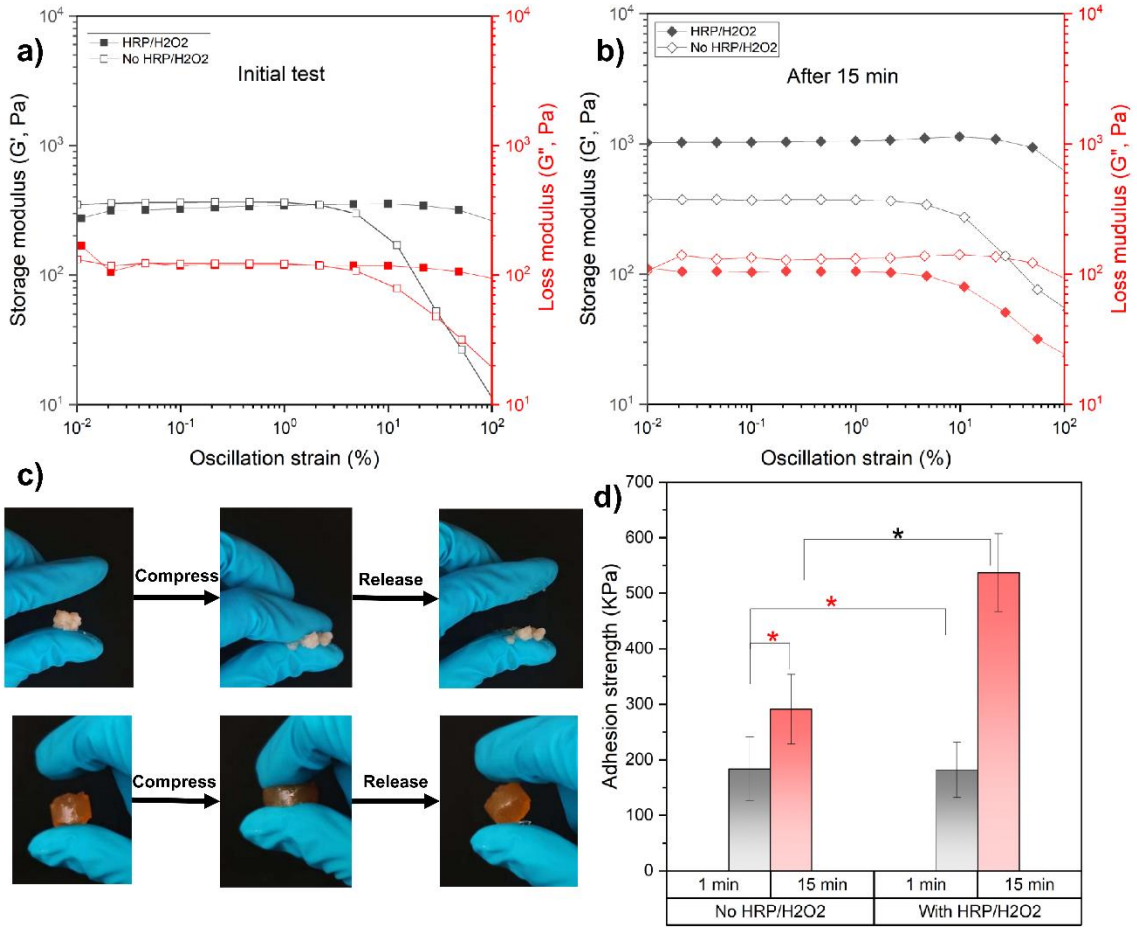

Figure 4.12 Rheological measurements of ChiC coacervates with or without HRP/H_2O_2 treatment tested a) initially or b) after 15-minutes curability. c) A vision compression-release figure test. d) Underwater tensile adhesion strength as a function of curing time with or without HRP/H_2O_2 treatment. Statistical analysis was performed and considered significant when $p^* < 0.001$, the red asterisk means no difference.

This study highlights the potential of ChiC precipitate as an effective underwater adhesive, especially when treated with HRP/H_2O_2 for curability. In summary, the key findings of this study are as follows:

- ChiC precipitates demonstrate adjustable physical and mechanical properties, which are influenced by catechol contents and ionic strength.
- With increasing ionic strength or catechol content, ChiC precipitates exhibit a hierarchical range of properties, transitioning from a watery state to an injectable state and finally to a solid state.
- Inspired by mussel adhesives, the use of curing chemistry holds great potential for significantly enhancing the underwater adhesion strength, increasing it from 200 to 600 kPa.

5. PERSPECTIVES

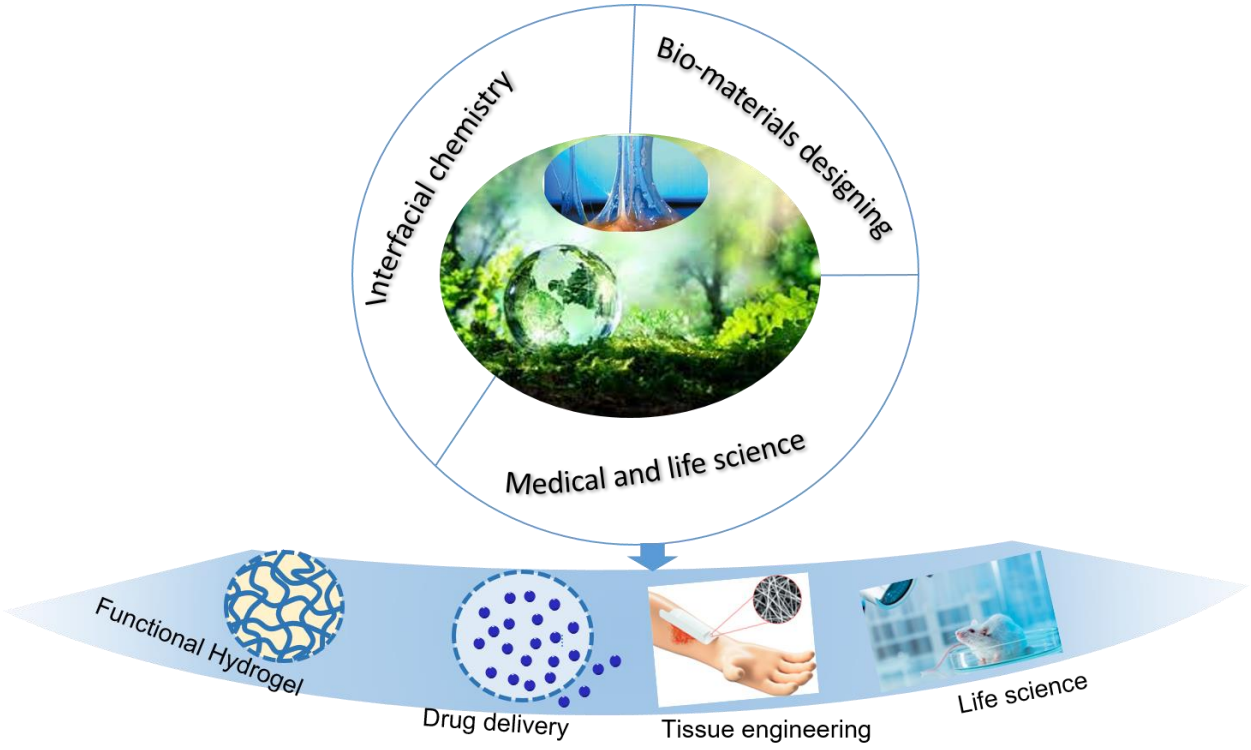

5. Perspectives

The perspectives of mussel-inspired wet adhesives offer numerous directions for further exploration. In addition to the three mechanisms already mimicked in bio-based adhesives, the coordination chemistry within mussel adhesive plaques remains an intriguing area of study. Specifically, the reversible interactions between proteins and metal ions (as discussed in Section 2.1.4.2), highlight the significance of coordination crosslinking in the extensibility of mussel adhesives.[168] It is therefore expected that mimicking this coordination chemistry could lead to the development of materials (i.e., hydrogel) with self-healing properties. By focusing on this aspect, one assumed that mimicking coordination chemistry could lead to the development of innovative materials with versatile functionalities.

Another perspective lies in the versatility of mussel-inspired adhesives. Researchers are continuously exploring new formulations and modifications to enhance their adhesive strength, durability, and versatility. By incorporating additional components, such as nanocomposites,[70,169,170] cross-linking agents,[171] or bioactive molecules,[172] researchers can tailor the adhesive properties to meet specific application requirements. For instance, the incorporation of nanoparticles can enhance the mechanical strength, adhesion, and stability of mussel-inspired adhesives. These nanocomposites can reinforce the adhesive matrix and provide additional functionalities, such as antimicrobial properties or controlled release of therapeutic agents.[173] Furthermore, the exploration of cross-linking agents can contribute to the development of adhesive systems with tunable properties. Cross-linking agents enable the control of adhesive strength, flexibility, and degradation rate, allowing for customized adhesive formulations suitable for different applications.[145] Incorporating bioactive molecules into mussel-inspired adhesives presents another avenue for future research. By doing this, one expect these adhesives can promote

tissue regeneration,[167,174,175] prevent infections,[44,176] or provide localized drug delivery capabilities.[117] Exploring new compounds, functionalities, and their interactions with substrates will pave the way for the development of advanced adhesive materials with improved performance and expanded applications.

In conclusion, the perspectives of mussel-inspired wet adhesives are highly promising, offering solutions for challenging adhesive scenarios, environmentally conscious applications, and versatile adhesive systems. Continued research and development in this field will undoubtedly lead to exciting advancements and practical implementations in the future.

6. REFERENCE

6. Reference

1. Lee, H., Scherer, N. F. & Messersmith, P. B. Single-molecule mechanics of mussel adhesion. *Proc. Natl. Acad. Sci. U. S. A.* **103**, 12999–13003 (2006).

2. ZajforoushanMoghaddam, S., Qie, R. & Thormann, E. Making Protein-Based Adhesives Water Resistant: Role of Protein Water Solubility, Galloyl Modification, and Complexation. *ACS Appl. Polym. Mater.* **0**, (2021).

3. Silverman, H. G. & Roberto, F. F. Understanding Marine Mussel Adhesion. *Mar. Biotechnol.* **9**, 661–681 (2007).

4. Waite, J. H. Mussel adhesion – essential footwork. *J. Exp. Biol.* **220**, 517–530 (2017).

5. Warner, S. C. & Waite, J. H. Expression of multiple forms of an adhesive plaque protein in an individual mussel, Mytilus edulis. *Mar. Biol. 1999 1344* **134**, 729–734 (1999).

6. Lee, B. P., Messersmith, P. B., Israelachvili, J. N. & Waite, J. H. Mussel-Inspired Adhesives and Coatings. *Annu. Rev. Mater. Res.* **41**, 99–132 (2011).

7. Silverman, H. G. & Roberto, F. F. Understanding marine mussel adhesion. *Mar. Biotechnol.* **9**, 661–681 (2007).

8. Lin, Q. *et al.* Adhesion mechanisms of the mussel foot proteins mfp-1 and mfp-3. *Proc. Natl. Acad. Sci. U. S. A.* **104**, 3782–3786 (2007).

9. Danner, E. W., Kan, Y., Hammer, M. U., Israelachvili, J. N. & Waite, J. H. Adhesion of mussel foot protein Mefp-5 to mica: An underwater superglue. *Biochemistry* **51**, 6511–6518 (2012).

10. Hwang, D. S. *et al.* Protein- and metal-dependent interactions of a prominent protein in mussel adhesive plaques. *J. Biol. Chem.* **285**, 25850–25858 (2010).

11. Hwang, D. S. *et al.* Protein- and Metal-dependent Interactions of a Prominent Protein in Mussel Adhesive Plaques. *J. Biol. Chem.* **285**, 25850 (2010).

12. Yu, J. *et al.* Mussel protein adhesion depends on interprotein thiol-mediated redox modulation. *Nat. Chem. Biol. 2011 79* **7**, 588–590 (2011).

13. Yu, J. Antioxidant is a Key Factor in Mussel Protein Adhesion. 31–41 (2014). doi:10.1007/978-3-319-06031-6_4

14. Zhao, H. & Waite, J. H. Linking Adhesive and Structural Proteins in the Attachment Plaque of Mytilus californianus. *J. Biol. Chem.* **281**, 26150–26158 (2006).

15. Wei, W. *et al.* A mussel-derived one component adhesive coacervate. *Acta Biomater.* **10**, 1663–1670 (2014).

16. Strathmann, H. & Kock, K. The formation mechanism of phase inversion membranes. *Desalination* **21**, 241–255 (1977).

17. Zhao, Q. *et al.* Underwater contact adhesion and microarchitecture in polyelectrolyte complexes actuated by solvent exchange. *Nat. Mater.* **15**, 407–412 (2016).

18. Li, S., Chen, J., Wang, J. & Zeng, H. Anti-biofouling materials and surfaces based on mussel-inspired chemistry. *Mater. Adv.* **2**, 2216–2230 (2021).

19. Li, L. & Zeng, H. Marine mussel adhesion and bio-inspired wet adhesives. *Biotribology* **5**, 44–51 (2016).

20. Yang, J., Stuart, M. A. C. & Kamperman, M. Jack of all trades: versatile catechol crosslinking mechanisms. *Chem. Soc. Rev.* **43**, 8271–8298 (2014).

21. Chen, J. & Zeng, H. Designing Bio-Inspired Wet Adhesives through Tunable Molecular Interactions. *J. Colloid Interface Sci.* **645**, 591–606 (2023).

22. Saiz-Poseu, J., Mancebo-Aracil, J., Nador, F., Busqué, F. & Ruiz-Molina, D. The Chemistry behind Catechol-Based Adhesion. *Angew. Chemie Int. Ed.* **58**, 696–714 (2019).

23. Yu, J., Wei, W., Danner, E., Israelachvili, J. N. & Waite, J. H. Effects of Interfacial Redox in Mussel Adhesive Protein Films on Mica. *Adv. Mater.* **23**, 2362–2366 (2011).

24. Anderson, T. H. *et al.* The Contribution of DOPA to Substrate–Peptide Adhesion and Internal Cohesion of Mussel-Inspired Synthetic Peptide Films. *Adv. Funct. Mater.* **20**, 4196–4205 (2010).

25. Ahn, B. K., Lee, D. W., Israelachvili, J. N. & Waite, J. H. Surface-initiated self-healing of polymers in aqueous media. *Nat. Mater. 2014 139* **13**, 867–872 (2014).

26. Yu, J., Wei, W., Danner, E., Israelachvili, J. N. & Waite, J. H. Effects of Interfacial Redox in Mussel Adhesive Protein Films on Mica. *Adv. Mater.* **23**, 2362–2366 (2011).

27. Kang, J. *et al.* Metal-Phenolic Networks Films: On-Site Surface Coordination Complexation via Mechanochemistry for Versatile Metal–Phenolic Networks Films (Adv. Mater. Interfaces 5/2019). *Adv. Mater. Interfaces* **6**, 1970031 (2019).

28. Stewart, R. J., Ransom, T. C. & Hlady, V. Natural underwater adhesives. *J. Polym. Sci. Part B Polym. Phys.* **49**, 757–771 (2011).

29. Zhu, H., Demirci, A., Liu, Y., Gong, J. & Mitsuishi, M. Robust, Reusable, and Antioxidative Supramolecular Adhesive to Inorganic Surfaces Based on Water-Stimulated Hydrogen Bonding. *ACS Appl. Polym. Mater.* (2022). doi:10.1021/ACSAPM.1C01353/SUPPL_FILE/AP1C01353_SI_001.PDF

30. Liu, Y., Meng, H., Messersmith, P. B., Lee, B. P. & Dalsin, J. L. Biomimetic adhesives and coatings based on mussel adhesive proteins. *Biol. Adhes. Second Ed.* 345–378 (2016). doi:10.1007/978-3-319-46082-6_15/FIGURES/9

31. Deng, J. H. *et al.* Π-π stacking interactions: Non-negligible forces for stabilizing porous supramolecular frameworks. *Sci. Adv.* **6**, (2020).

32. Shao, H. & Stewart, R. J. Biomimetic Underwater Adhesives with Environmentally Triggered Setting Mechanisms. doi:10.1002/adma.200902380

33. Barrett, D. G. *et al.* pH-Based Regulation of Hydrogel Mechanical Properties Through Mussel-Inspired Chemistry and Processing. *Adv. Funct. Mater.* **23**, 1111–1119 (2013).

34. Gallivan, J. P. & Dougherty, D. A. Cation-π interactions in structural biology. *Proc. Natl. Acad. Sci. U. S. A.* **96**, 9459–9464 (1999).

35. Crowley, P. B. & Golovin, A. Cation–π interactions in protein–protein interfaces. *Proteins Struct. Funct. Bioinforma.* **59**, 231–239 (2005).

36. Tiu, B. D. B., Delparastan, P., Ney, M. R., Gerst, M. & Messersmith, P. B. Cooperativity of Catechols and Amines in High-Performance Dry/Wet Adhesives. *Angew. Chemie Int. Ed.* **59**, 16616–16624 (2020).

37. Fan, H. *et al.* Adjacent cationic–aromatic sequences yield strong electrostatic adhesion of hydrogels in seawater. *Nat. Commun.* **10**, 1–8 (2019).

38. Shin, M. *et al.* The position of lysine controls the catechol-mediated surface adhesion and cohesion in underwater mussel adhesion. *J. Colloid Interface Sci.* **563**, 168–176 (2020).

39. Maier, G. P., Bernt, C. M. & Butler, A. Catechol oxidation: considerations in the design of wet adhesive materials. *Biomater. Sci.* **6**, 332–339 (2018).

40. Krogsgaard, M., Nue, V. & Birkedal, H. Mussel-Inspired Materials: Self-Healing through Coordination Chemistry. *Chem. – A Eur. J.* **22**, 844–857 (2016).

41. Singh, I., Dhawan, G., Gupta, S. & Kumar, P. Recent Advances in a Polydopamine-Mediated Antimicrobial Adhesion System. *Front. Microbiol.* **11**, 3326 (2021).

42. Pinnataip, R. & P. Lee, B. Oxidation Chemistry of Catechol Utilized in Designing Stimuli-Responsive Adhesives and Antipathogenic Biomaterials. *ACS Omega* **0**, (2021).

43. Na Lee, J., Yeon Lee, S. & Ho Park, W. Bioinspired Self-Healable Polyallylamine-Based Hydrogels for Wet Adhesion: Synergistic Contributions of Catechol-Amino Functionalities and Nanosilicate. *ACS Appl. Mater. Interfaces* **13**, 18324–18337 (2021).

44. Shin, M., Choi, J. H., Kim, K., Kim, S. & Lee, H. Hemostatic Needles: Controlling Hemostasis Time by a Catecholamine Oxidative Pathway. *ACS Appl. Mater. Interfaces* **13**, 10741–10747 (2021).

45. Maier, G. P., Rapp, M. V., Waite, J. H., Israelachvili, J. N. & Butler, A. Adaptive synergy between catechol and lysine promotes wet adhesion by surface salt displacement. *Science (80-.).* **349**, 628–632 (2015).

46. Maier, G. P., Rapp, M. V., Waite, J. H., Israelachvili, J. N. & Butler, A. Adaptive synergy between catechol and lysine promotes wet adhesion by surface salt displacement. *Science (80-.).* **349**, 628–632 (2015).

47. Mu, Y., Mu, P., Wu, X. & Wan, X. The two facets of the synergic effect of amine cation and catechol on the adhesion of catechol in underwater conditions. *Appl. Surf. Sci.* **530**, 146973 (2020).

48. Rapp, M. V. *et al.* Defining the Catechol-Cation Synergy for Enhanced Wet Adhesion to Mineral Surfaces. *J. Am. Chem. Soc.* **138**, 9013–9016 (2016).

49. Shin, M., Park, Y., Jin, S., Jung, Y. M. & Cha, H. J. Two Faces of Amine–Catechol Pair Synergy in Underwater Cation−π Interactions. *Chem. Mater.* **33**, 3196–3206 (2021).

50. Fischer, L. *et al.* Sequence-defined positioning of amine and amide residues to control catechol driven wet adhesion. *Chem. Sci.* **11**, 9919–9924 (2020).

51. Lsraelachvili Be, J. & Wennerstrom, H. Role of hydration and water structure in biological and colloidal interactions. *Nat.* · **379**, (1996).

52. Pashley, R. M. Hydration forces between mica surfaces in electrolyte solutions. *Adv. Colloid Interface Sci.* **16**, 57–62 (1982).

53. Yang, B., Lim, C., Hwang, D. S. & Cha, H. J. Switch of Surface Adhesion to Cohesion by Dopa-Fe3+ Complexation, in Response to Microenvironment at the Mussel Plaque/Substrate Interface. *Chem. Mater.* **28**, 7982–7989 (2016).

54. Yang, B. *et al.* Coacervation of Interfacial Adhesive Proteins for Initial Mussel Adhesion to a Wet Surface. *Small* **14**, 1803377 (2018).

55. Gucht, J. van der, Spruijt, E., Lemmers, M. & Cohen Stuart, M. A. Polyelectrolyte complexes: Bulk phases and colloidal systems. *J. Colloid Interface Sci.* **361**, 407–422 (2011).

56. Kim, H. J., Yang, B., Park, T. Y., Lim, S. & Cha, H. J. Complex coacervates based on recombinant mussel adhesive proteins: their characterization and applications. *Soft Matter* **13**, 7704–7716 (2017).

57. Perry, S. L. Phase separation: Bridging polymer physics and biology. *Curr. Opin. Colloid Interface Sci.* **39**, 86–97 (2019).

58. Stewart, R. J., Wang, C. S. & Shao, H. Complex coacervates as a foundation for synthetic underwater adhesives. *Adv. Colloid Interface Sci.* **167**, 85–93 (2011).

59. Narayanan, A., Menefee, J. R., Liu, Q., Dhinojwala, A. & Joy, A. Lower Critical Solution Temperature-Driven Self-Coacervation of Nonionic Polyester Underwater Adhesives.

ACS Nano **14**, 8359–8367 (2020).

60. Wei, W., Yu, J., Broomell, C., Israelachvili, J. N. & Waite, J. H. Hydrophobic enhancement of dopa-mediated adhesion in a mussel foot protein. *J. Am. Chem. Soc.* **135**, 377–383 (2013).

61. Nairm, J. G. *Coacervation-phase separation technology*. *Advances in Pharmaceutical Sciences* **7**, (1995).

62. Danielsen, S. P. O., McCarty, J., Shea, J. E., Delaney, K. T. & Fredrickson, G. H. Small ion effects on self-coacervation phenomena in block polyampholytes. *J. Chem. Phys.* **151**, 034904 (2019).

63. Wei, W., Yu, J., Broomell, C., Israelachvili, J. N. & Waite, J. H. Hydrophobic enhancement of dopa-mediated adhesion in a mussel foot protein. *J. Am. Chem. Soc.* **135**, 377–383 (2013).

64. Hwang, D. S. *et al.* Viscosity and interfacial properties in a mussel-inspired adhesive coacervate. *Soft Matter* **6**, 3232–3236 (2010).

65. Ahn, B. K. *et al.* High-performance mussel-inspired adhesives of reduced complexity. *Nat. Commun. 2015 61* **6**, 1–7 (2015).

66. Cui, M., Ren, S., Wei, S., Sun, C. & Zhong, C. Natural and bio-inspired underwater adhesives: Current progress and new perspectives. *APL Mater.* **5**, 116102 (2017).

67. Forooshani, P. K. & Lee, B. P. Recent approaches in designing bioadhesive materials inspired by mussel adhesive protein. *J. Polym. Sci. Part A Polym. Chem.* **55**, 9–33 (2017).

68. Yang, X. *et al.* Mussel-inspired structure evolution customizing membrane interface hydrophilization. *J. Memb. Sci.* **612**, (2020).

69. Hwang, D. S. *et al.* Protein- and metal-dependent interactions of a prominent protein in mussel adhesive plaques. *J. Biol. Chem.* **285**, 25850–25858 (2010).

70. Guo, Q., Chen, J., Wang, J., Zeng, H. & Yu, J. Recent progress in synthesis and application of mussel-inspired adhesives. *Nanoscale* **12**, 1307–1324 (2020).

71. Coombs, T. L. & Keller, P. J. Mytilus byssal threads as an environmental marker for

metals. *Aquat. Toxicol.* **1**, 291–300 (1981).

72. Guo, Q., Chen, J., Wang, J., Zeng, H. & Yu, J. Recent progress in synthesis and application of mussel-inspired adhesives. *Nanoscale* **12**, 1307–1324 (2020).

73. Holten-Andersen, N. *et al.* pH-induced metal-ligand cross-links inspired by mussel yield self-healing polymer networks with near-covalent elastic moduli. *Proc. Natl. Acad. Sci.* **108**, 2651–2655 (2011).

74. Harrington, M. J., Masic, A., Holten-Andersen, N., Waite, J. H. & Fratzl, P. Iron-clad fibers: A metal-based biological strategy for hard flexible coatings. *Science (80-.).* **328**, 216–220 (2010).

75. Zeng, H., Hwang, D. S., Israelachvili, J. N. & Waite, J. H. Strong reversible Fe3+-mediated bridging between dopa-containing protein films in water. *Proc. Natl. Acad. Sci. U. S. A.* **107**, 12850–12853 (2010).

76. Rodriguez, N. R. M., Das, S., Kaufman, Y., Israelachvili, J. N. & Waite, J. H. Interfacial pH during mussel adhesive plaque formation. *Biofouling* **31**, 221–227 (2015).

77. Sánchez-Ferrer, Á., Neptuno Rodríguez-López, J., García-Cánovas, F. & García-Carmona, F. Tyrosinase: a comprehensive review of its mechanism. *Biochim. Biophys. Acta - Protein Struct. Mol. Enzymol.* **1247**, 1–11 (1995).

78. Chan Choi, Y., Choi, J. S., Jung, Y. J. & Cho, Y. W. Human gelatin tissue-adhesive hydrogels prepared by enzyme-mediated biosynthesis of DOPA and Fe 3+ ion crosslinking. *J. Mater. Chem. B* **2**, 201–209 (2013).

79. Hou, J., Li, C., Guan, Y., Zhang, Y. & Zhu, X. X. Enzymatically crosslinked alginate hydrogels with improved adhesion properties. *Polym. Chem.* **6**, 2204–2213 (2015).

80. Seo, S. *et al.* Microphase Behavior and Enhanced Wet-Cohesion of Synthetic Copolyampholytes Inspired by a Mussel Foot Protein. *J. Am. Chem. Soc.* **137**, 9214–9217 (2015).

81. Ebnesajjad, S. Handbook of Biopolymers and Biodegradable Plastics: Properties, Processing and Applications. *Handb. Biopolym. Biodegrad. Plast. Prop. Process. Appl.* 1–

462 (2012). doi:10.1016/C2011-0-07342-8

82. Burchardt, B. 3 - Advances in polyurethane structural adhesives. in *Woodhead Publishing in Materials* (ed. Dillard, D. A. B. T.-A. in S. A. B.) 35–65 (Woodhead Publishing, 2010). doi:https://doi.org/10.1533/9781845698058.1.35

83. Balkenende, D. W. R., Olson, R. A., Balog, S., Weder, C. & Montero de Espinosa, L. Epoxy Resin-Inspired Reconfigurable Supramolecular Networks. *Macromolecules* **49**, 7877–7885 (2016).

84. Abbey, K. J. 2 - Advances in epoxy adhesives. in *Woodhead Publishing in Materials* (ed. Dillard, D. A. B. T.-A. in S. A. B.) 20–34 (Woodhead Publishing, 2010). doi:https://doi.org/10.1533/9781845698058.1.20

85. White, C., Tan, K., Wolf, A. & Carbary, L. 4 - Advances in structural silicone adhesives. in *Woodhead Publishing in Materials* (ed. Dillard, D. A. B. T.-A. in S. A. B.) 66–95 (Woodhead Publishing, 2010). doi:https://doi.org/10.1533/9781845698058.1.66

86. Klemarczyk, P. & Guthrie, J. 5 - Advances in anaerobic and cyanoacrylate adhesives. in *Woodhead Publishing in Materials* (ed. Dillard, D. A. B. T.-A. in S. A. B.) 96–131 (Woodhead Publishing, 2010). doi:https://doi.org/10.1533/9781845698058.1.96

87. Briggs, P. C. & Jialanella, G. L. 6 - Advances in acrylic structural adhesives. in *Woodhead Publishing in Materials* (ed. Dillard, D. A. B. T.-A. in S. A. B.) 132–150 (Woodhead Publishing, 2010). doi:https://doi.org/10.1533/9781845698058.1.132

88. Zhu, Y., Romain, C. & Williams, C. K. Sustainable polymers from renewable resources. *Nat. 2016 5407633* **540**, 354–362 (2016).

89. Heinrich, L. A. Future opportunities for bio-based adhesives – advantages beyond renewability. *Green Chem.* **21**, 1866–1888 (2019).

90. Suárez, J. C. Bioadhesives. *Handb. Adhes. Technol.* 1385–1408 (2011). doi:10.1007/978-3-642-01169-6_53

91. Mathias, J. D., Grédiac, M. & Michaud, P. Bio-based adhesives. *Biopolym. Biotech Admixtures Eco-Efficient Constr. Mater.* 369–385 (2016). doi:10.1016/B978-0-08-

100214-8.00016-6

92. Li, J. *et al.* Emerging Biopolymer-Based Bioadhesives. *Macromol. Biosci.* **22**, 2100340 (2022).

93. Lutz, T. M., Kimna, C., Casini, A. & Lieleg, O. Bio-based and bio-inspired adhesives from animals and plants for biomedical applications. *Mater. Today Bio* **13**, 100203 (2022).

94. Islam, M. N., Rahman, F., Das, A. K. & Hiziroglu, S. An overview of different types and potential of bio-based adhesives used for wood products. *Int. J. Adhes. Adhes.* **112**, 102992 (2022).

95. Ma, S., Li, T., Liu, X. & Zhu, J. Research progress on bio-based thermosetting resins. *Polym. Int.* **65**, 164–173 (2016).

96. Jenkins, C. L., Siebert, H. M. & Wilker, J. J. Integrating Mussel Chemistry into a Bio-Based Polymer to Create Degradable Adhesives. *Macromolecules* **50**, 561–568 (2017).

97. Gowda, A. H. J. *et al.* Design of tunable gelatin-dopamine based bioadhesives. *Int. J. Biol. Macromol.* **164**, 1384–1391 (2020).

98. Hou, J., Li, C., Guan, Y., Zhang, Y. & Zhu, X. X. Enzymatically crosslinked alginate hydrogels with improved adhesion properties. *Polym. Chem.* **6**, 2204–2213 (2015).

99. Kim, K., Kim, K., Ryu, J. H. & Lee, H. Chitosan-catechol: A polymer with long-lasting mucoadhesive properties. *Biomaterials* **52**, 161–170 (2015).

100. Cui, C. *et al.* Water-Triggered Hyperbranched Polymer Universal Adhesives: From Strong Underwater Adhesion to Rapid Sealing Hemostasis. *Adv. Mater.* **31**, 1905761 (2019).

101. S. Yavvari, P. & Aasheesh Srivastava. Robust, self-healing hydrogels synthesised from catechol rich polymers. *J. Mater. Chem. B* **3**, 899–910 (2015).

102. Ryu, J. H., Hong, S. & Lee, H. Bio-inspired adhesive catechol-conjugated chitosan for biomedical applications: A mini review. (2015). doi:10.1016/j.actbio.2015.08.043

103. Ma, S., Wu, Y. & Zhou, F. Bioinspired synthetic wet adhesives: from permanent bonding to reversible regulation. *Curr. Opin. Colloid Interface Sci.* **47**, 84–98 (2020).

104. Gowda, A. H. J. *et al.* Design of tunable gelatin-dopamine based bioadhesives. *Int. J. Biol. Macromol.* **164**, 1384–1391 (2020).

105. Schmidt, G., Hamaker, B. R. & Wilker, J. J. High Strength Adhesives from Catechol Cross-Linking of Zein Protein and Plant Phenolics. *Adv. Sustain. Syst.* **2**, 1700159 (2018).

106. Wang, Z. *et al.* The synergy between natural polyphenol-inspired catechol moieties and plant protein-derived bio-adhesive enhances the wet bonding strength. *Sci. Reports 2017 71* **7**, 1–10 (2017).

107. Kang, S. M. *et al.* One-Step Multipurpose Surface Functionalization by Adhesive Catecholamine. *Adv. Funct. Mater.* **22**, 2949–2955 (2012).

108. Shin, M., Choi, J. H., Kim, K., Kim, S. & Lee, H. Hemostatic Needles: Controlling Hemostasis Time by a Catecholamine Oxidative Pathway. *Cite This ACS Appl. Mater. Interfaces* **13**, 10741–10747 (2021).

109. Hong, S., Wang, Y., Park, S. Y. & Lee, H. Progressive fuzzy cation- assembly of biological catecholamines. *Sci. Adv.* **4**, 7457–7464 (2018).

110. Wang, Z. *et al.* Facile biomimetic self-coacervation of tannic acid and polycation: Tough and wide pH range of underwater adhesives. *Chem. Eng. J.* **404**, 127069 (2021).

111. Lee, D. *et al.* VATA: A Poly(vinyl alcohol)-and Tannic Acid-Based Nontoxic Underwater Adhesive. *Cite This ACS Appl. Mater. Interfaces* **12**, (2020).

112. Du, X. *et al.* UV-Triggered Dopamine Polymerization: Control of Polymerization, Surface Coating, and Photopatterning. *Adv. Mater.* **26**, 8029–8033 (2014).

113. Behboodi-Sadabad, F. *et al.* UV-Triggered Polymerization, Deposition, and Patterning of Plant Phenolic Compounds. *Adv. Funct. Mater.* **27**, 1700127 (2017).

114. Paez, J. I. *et al.* Gauging and Tuning Cross-Linking Kinetics of Catechol-PEG Adhesives via Catecholamine Functionalization. *Biomacromolecules* **16**, 3811–3818 (2015).

115. Sugumaran, M. Reactivities of Quinone Methides versus o-Quinones in Catecholamine Metabolism and Eumelanin Biosynthesis. *Int. J. Mol. Sci. 2016, Vol. 17, Page 1576* **17**, 1576 (2016).

116. Ganesh, K., Jung, J., Woo Park, J., Kim, B. S. & Seo, S. Effect of Substituents in Mussel-inspired Surface Primers on their Oxidation and Priming Efficiency. *ChemistryOpen* **10**, 852–859 (2021).

117. Hauser, D., Septiadi, D., Turner, J., Petri-Fink, A. & Rothen-Rutishauser, B. From Bioinspired Glue to Medicine: Polydopamine as a Biomedical Material. *Mater. 2020, Vol. 13, Page 1730* **13**, 1730 (2020).

118. Hong, Y. *et al.* A strongly adhesive hemostatic hydrogel for the repair of arterial and heart bleeds. *Nat. Commun. 2019 101* **10**, 1–11 (2019).

119. Cencer, M. *et al.* Effect of pH on the rate of curing and bioadhesive properties of dopamine functionalized poly(ethylene glycol) hydrogels. *Biomacromolecules* **15**, 2861–2869 (2014).

120. Narkar, A. R., D. Kelley, J., Pinnaratip, R. & P. Lee, B. Effect of Ionic Functional Groups on the Oxidation State and Interfacial Binding Property of Catechol-Based Adhesive. *Biomacromolecules* **19**, 1416–1424 (2017).

121. Zhang, X., Liu, H., Yue, L., Bai, Y. & He, J. Mussel-mimetic polymer underwater adhesives with l-Dopa functionality: influencing adhesion properties and simplified operation procedures. *J. Mater. Sci.* **55**, 7981–7997 (2020).

122. Wang, Z. *et al.* Facile biomimetic self-coacervation of tannic acid and polycation: Tough and wide pH range of underwater adhesives. *Chem. Eng. J.* **404**, 127069 (2021).

123. Tang, Z. *et al.* Mussel-inspired cellulose-based adhesive with biocompatibility and strong mechanical strength via metal coordination. *Int. J. Biol. Macromol.* **144**, 127–134 (2020).

124. Li, S. *et al.* Metal-crosslinked ε-poly-L-lysine tissue adhesives with high adhesive performance: Inspiration from mussel adhesive environment. *Int. J. Biol. Macromol.* **153**, 1251–1261 (2020).

125. Yu, M., Hwang, J. & Deming, T. J. Role of 1-3,4-dihydroxyphenylalanine in mussel adhesive proteins. *J. Am. Chem. Soc.* **121**, 5825–5826 (1999).

126. Yavvari, P. S. & Srivastava, A. Robust, self-healing hydrogels synthesised from catechol

rich polymers. *J. Mater. Chem. B* **3**, 899–910 (2015).

127. Matos-Pérez, C. R., White, J. D. & Wilker, J. J. Polymer composition and substrate influences on the adhesive bonding of a biomimetic, cross-linking polymer. *J. Am. Chem. Soc.* **134**, 9498–9505 (2012).

128. Tian, M. *et al.* Long-term and oxidative-responsive alginate-deferoxamine conjugates with a low toxicity for iron overload. *RSC Adv.* **6**, 32471–32479 (2016).

129. Meng, H., Liu, Y. & Lee, B. P. Model polymer system for investigating the generation of hydrogen peroxide and its biological responses during the crosslinking of mussel adhesive moiety. *Acta Biomater.* **48**, 144–156 (2017).

130. Lee, B. P., Dalsin, J. L. & Messersmith, P. B. Synthesis and gelation of DOPA-modified poly(ethylene glycol) hydrogels. *Biomacromolecules* **3**, 1038–1047 (2002).

131. Wang, R. *et al.* A Biomimetic Mussel-Inspired ε-Poly-l-lysine Hydrogel with Robust Tissue-Anchor and Anti-Infection Capacity. *Adv. Funct. Mater.* **27**, 1604894 (2017).

132. Pradyawong, S., Qi, G., Sun, X. S. & Wang, D. Laccase/TEMPO-modified lignin improved soy-protein-based adhesives: Adhesion performance and properties. *Int. J. Adhes. Adhes.* **91**, 116–122 (2019).

133. Seo, S. Y., Sharma, V. K. & Sharma, N. Mushroom tyrosinase: Recent prospects. *J. Agric. Food Chem.* **51**, 2837–2853 (2003).

134. Choi, S., Ahn, H. & Kim, S. H. Tyrosinase-mediated hydrogel crosslinking for tissue engineering. *J. Appl. Polym. Sci.* **139**, 51887 (2022).

135. Nakayama, Y. & Matsuda, T. Photocurable Surgical Tissue Adhesive Glues Composed of Photoreactive Gelatin and Poly(ethylene glycol) Diacrylate. (1999). doi:10.1002/(SICI)1097-4636(1999)48:4

136. Schmidt, G. *et al.* Strong Adhesives from Corn Protein and Tannic Acid. *Adv. Sustain. Syst.* **3**, 1900077 (2019).

137. Zhao, Q. *et al.* Tannin-Tethered Gelatin Hydrogels with Considerable Self-Healing and Adhesive Performances. *Macromol. Mater. Eng.* **304**, 1800664 (2019).

138. Liu, S. *et al.* H2O2-mediated tannin bio-based wood adhesive inspired by starfish structure and phenol-amine synergy. *Ind. Crops Prod.* **188**, 115714 (2022).

139. Yamada, K. *et al.* Chitosan based water-resistant adhesive. Analogy to mussel glue. *Biomacromolecules* **1**, 252–258 (2000).

140. Cordes, E. H., Jencks, W. P., Cordes, E. H. & Jencks, W. P. On the Mechanism of Schiff Base Formation and Hydrolysis1.

141. Pan, W. *et al.* Facile formation of injectable quaternized chitosan/tannic acid hydrogels with antibacterial and ROS scavenging capabilities for diabetic wound healing. *Int. J. Biol. Macromol.* **195**, 190–197 (2022).

142. Shao, Z. *et al.* Wound microenvironment self-adaptive hydrogel with efficient angiogenesis for promoting diabetic wound healing. *Bioact. Mater.* **20**, 561–573 (2023).

143. Fischer, M. J. E. Amine coupling through EDC/NHS: a practical approach. *Methods Mol. Biol.* **627**, 55–73 (2010).

144. Sahatsapan, N., Ngawhirunpat, T., Rojanarata, T., Opanasopit, P. & Patrojanasophon, P. Catechol-Functionalized Alginate Nanoparticles as Mucoadhesive Carriers for Intravesical Chemotherapy. *AAPS PharmSciTech* **21**, 1–9 (2020).

145. Lee, C. *et al.* Bioinspired, calcium-free alginate hydrogels with tunable physical and mechanical properties and improved biocompatibility. *Biomacromolecules* **14**, 2004–2013 (2013).

146. Lórenz-Fonfría, V. íctor A. & Padrós, E. Curve-fitting of Fourier manipulated spectra comprising apodization, smoothing, derivation and deconvolution. *Spectrochim. Acta Part A Mol. Biomol. Spectrosc.* **60**, 2703–2710 (2004).

147. Fan, R., Yang, X., Drury, C. F. & Zhang, Z. Curve-fitting techniques improve the mid-infrared analysis of soil organic carbon: a case study for Brookston clay loam particle-size fractions. *Sci. Reports 2018 81* **8**, 1–10 (2018).

148. Wang, L., Khor, E., Wee, A. & Lim, L. Y. Chitosan-alginate PEC membrane as a wound dressing: Assessment of incisional wound healing. *J. Biomed. Mater. Res.* **63**, 610–618

(2002).

149. Buriuli, M. & Verma, D. Polyelectrolyte complexes (PECs) for biomedical applications. *Adv. Struct. Mater.* **66**, 45–93 (2017).

150. Wang, S. *et al.* Preparation, in vitro and in vivo evaluation of chitosan-sodium alginate-ethyl cellulose polyelectrolyte film as a novel buccal mucosal delivery vehicle. *Eur. J. Pharm. Sci.* **168**, 106085 (2022).

151. Voinova, M. V, Rodahl, M., Jonson, M. & Kasemo, B. Viscoelastic Acoustic Response of Layered Polymer Films at Fluid-Solid Interfaces: Continuum Mechanics Approach. *Phys. Scr.* **59**, 391–396 (1999).

152. Fan, H. *et al.* Adjacent cationic–aromatic sequences yield strong electrostatic adhesion of hydrogels in seawater. *Nat. Commun. 2019 101* **10**, 1–8 (2019).

153. Mahadevi, A. S. & Sastry, G. N. Cation-π interaction: Its role and relevance in chemistry, biology, and material science. *Chem. Rev.* **113**, 2100–2138 (2013).

154. Clegg, J. R., Ludolph, C. M. & Peppas, N. A. QCM-D assay for quantifying the swelling, biodegradation, and protein adsorption of intelligent nanogels. *J. Appl. Polym. Sci.* **137**, 48655 (2020).

155. An, J., Dèdinaitè, A., Winnik, F. M., Qiu, X. P. & Claesson, P. M. Temperature-dependent adsorption and adsorption hysteresis of a thermoresponsive diblock copolymer. *Langmuir* **30**, 4333–4341 (2014).

156. Guo, L. *et al.* pH-induced structural transition during complexation and precipitation of sodium caseinate and ε-Poly-l-lysine. *Int. J. Biol. Macromol.* **154**, 644–653 (2020).

157. He, Z. *et al.* Sustained release of exendin-4 from tannic acid/Fe (III) nanoparticles prolongs blood glycemic control in a mouse model of type II diabetes. *J. Control. Release* **301**, 119–128 (2019).

158. Li, K. *et al.* Biomimetic development of a strong, mildew-resistant soy protein adhesive via mineral–organic system and phenol-amine synergy. *Ind. Crops Prod.* **187**, 115412 (2022).

159. Yang, J., Saggiomo, V., Velders, A. H., Stuart, M. A. C. & Kamperman, M. Reaction Pathways in Catechol/Primary Amine Mixtures: A Window on Crosslinking Chemistry. *PLoS One* **11**, e0166490 (2016).

160. Xin, Y. & Yuan, J. Schiff's base as a stimuli-responsive linker in polymer chemistry. doi:10.1039/c2py20290e

161. Chen, X. *et al.* Preparation and properties of a novel type of tannin-based wood adhesive. *https://doi.org/10.1080/00218464.2020.1863215* (2020). doi:10.1080/00218464.2020.1863215

162. urRehman, S., Sahiner, M., Sel, K., Siddiq, M. & Sahiner, N. Synthesis and characterization of new microgel from tris(2-aminoethyl)amine and glycerol diglycidyl ether as poly(TAEA-co-GDE). *Colloids Surfaces B Biointerfaces* **136**, 1156–1165 (2015).

163. Shechter, L. & Wynstra, J. Glycidyl Ether Reactions with Alcohols, Phenols, Carboxylic Acids, and Acid Anhydrides. *Ind. Eng. Chem.* **48**, 86–93 (2002).

164. Stropoli, S. J. & Elrod, M. J. Assessing the Potential for the Reactions of Epoxides with Amines on Secondary Organic Aerosol Particles. *J. Phys. Chem. A* **119**, 10181–10189 (2015).

165. Azizi, N. & Saidi, M. R. Highly chemoselective addition of amines to epoxides in water. *Org. Lett.* **7**, 3649–3651 (2005).

166. Hasanvand, E. & Rafe, A. Rheological and structural properties of rice bran protein-flaxseed (Linum usitatissimum L.) gum complex coacervates. *Food Hydrocoll.* **83**, 296–307 (2018).

167. Huang, W. *et al.* Noncompressible Hemostasis and Bone Regeneration Induced by an Absorbable Bioadhesive Self-Healing Hydrogel. *Adv. Funct. Mater.* 2009189 (2021). doi:10.1002/adfm.202009189

168. Birkedal, H. & Chen, Y. Mussel inspired self-healing materials: Coordination chemistry of polyphenols. *Adv. Inorg. Chem.* **76**, 269–298 (2020).

169. Hu, J. *et al.* Effect of interfacial interaction between graphene oxide derivatives and

poly(vinyl chloride) upon the mechanical properties of their nanocomposites. *J. Mater. Sci.* **49**, 2943–2951 (2014).

170. Na Lee, J., Yeon Lee, S. & Ho Park, W. Bioinspired Self-Healable Polyallylamine-Based Hydrogels for Wet Adhesion: Synergistic Contributions of Catechol-Amino Functionalities and Nanosilicate. *Cite This ACS Appl. Mater. Interfaces* **13**, 18324–18337 (2021).

171. Silverman, H. G. & Roberto, F. F. Review Understanding Marine Mussel Adhesion. doi:10.1007/s10126-007-9053-x

172. Xu, J. *et al.* Supramolecular Copolymerization of Short Peptides and Polyoxometalates: Toward the Fabrication of Underwater Adhesives. *Biomacromolecules* **18**, 3524–3530 (2017).

173. Zhang, M. *et al.* Mussel-inspired nanocomposite hydrogel based on alginate and antimicrobial peptide for infected wound repair. *Int. J. Biol. Macromol.* **219**, 1087–1099 (2022).

174. Shi, D. *et al.* Preparation and properties of dopamine-modified alginate/chitosan–hydroxyapatite scaffolds with gradient structure for bone tissue engineering. *J. Biomed. Mater. Res. - Part A* **107**, 1615–1627 (2019).

175. Costa, R. R., Soares da Costa, D., Reis, R. L. & Pashkuleva, I. Bioinspired baroplastic glycosaminoglycan sealants for soft tissues. *Acta Biomater.* **87**, 108–117 (2019).

176. Haseeb, M. *et al.* Effect of the Buffer on the Buildup and Stability of Tannic Acid/ Collagen Multilayer Films Applied as Antibacterial Coatings. *Cite This ACS Appl. Mater. Interfaces* **12**, (2020).

PAPER I

Self-cross-linkable Chitosan-Alginate Complexes Inspired by the Mussel Glue Chemistry

Journal:	*Langmuir*
Manuscript ID	la-2023-01750e
Manuscript Type:	Article
Date Submitted by the Author:	26-Jun-2023
Complete List of Authors:	Kang, Junjie; Technical University of Denmark, chemistry Zajforoushan Moghaddam, Saeed; Danmarks Tekniske Universitet, Department of Chemistry Thormann, Esben; Danmarks Tekniske Universitet, Department of Chemistry

Self-cross-linkable Chitosan-Alginate Complexes Inspired by the Mussel Glue Chemistry

Junjie Kang, Saeed Zajforoushan Moghaddam, Esben Thormann*

Department of Chemistry, Technical University of Denmark, 2800 Kgs. Lyngby, Denmark

*esth@kemi.dtu.dk

Abstract: In this study, a mussel-inspired chemistry, based on catechol–amine reactions, was adopted to develop self-cross-linkable chitosan–alginate (Chi–Alg) complexes. To do so, the biopolymers were each substituted with ~20% catechol groups (ChiC and AlgC), then four complex combinations (Chi–Alg, ChiC–Alg, Chi–AlgC, ChiC–AlgC) were prepared at surface and in bulk solution. Based on QCM-D and lap shear adhesion tests, the complex with catechol only on Chi (ChiC–Alg) did not show a significant variation from the control complex (Chi–Alg). Conversely, the complexes with catechol on alginate (Chi–AlgC and ChiC–AlgC) rendered a self-crosslinking property and enhanced cohesive properties.

Keywords: bio-inspired, polyelectrolyte complexation, chitosan, alginate, catechol

1. Introduction

Chitosan–Alginate (Chi–Alg) polyelectrolyte complexes have been investigated in various fields including biomedical and pharmaceutical applications.[1–3] These materials can be prepared in various forms including coatings,[4] vesicles,[3] scaffolds,[5,6] and nanofibers.[6,7] Aside from biocompatibility/biodegradability aspects, the preparation of such complexes is relatively straightforward, mainly requiring the control of pH and ionic strength.[8–10]

The stability of Chi–Alg complexes in response to pH and salinity of the environment is of importance in many applications.[11–14] In the complexed state, these oppositely charged weak biopolyelectrolytes are held together mainly by electrostatic interactions; hence, variations in pH and salinity perturb the charge balance and produce swelling/dissociation.[9] This inherent feature has been used to develop pH-responsive materials, e.g., vesicles releasing the encapsulated agent.[14–16] In many other systems though, one requires the complex to be stable against variations in pH and salt.[17–20] Herein, various chemical modifications are suggested to covalently cross-link the biopolymers, by post-modification of the complex through EDC/NHS coupling,[17] or using a cross-linker such as glutaraldehyde.[19] Such methods may not be always favorable considering the need for an extra post-modification step, as well as safety concerns over using volatile toxic reagents. Alternatively, the biopolymers can be chemically modified allowing self-cross-linking. In a previous study, we found that periodate oxidation of Alg, yielding Alg dialdehyde, enables preparing Chi–Alg complexes with tunable self-cross-linking and enhanced pH stability at elevated pH.[21–23] Despite the high efficiency of this approach, periodate oxidation is a rather rigorous chemical treatment whereby the biopolymer properties such as molecular weight can significantly vary.[24,25]

Sticky marine organisms, e.g., mussels, can be a source of inspiration for designing biopolymeric systems with novel functionalities.[26–29] Herein, various biomacromolecules are combined under a controlled acidic environment (pH~3-5), and the resulting multicomponent glue is then cured by exposure to the seawater (pH~8.1).[30] It is suggested that catechol–amine interactions play a critical role, in particular in the curing stage. The increased pH results in catechol oxidation to quinone, which can form covalent bonds with amines via Michael addition and Schiff base reactions.[31,32] Subsequently, the mussel glue cross-links and solidifies to provide a durable adhesive bond.

In this study, we investigated a mussel-inspired amine–catechol chemistry to develop self-cross-linkable Chi–Alg complexes. To do so, Chi and Alg were each substituted with a catechol content of ~20% (ChiC and AlgC), so they could (i) remain highly charged (ii) yet able to form catechol–amine interactions. Then, four complex combinations, i.e., Chi–Alg, ChiC–AlgC, Chi–AlgC, and ChiC–AlgC, were prepared at surface and in bulk solution, and their self-cross-linking and pH stability were examined.

2. Experimental Section

Materials: chitosan (degree of deacetylation ≥ 95%, viscosity 5 cps) was purchased from Heppe Medical Chitosan GmbH, Germany. Sodium Alginate (medium viscosity), Dopamine hydrochloride acid (DA·HCl, ≥ 98%), 3, 4-Dihydroxybenzaldehyde (DHBA, ≥ 97%), 3-glycidoxypropyltrimethoxysilan (GOPS, ≥ 98%), 1-ethyl-3-(3-dimethylaminopropyl)-carbodiimide hydrochloride (EDC, ≥ 98%), and N-hydroxysulfosuccinimide (NHS, ≥ 98%) were purchased from Sigma-Aldrich and used as received unless otherwise stated. Degassed ultrapure water (Arium® Pro) with a resistivity of 18.2 MΩ cm was used to prepare all solutions. All the solvents used in this study were HPLC grade from Sigma-Aldrich.

Synthesis: 2 g Chi (~13 mmol of repeating units) was added to 140 ml of 1 v/v% acetic acid solution. After stirring overnight, the pH was adjusted to 4.5 with the addition of 1 M HCl solution. 0.32 g DHBA was dissolved in a mixture of 40 ml water and 20 ml methanol, followed by adjusting pH to 4.5. The DHBA solution was then added to the Chi solution. The pH of the reaction solution was measured every 15 min and readjusted to 4.5. After 1 h, an excess amount of solid $NaCNBH_3$ (2 g) was gradually (in 15 min) added to the reaction solution and left stirring for 4 h. The product was then precipitated by adjusting the pH to 6.5. The supernatant phase was removed, followed by the addition of 50 ml HCl solution (pH 2) to re-dissolve the product. The resultant solution was then dialyzed (regenerated cellulose dialysis membrane, MWCO: 3.5 kDa) against HCl solution (pH 3.0-3.5) for 48 h (for the first 8 h, HCl solution was exchanged every 2 h). After 48 h, the solution was dialyzed against water for 4 h to remove HCl. The pH of the dialyzed polymer solution was then adjusted to 6.5 and the precipitated material was collected by centrifugation (6500 rpm, 5 min). Finally, around 1.5 g of dried ChiC powder was yielded via lyophilization.

2.0 g Alg (~10 mmol of repeating unit) was added to 200 ml water and stirred overnight to fully dissolve, followed by pH adjustment to 4.5 using 1 M HCl solution. 1.2 g EDC and 2.0 g NHS were step-wise added to the above solution. After 30 min, 2.0 g DA·HCl was added to the solution (1:1 molar ratio between DA·HCl and Alg). The reaction was conducted at room temperature overnight (pH remained at ~4.5). The reaction mixture was then dialyzed and subsequently lyophilized. Finally, ~1.8 g of dried AlgC powder was yielded.

Catechol substitution was confirmed by ^{1}H-NMR (Bruker Avance, 400 MHz), and the degree of catechol substitution was estimated by UV-Vis (Supporting Information, S1). The hydrodynamic size of the biopolymers was estimated using Dynamic Light Scattering (DLS, Malvern Zetasizer Nano ZS90). Herein, 2 mg ml^{-1} solutions of Chi/ChiC (in 0.1 M citric acid-

Na_2HPO_4 buffer; pH 3.0) and Alg/AlgC (in pure water; pH 6.0) were prepared and filtered using 0.45 µm polyether sulfone (PES) membrane.

Layer-by-layer (LbL) assembly: LbL deposition of multilayer films and their pH stability were examined by Quartz Crystal Microbalance (QCM-D, Biolin Scientific Q-SenseE1, Sweden). Silica-coated sensors (Biolin Scientific QSX 303) were rinsed with water and acetone, dried with compressed air, followed by plasma treatment (Harrick Plasma PDC-32G) for 5 min (medium power, water vapor pressure of 500 mTorr). The sensors were immediately immersed into 18 v/v% GOPS/acetone solution for 24 h, followed by rinsing with acetone three times to remove unreacted GOPS, then dried at 80 °C for 1 h. The epoxide-modified sensors were then immersed in Chi solution (200 ppm, pH 3.0) for 20 min, followed by rinsing to remove the unreacted Chi compounds.

The Chi-grafted sensor was mounted into the QCM-D module, and the background solution (NaCl 15 mM, pH 3) was loaded with a flow rate of 150 µl min^{-1}. When a stable baseline was obtained, a 200 ppm Alg solution was loaded for 20 min, followed by rinsing with the background solution for 20 min. Next, a 200 ppm Chi solution was loaded for 20 min, followed by 20 min rinsing. This procedure was repeated 7 times yielding Chi–Alg multilayer. A similar procedure was conducted to fabricate Chi–AlgC, ChiC–Alg, and ChiC–AlgC multilayers. For each case, 3 measurements were conducted (Supporting Information, S2). Next, the pH-responsiveness of each multilayer was examined. Herein, acidic (NaCl 15 mM, pH 3) and alkaline (NaCl 15 mM, pH 9) solutions were sequentially loaded for 20 min each, repeated in 3 cycles.

Bulk complexation: biopolymeric complexes were also prepared by mixing Chi/ChiC (10 mg ml^{-1}, pH 3) and Alg/AlgC (5 mg ml^{-1}, pH 3) solutions in a 1:1 volumetric ratio, followed by centrifugation (6.5 K rpm, 30 min).

Adhesion test: bulk complexes were examined in a lap shear adhesion test (Instron 34Sc, USA). Aluminum substrates (L×W×H: 50 mm × 12 mm × 10 mm) were polished and cleaned with ethanol/acetone. In each case, the prepared complex was clamped between two aluminum substrates (12 mm × 12 mm overlap area), then placed in water (pH 3.0 and pH 9) for 1, 3, 6, and 12 h. The samples were then tested in a single-lap shear mode (crosshead speed of 1.5 mm min^{-1}), and the maximum force was recorded. For each sample, 10 measurements were conducted in two independent experiments.

3. Results

3.1 Synthesis: Figure 1 summarizes the synthetic route and characterization of ChiC and AlgC. ChiC (Figure 1, top panel) was prepared by grafting DHBA onto Chi via Schiff base chemistry, followed by reductive amination using $NaCNBH_3$.[33–35] AlgC (Figure 1, bottom panel) was synthesized by grafting dopamine onto alginate via a carbodiimide coupling reaction using EDC/NHS.[36] Catechol substitution was confirmed for both biopolymers through ^{1}H-NMR analysis (Figure 1b, e). This confirmation was based on the presence of specific peaks at ~ 6.8 ppm, which are suggested to correspond to the grafted aromatic groups.[37,38] Notably, the differences in the shape/position of the aromatic peaks (when comparing ChiC and AlgC) can be attributed to structural differences between DA and DHBA, as well as contributions from the surrounding chemical groups on Chi and Alg.[39–41] In both cases, a catechol substitution of ~20% was targeted so the biopolymers can remain highly charged. Using UV-Vis spectroscopy (Figure 1c, f), the degree of catechol conjugation was determined to be 20.2% for ChiC and

18.7% for AlgC (Supporting Information, Figure S1-S2). In addition, the hydrodynamic size of the biopolymers was examined by DLS (Supporting Information, Figure S3), suggesting no significant effect of catechol substitution on the biopolymers' molecular size.

3.2 Surface complexation: four biopolymer complexes, i.e., Chi–Alg, ChiC–Alg, Chi–AlgC, and ChiC–AlgC, were prepared using a LbL assembly approach. In all cases, the LbL assembly was conducted at pH 3 to (i) preserve catechol groups from oxidation and (ii) ensure the dissolution of Chi and ChiC. Herein, one can expect different molecular interactions to be involved. The Chi–Alg complex is held together mainly through electrostatic interactions.[10,42–44] For the other three complexes though, one may expect additional catechol–amine interactions.

The LbL assembly of biopolymers was monitored by QCM-D (Figure 2a, b). In brief, the oppositely charged biopolymers were sequentially adsorbed onto the QCM-D sensor to yield 7 bilayers in total. Each deposition step was real-time monitored in terms of QCM-D frequency (F, Figure 2a) and dissipation (D, Figure 2b) shifts. In general, ΔF correlates to the effective mass (adsorbed polymer plus water content) coupled to the sensor, whereas ΔD reflects the capacity of the adsorbed layer to dissipate energy. Specifically, for viscoelastic films, both of these parameters are crucial in determining the adsorbed mass and viscoelastic properties.[45] The cumulative ΔF and ΔD measured for the deposition of 7 bilayers were compared between the complexes. Considering the standard deviation of the experiments (Supporting Information, Figure S4-S5 and Table S1), ΔF and ΔD values were found to be rather similar for different complexes. In other words, substituting 20% of the ionic units with catechol on one or both biopolymers appears to have a minimal effect on the degree of complexation or the affinity of the biopolymers to form complexes. Given the weak nature of ionizable groups,[46]

the biopolymers with catechol conjugation are still expected to be significantly charged; thus, long-ranged electrostatic interactions are expected to be the main driving force of complexation in all cases. This means that at each deposition step, the amount of the adsorbed biopolymer is controlled mainly by the electrostatic forces and that excessive overcharging cannot occur, which may explain the comparable ΔF values for all samples.[47,48]

While complex formation appears to be mainly dependent on long-range electrostatic interactions, the short-range catechol–amine interactions may affect the properties of the formed complexes, e.g., pH-responsiveness.[49–51] For the reference complex (Chi–Alg), electrostatic forces, as the main stabilizing interaction, are easily perturbed by a change in pH. If such a complex is prepared at pH 3 and then is exposed to a solution with pH 9, excess negative charge is created in the complex (i.e., Chi becomes less charged, Alg becomes more charged) that causes complex dissociation.[9,52] If catechol–amine interactions are present, one can first expect physical cation–π interactions. But more importantly, as in the case of the mussel glue cured when exposed to high-pH seawater, the catechol groups in the complex getting oxidized may form covalent bonds with the amine groups on Chi and thus stabilize/cross-link the complex.[53]

This idea was examined by alternately exposing the LbL-assembled complexes to pH 3 and pH 9, respectively (Figure 2c-f). An electrostatic-based system is expected to show large and irreversible structural changes (F and D shifts) in each swelling/collapse cycle. Having stabilizing catechol–amine interactions should render reversible swell/collapse cycles with reduced structural changes. Based on QCM-D data, the Chi–Alg multilayer (Figure 2c), as expected, shows quite large shifts in F and D (when pH is changed from 3 to 9), which also grow in magnitude with each cycle. Moreover, a large structural hysteresis, evidenced by

large baseline shift after three cycles (Supporting Information, Table S2), was found. All these observations confirm the lack of stabilizing covalent interactions in the complex. Next, the effect of adding catechol to the complexes was investigated. Interestingly, the ChiC–Alg multilayer (Figure 2d) displays quite a similar behavior to Chi–Alg multilayer, suggesting a lack of cross-linking despite the presence of catechol groups. Having catechol only on Chi, one can expect catechol–amine interactions only between Chi chains, and not including Alg chains. Accordingly, even if catechol–amine interactions between Chi chains are present, they appear ineffective in improving the complex stability.

In contrast, Chi–AlgC (Figure 2e) and ChiC–AlgC (Figure 2f) multilayers demonstrated a more stable and reversible swelling-collapse behavior. The shifts in F and D (when pH is changed from 3 to 9) are significantly reduced, and the structural hysteresis (Supporting Information, Table S2) is negligible. By having catechol on Alg, one can expect catechol–amine interactions that can cross-link Chi and Alg chains. Based on the QCM-D data, these interactions appear to render Chi–AlgC and ChiC–AlgC complexes with a self-cross-linking property.[54]

3.2 Bulk complexation: To further investigate the effect of catechol substitution on the complex properties, the four complex combinations were also prepared in the bulk state (Figure 3). It is worth mentioning that bulk complexation requires more care to control homogeneity in both composition and morphology of the complex, and various factors such as mixing speed can affect the complex properties.[10,55,56] For this reason, we prepared all four complex combinations under identical conditions. In each case, mixing the solutions of oppositely charged biopolymers produces instant cloudiness; the resulting complex material is then collectible by centrifugation (Figure 3a). Since our complex design is inspired by mussel glue, we herein also examined the underwater adhesive properties of the complexes. The

four complexes were tested in single-lap shear mode (Figure 3b), where the adhesion strength was measured after immersion in either pH 3 or pH 9 solutions, for different durations (1-12 h).

Figure 3c displays the lap shear strength measured for the complexes after immersion in pH 3. Firstly, for a given immersion time, it is shown that having catechol on Alg corresponds to an improved lap shear strength. For example, for 1 h immersion, Chi–Alg reference complex demonstrated the weakest lap shear strength of ~40 KPa. Also, when having catechol only on Chi (ChiC–Alg complex), no significant improvement in the adhesion strength was found. Conversely, Chi–AlgC showed a nearly two-fold increment in the lap shear strength. Lastly, having catechol on both biopolymers (ChiC–AlgC) rendered the largest lap shear strength of ~130 kPa. The larger lap shear strength herein may be attributed to the larger net content of catechol groups present. In this case, besides catechol–amine interactions, one may expect catechol–catechol interactions between ChiC and AlgC chains as well. Secondly, for different immersion times, two distinct trends were found. For Chi–Alg and ChiC–Alg complexes, the lap shear strength appears to slightly increase for up to 6 h immersion time; however, the lap shear strength is significantly reduced after 12 h immersion. This observation suggests the instability of these complexes and possible dissolution over time. Hypothetically, the gain in lap shear strength for (up to 6 h immersion) can be attributed to an enhanced complex-substrate contact area.[57] In contrast, for Chi–AlgC and ChiC–AlgC complexes, a monotonic gain in lap shear strength was found. Accordingly, for these two complexes, it appears that catechol–amine interactions are involved and prevent complex disintegration.

Figure 3d demonstrates the lap shear strength for the complexes after immersion in pH 9 solution. Overall, the same trends observed in Figure 3c are shown herein. Importantly, a

comparison of Figure 3c and Figure 3d can confirm the stabilizing effect of catechol–amine interactions for Chi–AlgC and ChiC–AlgC complexes. A switch to pH 9 is expected to disrupt the charge neutrality and thus destabilize the complex if only electrostatic interactions are mainly in control. As shown in Figure 3d, Chi–Alg and ChiC–Alg complexes show a decaying lap shear strength with time, which implies complex instability. In contrast, Chi–AlgC and ChiC-AlgC complexes demonstrated a growing lap shear strength with time, which can hint to catechol–amine interactions.

Overall, from the studied system herein, it can be inferred that having catechol, on either Alg alone or both biopolymers, can add stabilizing non-electrostatic interactions in the biopolyelectrolyte complex. Contrarily, having catechol only on Chi appears ineffective and did not enhance the cohesiveness/stability of the complex. As depicted in Figure 3e, it is suggested that by having catechol only on Chi, catechol–amine interactions are only possible between Chi units (interchain and intrachain), while Alg will be excluded from the cross-linked network. On the other hand, catechol on Alg seems to enable a whole network cross-linking of Chi and Alg chains.

Conclusion

Self-cross-linkable Chi-Alg complexes can be obtained by using mussel-inspired chemistry. Catechol substitution onto one or both of the biopolymers introduces various catechol–amine interactions. When preserved from catechol oxidation (e.g., at acidic pH), these interactions are expected to be mainly of physical origin, e.g., cation-π interactions. Under oxidizing environments (e.g., at alkaline pH), covalent interactions between quinone and amine are expected. These interactions all together were shown to produce self-cross-linking and improve the mechanical properties and pH stability of the complexes. Notably, it was found

that having catechol only on Chi appears ineffective. This may be due to catechol–amine interactions occurring only between Chi chains, while Alg chains are not included in the cross-linked network.

Author Information

Junie Kang, jukan@kemi.dtu.dk

Saeed Zajforoushan Moghaddam, saza@kemi.dtu.dk

Esben Thormann (corresponding author), esth@kemi.dtu.dk

Acknowledgment

J. K. acknowledges a stipend from the China Scholarship Council (CSC). S. Z. M. and E. T. acknowledge financial support from Innovation Fund Denmark through the Grand Solutions Project 0175-00008B.

Supplementary Information is available at:

- Calculation of catechol substitution by UV-Vis, determination of hydrodynamic size via DLS, and QCM-D raw data

Reference

(1) Wang, L.; Khor, E.; Wee, A.; Lim, L. Y. Chitosan-Alginate PEC Membrane as a Wound Dressing: Assessment of Incisional Wound Healing. *J. Biomed. Mater. Res.* **2002**, *63* (5), 610–618. https://doi.org/10.1002/JBM.10382.

(2) Buriuli, M.; Verma, D. Polyelectrolyte Complexes (PECs) for Biomedical Applications. *Adv. Struct. Mater.* **2017**, *66*, 45–93. https://doi.org/10.1007/978-981-10-3328-5_2/FIGURES/4.

(3) Wang, S.; Gao, Z.; Liu, L.; Li, M.; Zuo, A.; Guo, J. Preparation, in Vitro and in Vivo Evaluation of Chitosan-Sodium Alginate-Ethyl Cellulose Polyelectrolyte Film as a Novel Buccal Mucosal Delivery Vehicle. *Eur. J. Pharm. Sci.* **2022**, *168*, 106085. https://doi.org/10.1016/J.EJPS.2021.106085.

(4) Nayef, L.; Castiello, R.; Tabrizian, M.; Nayef, L.; Castiello, R.; Tabrizian, M. Washless Method Enables Multilayer Coating of an Aggregation-Prone Nanoparticulate Drug Delivery System with Enhanced Yields, Colloidal Stability, and Scalability. *Macromol. Biosci.* **2017**, *17* (6),

1600535. https://doi.org/10.1002/MABI.201600535.

(5) Florczyk, S. J.; Kim, D. J.; Wood, D. L.; Zhang, M. Influence of Processing Parameters on Pore Structure of 3D Porous Chitosan–Alginate Polyelectrolyte Complex Scaffolds. *J. Biomed. Mater. Res. Part A* **2011**, *98A* (4), 614–620. https://doi.org/10.1002/JBM.A.33153.

(6) Jeong, S. I.; Krebs, M. D.; Bonino, C. A.; Samorezov, J. E.; Khan, S. A.; Alsberg, E. Electrospun Chitosan-Alginate Nanofibers with in Situ Polyelectrolyte Complexation for Use as Tissue Engineering Scaffolds. *Tissue Eng. - Part A* **2011**, *17* (1–2), 59–70. https://doi.org/10.1089/TEN.TEA.2010.0086/ASSET/IMAGES/LARGE/FIGURE11.JPEG.

(7) Liu, H.; Wang, Y.; Yu, Y.; Chen, W.; Jiang, L.; Qin, J. Simple Fabrication of Inner Chitosan-Coated Alginate Hollow Microfiber with Higher Stability. *J. Biomed. Mater. Res. Part B Appl. Biomater.* **2019**, *107* (8), 2527–2536. https://doi.org/10.1002/JBM.B.34343.

(8) Gorshkova, M.; Volkova, I. Preparation of PH-Tunable Polyelectrolyte Complexes of Alginate Sodium Salt and N-[(2-Hydroxy-3-Trimethylammonium) Propyl] Chitosan Chloride. *J. Polym. Res.* **2021**, *28* (3), 1–8. https://doi.org/10.1007/S10965-021-02451-Y/TABLES/3.

(9) Gierszewska, M.; Ostrowska-Czubenko, J.; Chrzanowska, E. PH-Responsive Chitosan/Alginate Polyelectrolyte Complex Membranes Reinforced by Tripolyphosphate. *Eur. Polym. J.* **2018**, *101*, 282–290. https://doi.org/10.1016/j.eurpolymj.2018.02.031.

(10) Sæther, H. V.; Holme, H. K.; Maurstad, G.; Smidsrød, O.; Stokke, B. T. Polyelectrolyte Complex Formation Using Alginate and Chitosan. *Carbohydr. Polym.* **2008**, *74* (4), 813–821. https://doi.org/10.1016/J.CARBPOL.2008.04.048.

(11) Park, J. W.; Park, K. H.; Seo, S. Natural Polyelectrolyte Complex-Based PH-Dependent Delivery Carriers Using Alginate and Chitosan. *J. Appl. Polym. Sci.* **2019**, *136* (43), 48143. https://doi.org/10.1002/APP.48143.

(12) Wang, X.; Wang, J.; Song, S.; Rao, P.; Wang, R.; Liu, S. Preparation and Properties of Soil Conditioner Microspheres Based on Self-Assembled Potassium Alginate and Chitosan. *Int. J. Biol. Macromol.* **2020**, *147*, 877–889. https://doi.org/10.1016/J.IJBIOMAC.2019.09.247.

(13) Lv, X.; Zhang, W.; Liu, Y.; Zhao, Y.; Zhang, J.; Hou, M. Hygroscopicity Modulation of Hydrogels Based on Carboxymethyl Chitosan/Alginate Polyelectrolyte Complexes and Its Application as PH-Sensitive Delivery System. *Carbohydr. Polym.* **2018**, *198*, 86–93. https://doi.org/10.1016/J.CARBPOL.2018.06.058.

(14) Omer, A. M.; Ahmed, M. S.; El-subruiti, G. M.; Khalifa, R. E.; Eltaweil, A. S. PH-Sensitive Alginate/Carboxymethyl Chitosan/Aminated Chitosan Microcapsules for Efficient Encapsulation and Delivery of Diclofenac Sodium. *Pharm. 2021, Vol. 13, Page 338* **2021**, *13* (3), 338. https://doi.org/10.3390/PHARMACEUTICS13030338.

(15) Quemeneur, F.; Rinaudo, M.; Pépin-Donat, B. Influence of Molecular Weight and PH on Adsorption of Chitosan at the Surface of Large and Giant Vesicles. *Biomacromolecules* **2008**, *9* (1), 396–402. https://doi.org/10.1021/BM700943J/ASSET/IMAGES/LARGE/BM-2007-00943J_0009.JPEG.

(16) Pham, T. T.; Pham, T. D.; Yusa, S. I. PH-and Thermo-Responsive Water-Soluble Smart Polyion Complex (PIC) Vesicle with Polyampholyte Shells. *Polymers (Basel).* **2022**, *14* (9), 1659. https://doi.org/10.3390/POLYM14091659/S1.

(17) Schirmer, U.; Ludolph, J.; Rothe, H.; Hauptmann, N.; Behrens, C.; Bittrich, E.; Schliephake, H.; Liefeith, K. Tailored Polyelectrolyte Multilayer Systems by Variation of Polyelectrolyte Composition and EDC/NHS Cross-Linking: Physicochemical Characterization and In Vitro

Evaluation. *Nanomaterials* **2022**, *12* (12), 2054. https://doi.org/10.3390/NANO12122054/S1.

(18) Shin, M. G.; Choi, W.; Lee, J. H. Highly Selective and PH-Stable Reverse Osmosis Membranes Prepared via Layered Interfacial Polymerization. *Membr. 2022, Vol. 12, Page 156* **2022**, *12* (2), 156. https://doi.org/10.3390/MEMBRANES12020156.

(19) Liu, Y.; Zhu, M.; Zhao, Q.; An, Q.; Qian, J.; Lee, K.; Lai, J. The Chemical Crosslinking of Polyelectrolyte Complex Colloidal Particles and the Pervaporation Performance of Their Membranes. *J. Memb. Sci.* **2011**, *385–386* (1), 132–140. https://doi.org/10.1016/J.MEMSCI.2011.09.033.

(20) Mu, B.; Lu, C.; Liu, P. Disintegration-Controllable Stimuli-Responsive Polyelectrolyte Multilayer Microcapsules via Covalent Layer-by-Layer Assembly. *Colloids Surfaces B Biointerfaces* **2011**, *82* (2), 385–390. https://doi.org/10.1016/J.COLSURFB.2010.09.024.

(21) Huang, J.; Liu, X.; Thormann, E. Surface Forces between Highly Charged Cationic Polyelectrolytes Adsorbed to Silica: How Control of PH and the Adsorbed Amount Determines the Net Surface Charge. *Langmuir* **2018**, *34* (25), 7264–7271. https://doi.org/10.1021/acs.langmuir.8b00909.

(22) Huang, J.; Zajforoushan Moghaddam, S.; Thormann, E. Structural Investigation of a Self-Cross-Linked Chitosan/Alginate Dialdehyde Multilayered Film with in Situ QCM-D and Spectroscopic Ellipsometry. *ACS Omega* **2019**, *4* (1), 2019–2029. https://doi.org/10.1021/acsomega.8b03145.

(23) Huang, J.; Zajforoushan Moghaddam, S.; Maroni, P.; Thormann, E. Swelling Behavior, Interaction, and Electrostatic Properties of Chitosan/Alginate Dialdehyde Multilayer Films with Different Outermost Layer. *Langmuir* **2020**, *36* (14), 3782–3791. https://doi.org/10.1021/ACS.LANGMUIR.0C00330/ASSET/IMAGES/LARGE/LA0C00330_0006.JPEG.

(24) Gupta, B.; Tummalapalli, M.; Deopura, B. L.; Alam, M. S. Functionalization of Pectin by Periodate Oxidation. *Carbohydr. Polym.* **2013**, *98* (1), 1160–1165. https://doi.org/10.1016/J.CARBPOL.2013.06.069.

(25) Balakrishnan, B.; Lesieur, S.; Labarre, D.; Jayakrishnan, A. Periodate Oxidation of Sodium Alginate in Water and in Ethanol–Water Mixture: A Comparative Study. *Carbohydr. Res.* **2005**, *340* (7), 1425–1429. https://doi.org/10.1016/J.CARRES.2005.02.028.

(26) Carmagnola, I.; Chiono, V.; Ruocco, G.; Scalzone, A.; Gentile, P.; Taddei, P.; Ciardelli, G. PLGA Membranes Functionalized with Gelatin through Biomimetic Mussel-Inspired Strategy. *Nanomater. 2020, Vol. 10, Page 2184* **2020**, *10* (11), 2184. https://doi.org/10.3390/NANO10112184.

(27) Yang, Q.; Tang, L.; Guo, C.; Deng, F.; Wu, H.; Chen, L.; Huang, L.; Lu, P.; Ding, C.; Ni, Y.; Zhang, M. A Bioinspired Gallol-Functionalized Collagen as Wet-Tissue Adhesive for Biomedical Applications. *Chem. Eng. J.* **2021**, *417*, 127962. https://doi.org/10.1016/J.CEJ.2020.127962.

(28) Li, K.; Jin, S.; Zhang, F.; Zhou, Y.; Zeng, G.; Li, J.; Shi, S. Q.; Li, J. Bioinspired Phenol-Amine Chemistry for Developing Bioadhesives Based on Biomineralized Cellulose Nanocrystals. *Carbohydr. Polym.* **2022**, *296*. https://doi.org/10.1016/J.CARBPOL.2022.119892.

(29) Liu, S.; Liu, X.; Ren, Y.; Wang, P.; Pu, Y.; Yang, R.; Wang, X.; Tan, X.; Ye, Z.; Maurizot, V.; Chi, B. Mussel-Inspired Dual-Cross-Linking Hyaluronic Acid/ϵ-Polylysine Hydrogel with Self-Healing and Antibacterial Properties for Wound Healing. *ACS Appl. Mater. Interfaces* **2020**, *12* (25), 27876–27888. https://doi.org/10.1021/ACSAMI.0C00782/ASSET/IMAGES/LARGE/AM0C00782_0003.JPEG.

(30) Waite, J. H. Mussel Adhesion – Essential Footwork. *J. Exp. Biol.* **2017**, *220* (4), 517–530. https://doi.org/10.1242/JEB.134056.

(31) Pinnataip, R.; P. Lee, B. Oxidation Chemistry of Catechol Utilized in Designing Stimuli-Responsive Adhesives and Antipathogenic Biomaterials. *ACS Omega* **2021**, *0* (0). https://doi.org/10.1021/acsomega.1c00006.

(32) Maier, G. P.; Bernt, C. M.; Butler, A. Catechol Oxidation: Considerations in the Design of Wet Adhesive Materials. *Biomater. Sci.* **2018**, *6* (2), 332–339. https://doi.org/10.1039/C7BM00884H.

(33) S. Yavvari, P.; Aasheesh Srivastava. Robust, Self-Healing Hydrogels Synthesised from Catechol Rich Polymers. *J. Mater. Chem. B* **2015**, *3* (5), 899–910. https://doi.org/10.1039/C4TB01307G.

(34) Pan, W.; Qi, X.; Xiang, Y.; You, S.; Cai, E.; Gao, T.; Tong, X.; Hu, R.; Shen, J.; Deng, H. Facile Formation of Injectable Quaternized Chitosan/Tannic Acid Hydrogels with Antibacterial and ROS Scavenging Capabilities for Diabetic Wound Healing. *Int. J. Biol. Macromol.* **2022**, *195*, 190–197. https://doi.org/10.1016/J.IJBIOMAC.2021.12.007.

(35) Shao, Z.; Yin, T.; Jiang, J.; He, Y.; Xiang, T.; Zhou, S. Wound Microenvironment Self-Adaptive Hydrogel with Efficient Angiogenesis for Promoting Diabetic Wound Healing. *Bioact. Mater.* **2023**, *20*, 561–573. https://doi.org/10.1016/J.BIOACTMAT.2022.06.018.

(36) Lee, C.; Shin, J.; Lee, J. S.; Byun, E.; Ryu, J. H.; Um, S. H.; Kim, D. I.; Lee, H.; Cho, S. W. Bioinspired, Calcium-Free Alginate Hydrogels with Tunable Physical and Mechanical Properties and Improved Biocompatibility. *Biomacromolecules* **2013**, *14* (6), 2004–2013. https://doi.org/10.1021/bm400352d.

(37) Kim, K.; Ryu, J. H.; Lee, D. Y.; Lee, H. Bio-Inspired Catechol Conjugation Converts Water-Insoluble Chitosan into a Highly Water-Soluble, Adhesive Chitosan Derivative for Hydrogels and LbL Assembly. *Biomater. Sci.* **2013**, *1* (7), 783–790. https://doi.org/10.1039/c3bm00004d.

(38) Lee, Y.-K.; Lee, S.-Y. A Colorimetric Alginate-Catechol Hydrogel Suitable as a Spreadable PH Indicator. *Dye. Pigment.* **2014**, *108*, 1–6. https://doi.org/10.1016/j.dyepig.2014.04.014.

(39) Hoffman, R. V. *Structure Determination of Organic Compounds*; 2005. https://doi.org/10.1002/0471648736.ch11.

(40) Harris, R. K.; Becker, E. D.; Cabral De Menezes, S. M.; Granger, P.; Hoffman, R. E.; Zilm, K. W. Further Conventions for NMR Shielding and Chemical Shifts (IUPAC Recommendations 2008). *Pure Appl. Chem.* **2008**, *80* (1), 59–84. https://doi.org/10.1351/PAC200880010059/MACHINEREADABLECITATION/RIS.

(41) Jameson, C. J. UNDERSTANDING NMR CHEMICAL SHIFTS. *https://doi.org/10.1146/annurev.physchem.47.1.135* **2003**, *47*, 135–169. https://doi.org/10.1146/ANNUREV.PHYSCHEM.47.1.135.

(42) Caridade, S. G.; Monge, C.; Gilde, F.; Boudou, T.; Mano, J. F.; Picart, C. Free-Standing Polyelectrolyte Membranes Made of Chitosan and Alginate. *Biomacromolecules* **2013**, *14* (5), 1653–1660. https://doi.org/10.1021/BM400314S.

(43) Aston, R.; Wimalaratne, M.; Brock, A.; Lawrie, G.; Grøndahl, L. Interactions between Chitosan and Alginate Dialdehyde Biopolymers and Their Layer-by-Layer Assemblies. *Biomacromolecules* **2015**, *16* (6), 1807–1817. https://doi.org/10.1021/ACS.BIOMAC.5B00383.

(44) Hoogeveen, N. G.; Cohen Stuart, M. A.; Fleer, G. J.; Böhmer, M. R. Formation and Stability of Multilayers of Polyelectrolytes. *Langmuir* **1996**, *12* (15), 3675–3681.

https://doi.org/10.1021/LA951574Y/ASSET/IMAGES/MEDIUM/LA951574YE00002.GIF.

(45) Voinova, M. V; Rodahl, M.; Jonson, M.; Kasemo, B. Viscoelastic Acoustic Response of Layered Polymer Films at Fluid-Solid Interfaces: Continuum Mechanics Approach. *Phys. Scr.* **1999**, *59* (5), 391–396. https://doi.org/10.1238/PHYSICA.REGULAR.059A00391/XML.

(46) Yavvari, P. S.; Srivastava, A. Robust, Self-Healing Hydrogels Synthesised from Catechol Rich Polymers. *J. Mater. Chem. B* **2015**, *3* (5), 899–910. https://doi.org/10.1039/c4tb01307g.

(47) Linse, P. Adsorption of Weakly Charged Polyelectrolytes at Oppositely Charged Surfaces. *Macromolecules* **1996**, *29* (1), 326–336. https://doi.org/10.1021/MA950539V/ASSET/IMAGES/LARGE/MA950539VF00011.JPEG.

(48) Hayashi, Y.; Ullner, M.; Linse, P. A Monte Carlo Study of Solutions of Oppositely Charged Polyelectrolytes. *J. Chem. Phys.* **2002**, *116* (15), 6836–6845. https://doi.org/10.1063/1.1460859.

(49) Fan, H.; Wang, J.; Tao, Z.; Huang, J.; Rao, P.; Kurokawa, T.; Gong, J. P. Adjacent Cationic–Aromatic Sequences Yield Strong Electrostatic Adhesion of Hydrogels in Seawater. *Nat. Commun. 2019 101* **2019**, *10* (1), 1–8. https://doi.org/10.1038/s41467-019-13171-9.

(50) Mahadevi, A. S.; Sastry, G. N. Cation-π Interaction: Its Role and Relevance in Chemistry, Biology, and Material Science. *Chem. Rev.* **2013**, *113* (3), 2100–2138. https://doi.org/10.1021/CR300222D/ASSET/IMAGES/CR300222D.SOCIAL.JPEG_V03.

(51) Gallivan, J. P.; Dougherty, D. A. Cation-π Interactions in Structural Biology. *Proc. Natl. Acad. Sci. U. S. A.* **1999**, *96* (17), 9459–9464. https://doi.org/10.1073/PNAS.96.17.9459/ASSET/8B7D3B1F-50F5-4DAA-8EBA-A5F46162B601/ASSETS/GRAPHIC/PQ1792486006.JPEG.

(52) Huang, J.; Moghaddam, S. Z.; Maroni, P.; Thormann, E. Swelling Behavior, Interaction, and Electrostatic Properties of Chitosan/Alginate Dialdehyde Multilayer Films with Different Outermost Layer. *36*, 52. https://doi.org/10.1021/acs.langmuir.0c00330.

(53) An, S.; Jeon, E. J.; Han, Y.; Jeon, J.; Lee, M. J.; Kim, S.; Shin, M.; Cho, S.-W.; An, S.; Jeon, E. J.; Han, S. Y.; Jeon, J.; Lee, M. J.; Kim, S.; Cho, S.-W.; Shin, M. PH-Universal Catechol-Amine Chemistry for Versatile Hyaluronic Acid Bioadhesives. *Small* **2022**, 2202729. https://doi.org/10.1002/SMLL.202202729.

(54) Shin, M.; Choi, J. H.; Kim, K.; Kim, S.; Lee, H. Hemostatic Needles: Controlling Hemostasis Time by a Catecholamine Oxidative Pathway. *ACS Appl. Mater. Interfaces* **2021**, *13*, 10741–10747. https://doi.org/10.1021/acsami.0c22223.

(55) Rusu-Balaita, L.; Desbrières, J.; Rinaudo, M. Formation of a Biocompatible Polyelectrolyte Complex: Chitosan-Hyaluronan Complex Stability. *Polym. Bull.* **2003**, *50* (1–2), 91–98. https://doi.org/10.1007/S00289-003-0144-1/METRICS.

(56) Becherán-Marón, L.; Peniche, C.; Argüelles-Monal, W. Study of the Interpolyelectrolyte Reaction between Chitosan and Alginate: Influence of Alginate Composition and Chitosan Molecular Weight. *Int. J. Biol. Macromol.* **2004**, *34* (1–2), 127–133. https://doi.org/10.1016/J.IJBIOMAC.2004.03.010.

(57) Li, J.; Yu, X.; Enciso Martinez, E.; Zhu, J.; Wang, T.; Shi, S.; Shin, S. R.; Hassan, S.; Guo, C.; Li, J.; Yu, X.; Guo, C.; Zhu, J.; Shi, S.; Martinez, E. E.; León, N.; Wang, M. T.; Shin, S. R.; Hassan, S. Emerging Biopolymer-Based Bioadhesives. *Macromol. Biosci.* **2022**, *22* (2), 2100340. https://doi.org/10.1002/MABI.202100340.

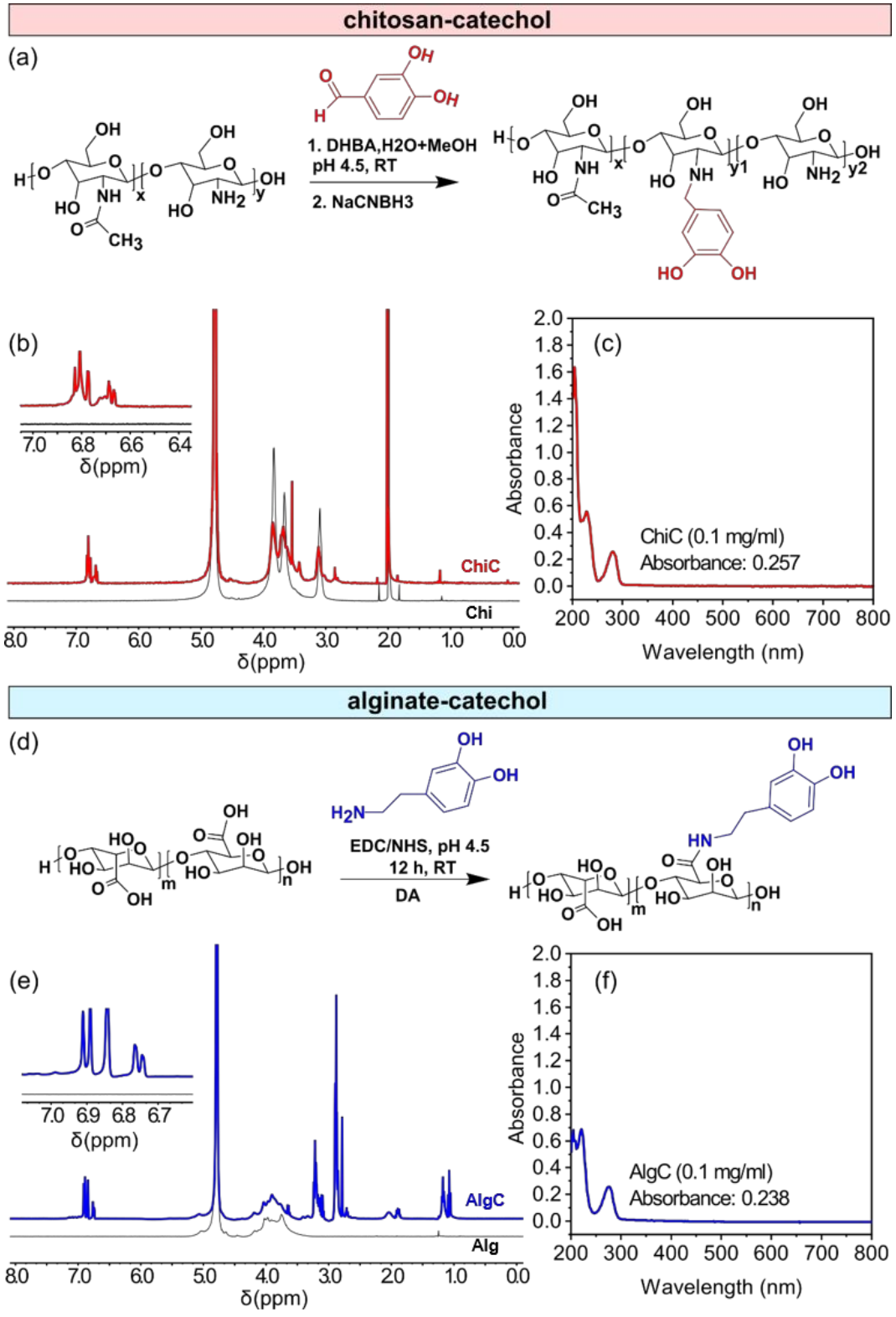

Figure 1 synthetic route and characterization of catechol-substituted chitosan (ChiC, top panel) and alginate (AlgC, bottom panel). (a)(d) schematic illustration of synthesis, (b)(e) ^{1}H-NMR spectra, (c)(f) UV-Vis spectra.

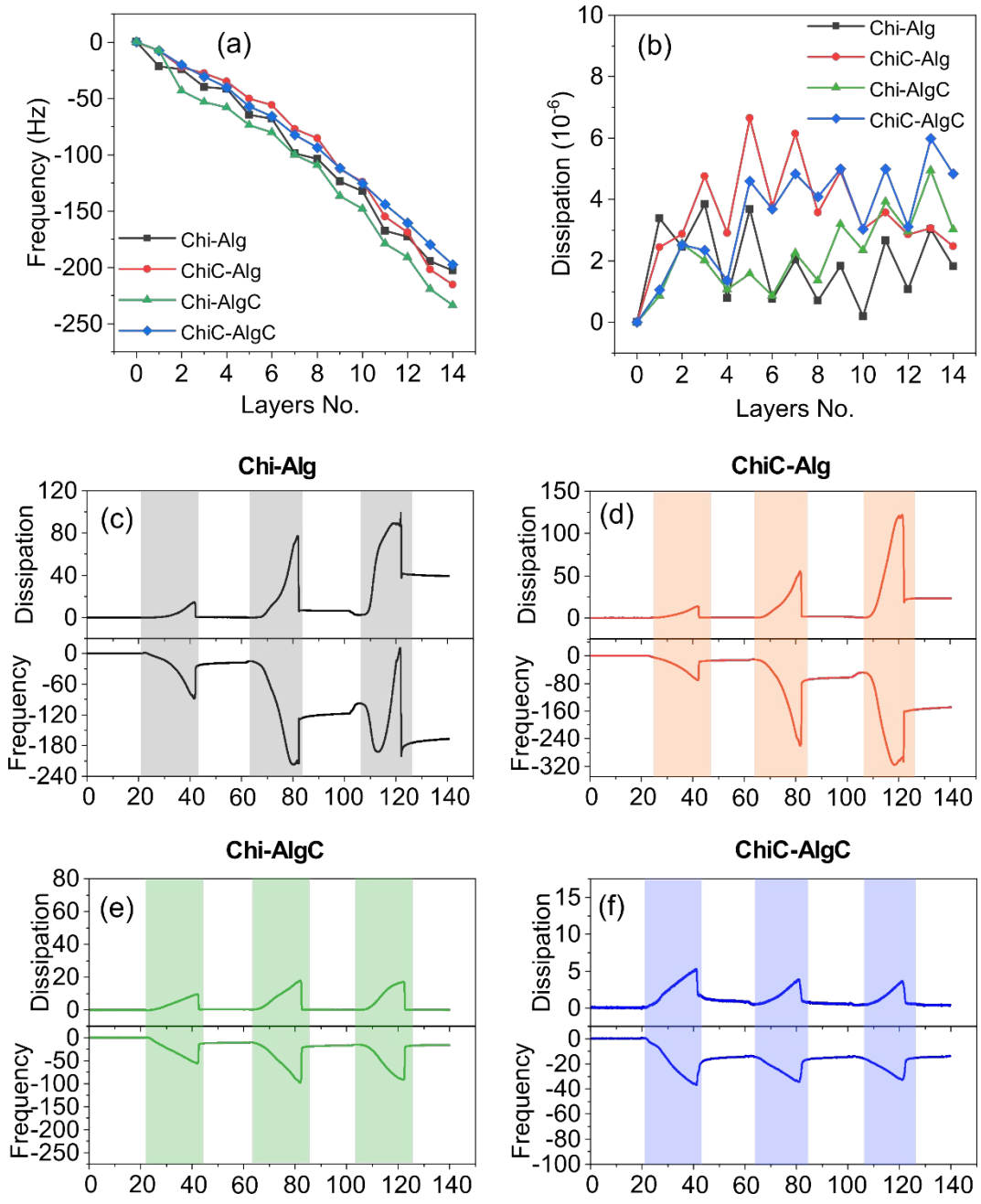

Figure 2 Complexation at surface (LbL assembly); multilayer growth monitored by QCM-D (a) frequency and (b) dissipation shifts as a function of layer number (*note:* odd layers: Alg or AlgC, even layers: Chi or ChiC polymer); pH cycle (3-to-9-to-3) of (c) Chi-Alg, (d) ChiC-Alg, (e) Chi-AlgC, and (f) ChiC-AlgC multilayer complex films (note: blank and highlighted regions represent pH 3 and pH 9, respectively). In all cases, F and D for the 3rd overtone is displayed.

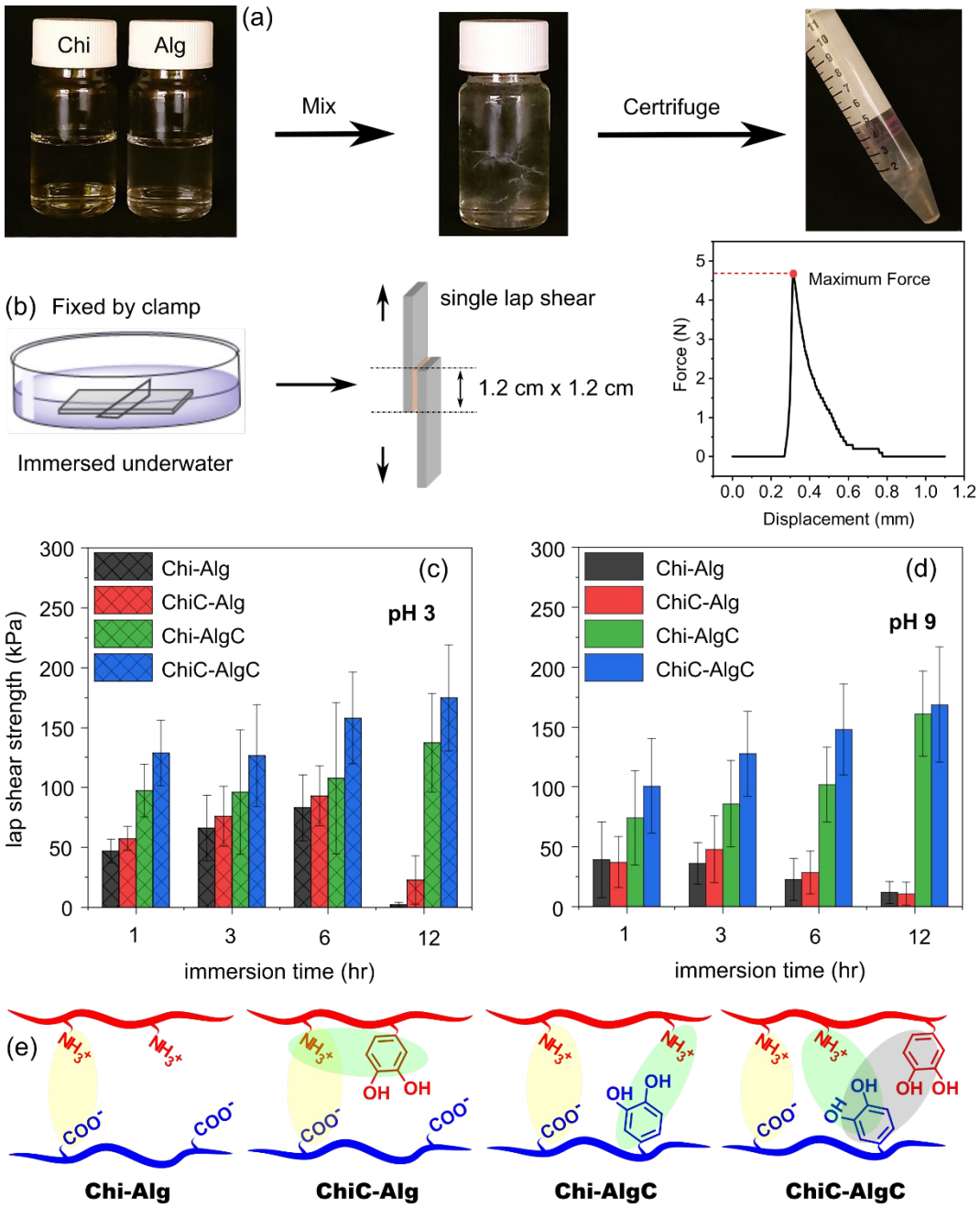

Figure 3 Bulk complexation; (a) preparation route, (b) lap shear test, (c)(d) maximum lap shear strength of four complexes after various immersion times in pH 3 and pH 9, (e) schematic illustration of molecular interactions in four complexes

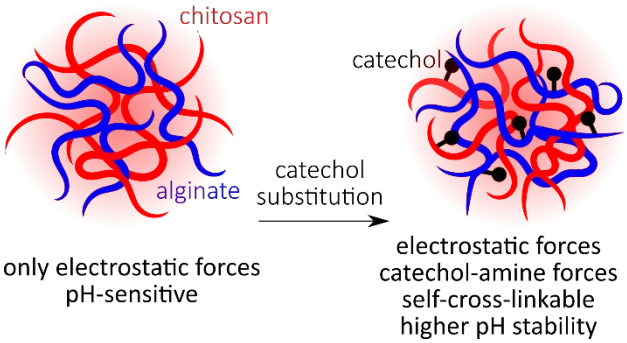

Graphical abstract

Supporting information

Self-cross-linkable Chitosan-Alginate Complexes Inspired by the Mussel Glue Chemistry

Junjie Kang, Saeed Zajforoushan Moghaddam, Esben Thormann*

Department of Chemistry, Technical University of Denmark, 2800 Kgs. Lyngby, Denmark

*esth@kemi.dtu.dk

S1 Catechol Substitution:

UV-Vis spectra (200 to 800 nm) were collected using NanoDrop 2000c Spectrophotometer. Quartz cuvettes with a path length of 10 mm were used, and the background absorption was subtracted before measurement.

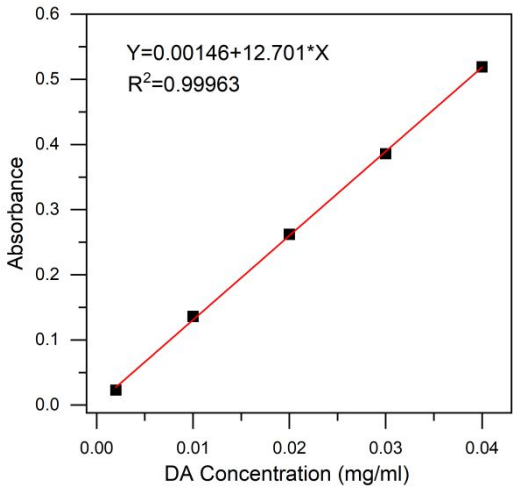

Figure S1 standard UV-Vis standard curve for different dopamine (DA) concentrations

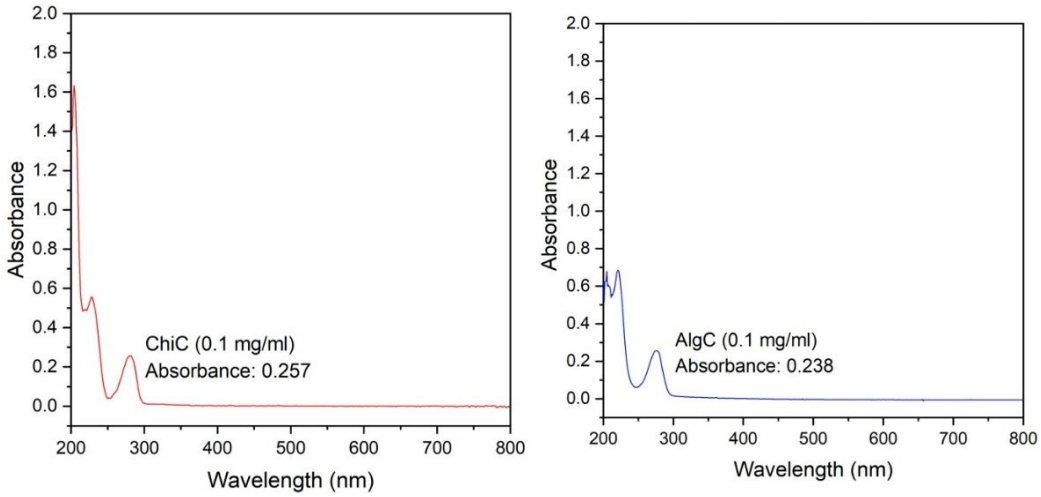

Figure S2 UV-Vis spectra of ChiC and AlgC solutions (0.1 mg/ml)

Solutions of dopamine (DA), ChiC, and AlgC were prepared in aqueous acetic buffer with pH = 3.0. A series of DA solutions at different concentrations have been prepared by diluting the stock solution (10 mg/ml). The standard curve (Figure S1) of absorbance at 280 nm was generated (R^2 = 0.99963). UV-Vis spectra for ChiC and AlgC solutions (0.10 mg/ml) were

measured (Figure S2) and the absorbance at 280 nm was used to calculate catechol substitution from Figure S1, i.e., 20.2% for ChiC and 18.7% for AlgC.

The hydrodynamic size of biopolymers was examined by DLS (Figure S3). Chi/ChiC (2 mg/ml in 0.1 M citric acid-Na_2HPO_4 buffer; pH 3.0) and Alg/AlgC (2 mg/ml in pure water; pH 6.0) were prepared, then filtered using 0.45 µm polyether sulfone (PES) membrane. All measurements were performed at room temperature (3 x 10 runs for each sample).

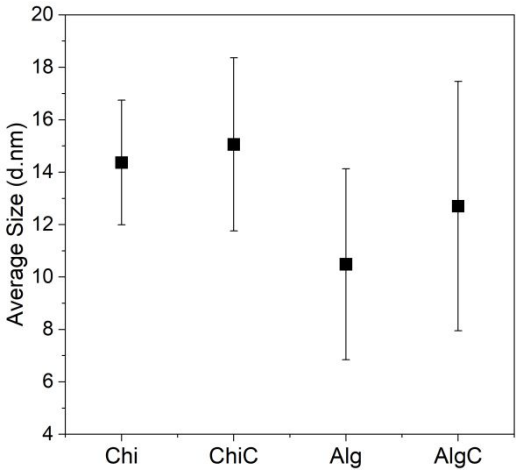

Figure S3 hydrodynamic diameter of biopolymers

S2 QCM-D: Layer-by-layer Assembly

Figure S4-S5 display QCM-D shifts corresponding to LbL assembly of 4 multilayer combinations. In each case, 3 replicas were collected.

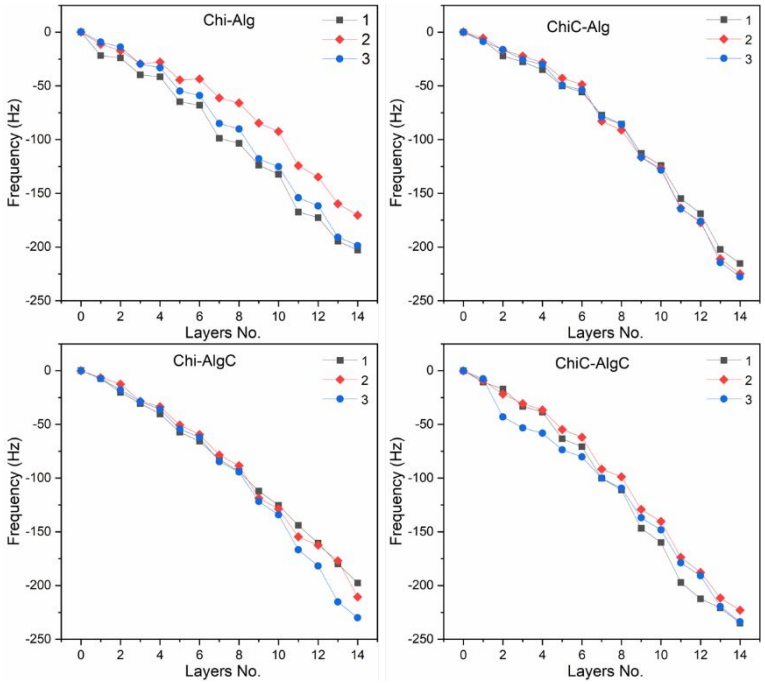

Figure S4 LbL assembly of biopolymers; QCM-D frequency shifts for 3rd overtone

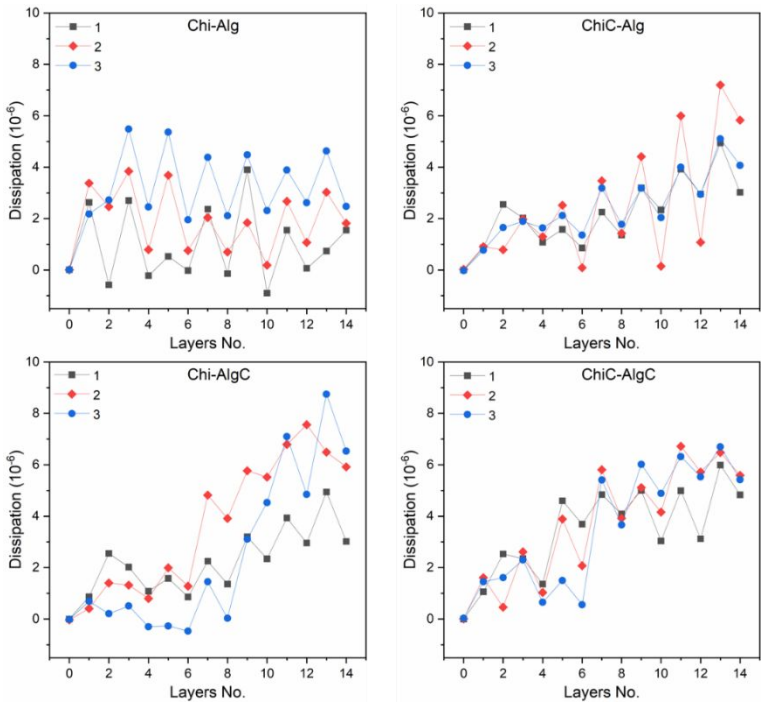

Figure S5 LbL assembly of biopolymers; QCM-D dissipation shifts for 3rd overtone

The adsorbed mass (Δm) was estimated from the ΔF using the Sauerbrey equation[1]:

$$\Delta \mathrm{m} = -\frac{\sqrt{\rho_q u_q}}{2{f_0}^2} \cdot \frac{\Delta f_n}{n}$$

where ρ_q is the density of quartz (2.648 g cm^{-3}), μ_q is the shear modulus of quartz for an AT-cut crystal (29.47 GPa), f_0 is the resonant frequency of the fundamental mode (4.95 MHz), C is the mass sensitivity constant (17.7 ng cm^{-2} Hz^{-1}), and n is the overtone number (in the present case = 3).[2] The above equation can provide a valid estimation only if the ratio of dissipation and normalized frequency shifts ($(\Delta D_n)/(-\Delta f_n/n)$) is smaller than 4×10^{-7} Hz^{-1}.[2,3] All of cases herein demonstrated ratios smaller than 3.0×10^{-8} Hz^{-1}.

Table S1 ΔF, ΔD, and Sauerbrey Δm for different complexes

	ΔF±S.D (Hz)	ΔD±S.D (x10^{-6})	Δm±S.D (ng cm^{-2})
Chi–Alg	-190.6±17.6	1.95±0.47	1124±104
ChiC–Alg	-217.9±8.8	4.13±1.66	1285±52
Chi–AlgC	-217.4±17.4	6.16±2.97	1283±103
ChiC–AlgC	-222.2±20.4	5.16±0.21	1311±121

S3 QCM-D: pH cycles

Figure S6 displays QCM-D data obtained for the pH cycles (3 replicas for each multilayer system). It can be seen that Chi-Alg and ChiC-Alg multilayers show large shifts at each cycle, which seem to grow in magnitude after each cycle as well. This can suggest lack of covalent bonds that could preserve the structural integrity of the multilayer. Conversely, Chi-AlgC and ChiC-AlgC multilayers show relatively smaller shifts, which also demonstrate less dependence on the number of cycles. This observation suggests improved stability of the multilayer through covalent cross-linking, mediated by catechol-amine interactions.

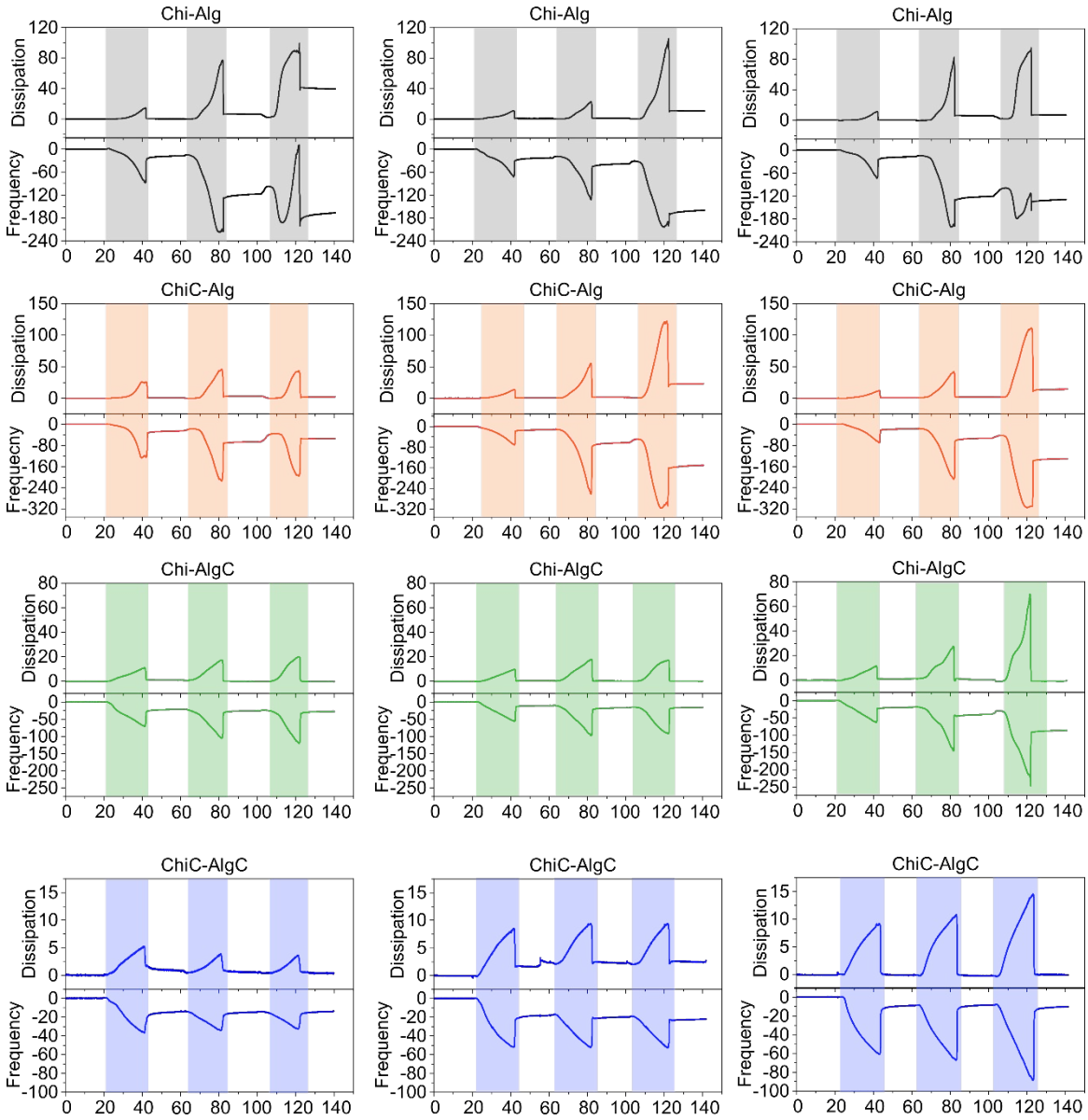

Figure S6 QCM-D data for pH cycles of different complexes

Table S2 also provides the calculated hysteresis after three pH cycles, i.e., the relative shifts in F and D baselines after the third cycle. The trends here also hint to lack of cross-linking in case of Chi-Alg and ChiC-Alg multilayers as indicated by rather large hysteresis in both F and D, suggesting irreversible structural changes in the multilayers. Conversely, Chi-AlgC and ChiC-AlgC multilayers are characterized by relatively smaller hysteresis in F and negligible baseline shift in D, which can hint to a reversible swelling-collapse cycles due to efficient cross-linking.

Table S2 baseline shift (hysteresis = baseline after 3rd cycle - baseline before 1st cycle) as a result of three pH cycles

Sample		D hysteresis after three pH cycle test	ΔD at Mean ± S.D	F hysteresis after three pH cycle test	ΔF at Mean ± S.D
Chi-Alg	1	39.62	18.96±18.00	-169.05	-153.83±19.97
	2	10.52		-161.22	
	3	6.73		-131.21	
ChiC-Alg	1	2.27	13.15±10.46	-54.45	-111.74±50.58
	2	23.13		-150.19	
	3	14.04		-130.59	
Chi-AlgC	1	-0.19	-0.34±0.50	-28.03	-43.76±38.03
	2	0.06		-16.12	
	3	-0.90		-87.13	
ChiC-AlgC	1	0.32	1.00±1.38	-14.55	-16.03±6.12
	2	2.59		-22.75	
	3	0.09		-10.78	

5. Reference

(1) Sauerbrey, G. Verwendung von Schwingquarzen Zur Wägung Dünner Schichten Und Zur Mikrowägung. *Zeitschrift für Phys. 1959 1552* **1959**, *155* (2), 206–222. https://doi.org/10.1007/BF01337937.

(2) Huang, J.; Zajforoushan Moghaddam, S.; Thormann, E. Structural Investigation of a Self-Cross-Linked Chitosan/Alginate Dialdehyde Multilayered Film with in Situ QCM-D and Spectroscopic Ellipsometry. *ACS Omega* **2019**, *4* (1), 2019–2029. https://doi.org/10.1021/acsomega.8b03145.

(3) Huang, J.; Liu, X.; Thormann, E. Surface Forces between Highly Charged Cationic Polyelectrolytes Adsorbed to Silica: How Control of PH and the Adsorbed Amount Determines the Net Surface Charge. *Langmuir* **2018**, *34* (25), 7264–7271. https://doi.org/10.1021/acs.langmuir.8b00909.

PAPER II

A biomimetic water-resistant adhesive based on □-polylysine/tannic acid complexation

Journal:	*ACS Applied Polymer Materials*
Manuscript ID	ap-2023-01400g
Manuscript Type:	Article
Date Submitted by the Author:	28-Jun-2023
Complete List of Authors:	Kang, Junjie; Technical University of Denmark, chemistry Zajforoushan Moghaddam, Saeed; Danmarks Tekniske Universitet, Department of Chemistry Larsen, René; Danmarks Tekniske Universitet, Department of Chemistry Thormann, Esben; Danmarks Tekniske Universitet, Department of Chemistry

A biomimetic water-resistant adhesive based on ε-polylysine/tannic acid complexation

Junjie Kang, Saeed Zajforoushan Moghaddam, René Wugt Larsen, Esben Thormann*

Department of Chemistry, Technical University of Denmark, 2800 Kgs. Lyngby, Denmark

*esth@kemi.dtu.dk

Abstract: This study investigates the potential of combining ε-polylysine and tannic acid to develop bio-based adhesives with enhanced water resistance. The two biomolecules exhibited complexation/precipitation in aqueous solutions with a pH range of 5-9. Water-based adhesives were prepared using complexes formed at pH 5, 7, and 9, followed by evaluating their adhesion properties in both dry and wet lap shear tests. The complexes prepared at higher pH values showed larger adhesion strength and improved water resistance. To further enhance the adhesive properties, an epoxide-based reagent was utilized to double-cross-link the complexes, resulting in a lap shear strength of ~2 MPa after being submerged in water for 7 days.

Keywords: bio-based adhesive, water resistance, polylysine, tannic acid, marine-inspired adhesive

1. Introduction

Extensive research is dedicated to the development of novel adhesives from renewable and less hazardous resources, known as bio-based adhesives.[1,2] Several challenges need to be tackled on this path, with one notable obstacle being the poor water resistance of bio-based adhesives.[3–6] Most biomacromolecules used in developing bio-based adhesives show significant water adsorption and swelling. As a result, such adhesives cannot maintain bonding in humid or wet environments, which limits their widespread use.[7] To overcome this challenge, research is focused on exploring innovative strategies to improve the water resistance of bio-based adhesives.[8–11]

The emulation of adhesion mechanisms found in marine organisms is being actively investigated as a promising strategy for the development of innovative adhesives.[8,12] Organisms such as sea mussels, have evolved intricate adhesion mechanisms that allow them to attach firmly to seashores and underwater environments.[13,14] These natural adhesives, composed primarily of proteins, reveal that biomolecules with precisely optimized compositions could exhibit remarkable water resistance. Research is thus focused on (i) uncovering the underlying physicochemical mechanisms responsible for the wet adhesion of marine organisms and (ii) harnessing this knowledge to develop bio-based adhesives with enhanced water resistance.[15,16]

Several mechanisms are suggested to play a substantial role in mussel adhesion,[14] three of which have been taken as inspiration in our recent studies.[11,17] The first mechanism revolves around the signature amino acid found in the mussel adhesive, i.e., l-3,4-dihydroxyphenylalanine (l-DOPA). The catechol moiety of l-DOPA can form various covalent/non-covalent interactions,[18] enabling robust interfacial adhesion to substrates of

different chemistries,[19] as well as cross-linking and curing of the adhesive proteins.[20] The second mechanism entails the synergistic effects of l-DOPA and lysine, or catechol–amine chemistry. This combination is proposed to facilitate catechol interaction with hydrated surfaces and regulate the cohesive strength of the adhesive through various pathways, including cation–π interactions, Michael addition, and Schiff base reactions.[21] The third mechanism underlines the role of physical phase transitions of the mussel adhesive proteins, particularly through coacervation.[22] This process leads to the formation of a condensed protein-rich phase, which exhibits a remarkable ability to spread onto underwater surfaces without dispersing in seawater.[23,24]

Therefore, as a potential strategy in developing water-resistant bio-based adhesives, one requires catechol or catechol-like groups, amine groups, and a complex condensed phase. This study aimed to explore a potential bio-based candidate that meets these criteria, i.e., ε-poly-l-lysine (ε-PL) and tannic acid (TA). ε-PL is a natural polypeptide composed of lysine building blocks, which is generally recognized as safe (GRAS) and is commercially used as an antimicrobial food preservative.[25] TA is a natural polyphenol with 2-12 galloyl (3,4,5-trihydroxyphenyl) groups, which is also classified as non-hazardous.[26] One of the primary reasons for choosing these two bio-based substances was their high water solubility (unlike most polyphenols and biomacromolecules), which simplifies the preparation process. However, we hypothesized that they, combined in a complex state, could exhibit water resistance given the similarities to the mussel glue chemistry. The amine–galloyl chemistry may mimic the interactions of lysine–Dopa and their corresponding benefits for wet adhesion. Moreover, our initial evaluations showed that the two biomolecules exhibit complex interactions leading to the formation of a dense precipitated phase. This material was

anticipated to show improved water resistance as compared to an adhesive composed of biomolecules in a non-condensed state. Therefore, various ε-PL–TA complexes were prepared under controlled conditions, and their adhesive properties and water resistance were assessed.

2. Experimental Section

2.1 Materials: ε-polylysine (ε-PL, ≥95%) was obtained from Handary (Belgium). Tannic acid (TA, M_w = 1701.20 Da) and glycerol diglycidyl ether (GDE, Mw = 204.22 Da, technical grade) were purchased from Sigma-Aldrich. All solutions were prepared using ultrapure water (Arium® Pro) with a resistivity of 18.2 MΩ cm. pH adjustment was carried out using 10 M NaOH and 10 M HCl aqueous solutions. Other solvents used were of HPLC grade and were not subjected to further purification. Additional characterization data of reagents are available as Supporting Information (Section S1).

2.2 Preparation of ε-PL–TA complexes: ε-PL (40 wt.%) and TA (20 wt.%) solutions were prepared in water without any pH adjustment. Once fully dissolved (after 2 h), the TA solution was added to the ε-PL solution in a 1:1 weight ratio under stirring. The resulting mixture was found to have a pH of ~2.3. The mixture solution was then subjected to different pH adjustments ranging from 3.0 to 10.0, and the resulting precipitate was collected by centrifugation at 6.5 K rpm min^{-1} for 10 min. The collected ε-PL–TA complexes were dried in a vacuum oven (Thermo Scientific, Germany) at 30 ℃ for two days. Subsequently, the dried complexes were finely ground using an agate mortar and stored in a desiccator. Additional characterization data of the dried ε-PL–TA complexes is provided as Supporting Information (Section S2).

2.3 Preparation of ε-PL–TA adhesives: ε-PL–TA adhesives were prepared by mixing ε-PL–TA complex powder with water in a 4:6 weight ratio (adhesive water content = 60 wt.%). In a separate set of adhesives, varying weight ratios of GDE were incorporated (Supporting Information, Section S4).

2.4 Adhesion testing: The lap shear strength of the ε-PL–TA adhesives was evaluated using a testing system (Instron 34Sc, USA) equipped with a 2 kN load cell. Before testing, pre-cut aluminum substrates (L×W×H: 50 mm × 12 mm × 10 mm) were polished and cleaned with ethanol/acetone. The adhesive was then placed between two aluminum substrates with an overlap area of 12 mm × 12 mm and clamped together. The clamped specimens were thermally cured in an oven at 120 ℃ for 10 minutes. After cooling for 1 h, the specimens were subjected to single lap shear testing at a controlled rate of 1.5 mm min^{-1}. To assess the water resistance of the adhesives, the cured specimens were immersed in water for 2 or 7 days, after which the lap shear strength was measured.

2.5 Water solubility: The specimen (dried) was weighed (m_d) and then added to 15 ml of water, followed by vortex mixing at room temperature for 2 days, and then centrifugation (6.5 k rpm min^{-1} for 10 min). The collected precipitate was dried until a final constant weight was achieved (m_r). The residual mass (RM) was calculated as (m_r/m_d) × 100.

2.6 IR Spectroscopy: ATR spectra of specimens were collected using a VERTEX80v Fourier transform vacuum spectrometer (Bruker Optics GmbH Fourier), equipped with a Germanium (Ge) on KBr beam splitter, a liquid N_2-cooled HgCdTe detector, and a thermal globar radiation source. Dried powder specimen was placed on the Ge crystal close-knit. The sample spectra were recorded in blocks of 300 scans within the wavenumber range of 700 and 3800 cm^{-1}, with a resolution of 2 cm^{-1}. Using the same parameters, background spectra of the cleaned

Ge crystal were collected before and after sample measurements. The data were processed and evaluated with the OPUS-7.2 software (Bruker Optik GmbH, Germany). Briefly, the absorption spectra were obtained by averaging the sample and background scans, and further adjustments were made to correct for any residual water vapor absorption occurring in the atmosphere. Following this, a baseline correction was then performed. Finally, an ATR correction was applied to account for the wavelength-dependent penetration depth of the infrared probe beam. **Curve Fitting:** each spectrum was first normalized based on the absorbance of peaks in two different ranges: i) 1416 cm^{-1} to 700 cm^{-1}, and ii) 1050 cm^{-1} to 700 cm^{-1} (Supporting information, Section S4). Wavelength within the ranges from 1250 cm^{-1} to 980 cm^{-1} were selected for Voigt modeling.

3. Results and discussion

3.1 ε-PL–TA complexation: Figure 1 depicts the chemistry, preparation, and characterization of ε-PL–TA complexes. ε-PL, a cationic polypeptide, becomes less charged with pH increment (pKa~9.4).[27] TA, a polyphenol with multiple galloyl groups, undergoes two pathways with increasing pH: (i) deprotonation of hydroxyl groups, resulting in a negative charge (pKa~6.0),[28] and (ii) oxidation into quinone species. The amine and galloyl groups, as well as their corresponding forms at elevated pH, are expected to interact through a variety of physical (hydrogen bonding and ionic bonding)[29] and chemical (covalent Michael addition[30] and reversible Schiff base formation[31,32]) mechanisms, all of which are pH-dependent (Figure 1b).[18] As a result, the net interaction between ε-PL and TA is expected to be pH-dependent.

Figure 1c displays the effect of pH (3-10 range) on the complexation of ε-PL and TA. The initial pH of the mixture containing ε-PL and TA in a 1:1 weight ratio was ~2.3, and no cloudiness or precipitation was observed. However, increasing the pH resulted in

complexation/precipitation, particularly within the pH range of 5-9 (as shown in Figure 1c, d). The absence of complexation/precipitation at pH<5, where TA is nearly uncharged,[28] and at pH>9, where ε-PL is minimally charged,[33] may suggest that ionic forces are the primary driving force behind the observed complexation/precipitation. An XPS analysis (Supporting Information, Section S2) indicated that the complexes produced at pH 5, 7, and 9 have a comparable ε-PL content, estimated to be ~50-60%. However, given that TA undergoes oxidation at ~ pH>7, the chemical structures and interactions of the complexes formed at different pH levels are expected to be different. This is evident from the color change (Figure 1c) observed in the dried complex powders, transitioning from light beige (prepared at pH 5) to dark brown (prepared at pH 9).

To explore the interactions within the complexes, additional investigation was performed using ATR analysis (Figure 1e). In particular, the absorbance bands related to C=O and C=N stretching in the range of 1800-1400 cm^{-1} was investigated. Herein, the complexes prepared at higher pH appear to contain a larger content of these functional groups. The increased content of C=O (1630-1570 cm^{-1}) groups can indicate a larger quinone content with increasing pH. These quinone moieties may form covalent bonds with the amine groups of ε-PL through Michael Addition and Schiff base reactions, producing C-N covalent bonds and dynamic/reversible C=N bonds, respectively. In Figure 1e, with pH increasing, a noticeable gain in the absorbance peak of both C-N (1150-1050 cm^{-1}) and C=N (1700-1630 cm^{-1}) bonds is also found, suggesting oxidative cross-linking reactions. Notably, the relatively larger increase in absorbance for the C=N bond, compared to C-N, as the pH increases from 5 to 9, suggests that Schiff base formation is the primary oxidative coupling reaction. A TGA analysis (Supporting Information, Section S2) also indicated increased thermal stability with increasing pH, which can further affirm covalent cross-linking at higher pH. Such covalent cross-linking

of ε-PL and TA is expected to reduce water solubility and swelling. Consequently, ε-PL–TA complexes prepared at pH 5, 7, and 9 were selected for further investigation of their adhesive properties and water resistance.

3.2 ε-PL–TA adhesives: Figure 2 compares the lap shear strength of ε-PL–TA adhesives (from complexes produced at pH 5, 7, and 9). To make the ε-PL–TA adhesives, the dried complex was mixed with water in a 4:6 weight ratio (Figure 2a). The resulting mixture was applied onto aluminum substrates, clamped, and subjected to thermal curing. Notably, it was found that a thermal curing process of 10 min at 120 °C was necessary for optimal adhesive performance (Supporting Information, Section S3). The bonded specimens were then tested either in dry state or after being submerged in water for 2 and 7 days.

The lap shear adhesion data of ε-PL–TA adhesives under dry and wet conditions are compared in Figure 2b. It was found that complexes produced at higher pH levels result in greater dry adhesion strength (also see Supporting Information, Section S3). This finding confirms that changes in the chemical structure/interactions of the complex occur depending on the pH of the complex preparation. The enhanced adhesion strength might be due to mechanical reinforcement resulting from galloyl–amine covalent cross-linking.

The adhesives' water resistance was demonstrated to follow a similar trend, with the adhesive produced from the pH 9 complex exhibiting the highest water resistance. After 7 days of immersion in water, the adhesive specimens made from pH 5 and pH 7 complexes de-bonded. The adhesive made from pH 9 complex maintained some level of adhesion (0.35 MPa, ~15% of dry strength) under similar wet conditions. The increased water resistance of the complex made at pH 9 suggests higher cross-linking between ε-PL and TA. Comparison with the control specimen (aqueous solution of ε-PL (20 wt.%) and TA (20 wt.%) as the adhesive),

indicates that complexation of ε-PL and TA efficiently contributes to water resistance. Despite both TA and ε-PL being highly water-soluble, their water resistance is overall improved when they are in a complex/condensed state. Additionally, when complexation is combined with chemical cross-linking (as seen for pH 9 complex), it provides even greater water resistance.

Further confirmation of the observed trends is provided by testing the water solubility of ε-PL–TA adhesives (Figure 2c). Since both ε-PL and TA are highly soluble in water, the insoluble matter content can be attributed to the cross-linked part. The results indicate that the complexes prepared at elevated pH exhibit a larger insoluble content, providing additional evidence for covalent cross-linking between ε-PL and TA complexes formed at elevated pH.

3.3 Double-cross-linking via epoxide chemistry: Thus far, it is demonstrated that ε-PL and TA, both highly water-soluble, can be converted into a partly cross-linked and water-resistant adhesive by (i) complexation and (ii) controlling pH of complexation. However, it is worth investigating why the water resistance remains relatively low and whether it can be further enhanced. One potential reason for the relatively poor water resistance could be that the Schiff base bonds are the primary means of forming complex self-crosslinks (as argued in relation to Figure 1e). The imine bonds are reversible in nature,[34] sensitive to acidic pH and moisture,[35] and may alone not provide a prolonged source of cross-linking and water resistance.[32] Though, regardless of having reversible bonds or not, a secondary source of cross-linking is anticipated to further reinforce the adhesives' water resistance.

Having amine and aromatic alcohol functional groups in the complex, epoxide chemistry (Figure 3a) as a promising cross-linking approach was investigated. GDE was selected considering its ability to function as a plasticizer and its overall safe profile.[36–38] The epoxide groups on GDE may react with (i) the hydroxyl groups on TA, resulting in the production of

stable ether bonds (C-O),[36,38,39] and (ii) the amine groups found on ε-PL, producing covalent C-N bonds.[40,41]

The adhesion performance of ε-PL–TA adhesives, including 5 wt.% GDE (relative to the total dry content), is presented in Figure 3b. The optimal concentration of GDE was determined based on the adhesion strength and water resistance testing (Supporting Information, Section S4). The addition of GDE was observed to increase the dry lap shear strength of the complexes across all pH values. Notably, all the adhesives also exhibited enhanced water resistance. The adhesive made from pH 9 complex again demonstrated the highest water resistance, with a lap shear strength of 2.5 MPa (~70% of dry strength) after 2 days and 2.0 MPa (~55% of dry strength) after 7 days of submerging in water. Upon comparison with the control (aqueous solution of ε-PL 19 wt.%, TA 19 wt.%, and GDE 2 wt.%), the impact of complexation on water resistance is once again confirmed.

The water-solubility test was conducted to further investigate the cross-linking effect of GDE. Upon comparing Figure 3c with Figure 2c, it becomes evident that the addition of GDE leads to an increase in the insoluble content of all complexes. For instance, at pH 9, the insoluble content was increased approximately from 80% to 90%. Similarly, the ε-PL–TA adhesive produced from the pH 9 complex exhibited the highest stability. Thus, it can be deduced that GDE induces a cross-linking effect that leads to a decrease in the solubility of the complex adhesive and an improvement in dry and wet lap shear strength. Notably, it appears that the highest reinforcing effect of GDE is found in the complex produced at pH 9, which may indicate that this sample has a larger net degree of cross-linking.

ATR analysis was conducted to examine the interactions of the adhesives including 5 wt.% GDE. The anticipated epoxide–hydroxyl and epoxide–amine reactions are expected to show

an absorption band in the range of 1150-1050 cm^{-1}. Herein, the integrated area under the peak, as a measure of the net content of C-O and C-N groups, or as a measure of cross-linking, was compared for adhesives with and without GDE (Figure 4). For adhesives without GDE, it is shown that the integrated area decreases with increasing the pH of complex preparation. This may be due to the decreased number of hydroxyl groups resulting from the oxidation of TA. When adding GDE, the integrated peak area increases in general for all three complex systems, which may indicate further cross-linking. Notably, the adhesive made from pH 9 complex showed the largest relative gain in peak area (when GDE added), which may suggest a larger cross-linking effect of GDE on this complex.

Finally, dry and wet lap shear strength of the ε-PL–TA adhesive was compared with two commercial bio-based adhesives (UHU Glue and Pritt Glue) and several recently reported mussel-inspired bio-based adhesives (Table 1). The results show that ε-PL–TA/GDE exhibits higher adhesion strength in wet conditions compared to both the commercial controls and the bio-based adhesives reported in the literature, indicating the potential of this system for developing a new generation of bio-based adhesives with enhanced wet adhesion.

4. Conclusion

ε-PL and TA combined show promise as a compelling choice for developing bio-based adhesives with improved water-resistance. Both substances possess a relatively safe profile and readily dissolve in water, making them suitable for preparation methods. Additionally, the two components undergo complexation, which was demonstrated to enhance water-resistance. Particularly, this complexation process is pH-dependent, meaning that the properties of the complex, including the adhesion properties, are adjustable by pH of complex preparation. Herein, it was demonstrated that complexes prepared at higher pH values

exhibit the highest dry and wet adhesion strength. Moreover, the amine- and galloyl-rich composition of ε-PL–TA allows for additional cross-linking chemistries. Herein, we demonstrated that by utilizing an epoxide-based reagent, it is possible to further cross-link the complex and enhance the water resistance of the adhesive.

Author Information

Junie Kang, jukan@kemi.dtu.dk

Saeed Zajforoushan Moghaddam, saza@kemi.dtu.dk

René Wugt Larsen, rewl@kemi.dtu.dk

Esben Thormann (corresponding author), esth@kemi.dtu.dk

Acknowledgment

J. K. acknowledges a stipend from the China Scholarship Council (CSC). S. Z. M. and E. T. acknowledge financial support from Innovation Fund Denmark through the Grand Solutions Project 0175-00008B.

Supplementary Information is available at:

- Characterization data of ε-PL and TA, XPS and TGA characterization of ε-PL–TA complexes, optimization of the ε-PL–TA adhesive composition and thermal curing method, optimization of GDE content based on lap shear testing, and details of ATR-FTIR spectra normalization.

5. Reference

(1) Heinrich, L. A. Future Opportunities for Bio-Based Adhesives – Advantages beyond Renewability. *Green Chem.* **2019**, *21* (8), 1866–1888. https://doi.org/10.1039/C8GC03746A.

(2) Li, J.; Yu, X.; Enciso Martinez, E.; Zhu, J.; Wang, T.; Shi, S.; Shin, S. R.; Hassan, S.; Guo, C.;

Li, J.; Yu, X.; Guo, C.; Zhu, J.; Shi, S.; Martinez, E. E.; León, N.; Wang, M. T.; Shin, S. R.; Hassan, S. Emerging Biopolymer-Based Bioadhesives. *Macromol. Biosci.* **2022**, *22* (2), 2100340. https://doi.org/10.1002/MABI.202100340.

(3) Yamada, K.; Chen, T.; Kumar, G.; Vesnovsky, O.; D. Timmie Topoleski, L.; F. Payne, G. Chitosan Based Water-Resistant Adhesive. Analogy to Mussel Glue. *Biomacromolecules* **2000**, *1* (2), 252–258. https://doi.org/10.1021/bm0003009.

(4) Zhu, X.; Song, C.; Sun, X.; Wang, D.; Cai, D.; Wang, Z.; Chen, Y.; Chen, X. Improved Water Resistance of TA-Modified Soy Adhesive: Effect of Complexation. *Int. J. Adhes. Adhes.* **2021**, 102858. https://doi.org/10.1016/j.ijadhadh.2021.102858.

(5) David B. Tiu, B.; Delparastan, P.; R. Ney, M.; Gerst, M.; B. Messersmith, P. Enhanced Adhesion and Cohesion of Bioinspired Dry/Wet Pressure-Sensitive Adhesives. *ACS Appl. Mater. & Interfaces* **2019**, *11* (31), 28296–28306. https://doi.org/10.1021/acsami.9b08429.

(6) Cui, C.; Liu, W. Recent Advances in Wet Adhesives: Adhesion Mechanism, Design Principle and Applications. *Prog. Polym. Sci.* **2021**, 101388. https://doi.org/10.1016/j.progpolymsci.2021.101388.

(7) Suárez, J. C. Bioadhesives. *Handb. Adhes. Technol.* **2011**, 1385–1408. https://doi.org/10.1007/978-3-642-01169-6_53.

(8) Stewart, R. J.; Ransom, T. C.; Hlady, V. Natural Underwater Adhesives. *J. Polym. Sci. Part B Polym. Phys.* **2011**, *49* (11), 757–771. https://doi.org/10.1002/POLB.22256.

(9) Kollbe Ahn, B. Perspectives on Mussel-Inspired Wet Adhesion. *J. Am. Chem. Soc.* **2017**, *139* (30), 10166–10171. https://doi.org/10.1021/jacs.6b13149.

(10) Zeng, G.; Zhou, Y.; Wang, T.; Li, K.; Dong, Y.; Li, J.; Li, J.; Fang, Z. A Bio-Based Adhesive Reinforced with Functionalized Nanomaterials to Build Multiple Strong and Weak Cross-Linked Networks with High Strength and Excellent Mold Resistance. *Chem. Eng. J.* **2023**, *453*, 139761. https://doi.org/10.1016/J.CEJ.2022.139761.

(11) ZajforoushanMoghaddam, S.; Qie, R.; Thormann, E. Making Protein-Based Adhesives Water Resistant: Role of Protein Water Solubility, Galloyl Modification, and Complexation. *ACS Appl.*

Polym. Mater. **2021**, *0* (0). https://doi.org/10.1021/acsapm.1c01089.

(12) Cui, M.; Ren, S.; Wei, S.; Sun, C.; Zhong, C. Natural and Bio-Inspired Underwater Adhesives: Current Progress and New Perspectives. *APL Mater.* **2017**, *5* (11), 116102. https://doi.org/10.1063/1.4985756.

(13) Silverman, H. G.; Roberto, F. F. Understanding Marine Mussel Adhesion. *Mar. Biotechnol.* **2007**, *9* (6), 661–681. https://doi.org/10.1007/S10126-007-9053-X/FIGURES/5.

(14) Waite, J. H. Mussel Adhesion – Essential Footwork. *J. Exp. Biol.* **2017**, *220* (4), 517–530. https://doi.org/10.1242/JEB.134056.

(15) Cai, C.; Chen, Z.; Chen, Y.; Li, H.; Yang, Z.; Liu, H. Mechanisms and Applications of Bioinspired Underwater/Wet Adhesives. *J. Polym. Sci.* **2021**, *59* (23), 2911–2945. https://doi.org/10.1002/POL.20210521.

(16) Ma, Y.; Zhang, B.; Frenkel, I.; Zhang, Z.; Pei, X.; Zhou, F.; He, X. Mussel-Inspired Underwater Adhesives-from Adhesion Mechanisms to Engineering Applications: A Critical Review. **2021**, *6*, 739–760. https://doi.org/10.7569/RAA.2021.097308.

(17) Qie, R.; Zajforoushan Moghaddam, S.; Thormann, E. A Curable Underwater Adhesive Based on Poly(Propylene Oxide) and Tannic Acid Coacervate. *ACS Appl. Polym. Mater.* **2022**, *5*. https://doi.org/10.1021/ACSAPM.2C02018/ASSET/IMAGES/LARGE/AP2C02018_0002.JPEG.

(18) Yang, J.; Stuart, M. A. C.; Kamperman, M. Jack of All Trades: Versatile Catechol Crosslinking Mechanisms. *Chem. Soc. Rev.* **2014**, *43* (24), 8271–8298. https://doi.org/10.1039/C4CS00185K.

(19) Yang, B.; Lim, C.; Hwang, D. S.; Cha, H. J. Switch of Surface Adhesion to Cohesion by Dopa-Fe3+ Complexation, in Response to Microenvironment at the Mussel Plaque/Substrate Interface. *Chem. Mater.* **2016**, *28* (21), 7982–7989. https://doi.org/10.1021/ACS.CHEMMATER.6B03676/ASSET/IMAGES/LARGE/CM-2016-03676M_0007.JPEG.

(20) Maier, G. P.; Bernt, C. M.; Butler, A. Catechol Oxidation: Considerations in the Design of Wet Adhesive Materials. *Biomater. Sci.* **2018**, *6* (2), 332–339.

https://doi.org/10.1039/C7BM00884H.

(21) Guo, Q.; Chen, J.; Wang, J.; Zeng, H.; Yu, J. Recent Progress in Synthesis and Application of Mussel-Inspired Adhesives. *Nanoscale* **2020**, *12* (3), 1307–1324. https://doi.org/10.1039/c9nr09780e.

(22) Wei, W.; Tan, Y.; Martinez Rodriguez, N. R.; Yu, J.; Israelachvili, J. N.; Waite, J. H. A Mussel-Derived One Component Adhesive Coacervate. *Acta Biomater.* **2014**, *10* (4), 1663–1670. https://doi.org/10.1016/j.actbio.2013.09.007.

(23) Kim, H. J.; Yang, B.; Park, T. Y.; Lim, S.; Cha, H. J. Complex Coacervates Based on Recombinant Mussel Adhesive Proteins: Their Characterization and Applications. *Soft Matter* **2017**, *13* (42), 7704–7716. https://doi.org/10.1039/C7SM01735A.

(24) Forooshani, P. K.; Lee, B. P. Recent Approaches in Designing Bioadhesive Materials Inspired by Mussel Adhesive Protein. *J. Polym. Sci. Part A Polym. Chem.* **2017**, *55* (1), 9–33. https://doi.org/10.1002/POLA.28368.

(25) Bo, T.; Han, P. P.; Su, Q. Z.; Fu, P.; Guo, F. Z.; Zheng, Z. X.; Tan, Z. L.; Zhong, C.; Jia, S. R. Antimicrobial ε-Poly-l-Lysine Induced Changes in Cell Membrane Compositions and Properties of Saccharomyces Cerevisiae. *Food Control* **2016**, *61*, 123–134. https://doi.org/10.1016/J.FOODCONT.2015.09.018.

(26) Guo, J.; Sun, W.; Kim, J. P.; Lu, X.; Li, Q.; Lin, M.; Mrowczynski, O.; Rizk, E. B.; Cheng, J.; Qian, G.; Yang, J. Development of Tannin-Inspired Antimicrobial Bioadhesives. *Acta Biomater.* **2018**, *72*, 35–44. https://doi.org/10.1016/J.ACTBIO.2018.03.008.

(27) Guo, L.; Fang, Y.; Shao, Z.; Fang, S.; Li, Y.; Chen, J.; Meng, Y. PH-Induced Structural Transition during Complexation and Precipitation of Sodium Caseinate and ε-Poly-l-Lysine. *Int. J. Biol. Macromol.* **2020**, *154*, 644–653. https://doi.org/10.1016/J.IJBIOMAC.2020.03.062.

(28) He, Z.; Hu, Y.; Gui, Z.; Zhou, Y.; Nie, T.; Zhu, J.; Liu, Z.; Chen, K.; Liu, L.; Leong, K. W.; Cao, P.; Chen, Y.; Mao, H. Q. Sustained Release of Exendin-4 from Tannic Acid/Fe (III) Nanoparticles Prolongs Blood Glycemic Control in a Mouse Model of Type II Diabetes. *J. Control. Release* **2019**, *301*, 119–128. https://doi.org/10.1016/J.JCONREL.2019.03.014.

(29) Li, K.; Jin, S.; Zeng, G.; Zhou, Y.; Zhang, F.; Li, J.; Shi, S. Q.; Li, J. Biomimetic Development of a Strong, Mildew-Resistant Soy Protein Adhesive via Mineral–Organic System and Phenol-Amine Synergy. *Ind. Crops Prod.* **2022**, *187*, 115412. https://doi.org/10.1016/J.INDCROP.2022.115412.

(30) Lee, H.; Scherer, N. F.; Messersmith, P. B. Single-Molecule Mechanics of Mussel Adhesion. *Proc. Natl. Acad. Sci. U. S. A.* **2006**, *103* (35), 12999–13003. https://doi.org/10.1073/PNAS.0605552103/SUPPL_FILE/05552SUPPTEXT.PDF.

(31) Yang, J.; Saggiomo, V.; Velders, A. H.; Stuart, M. A. C.; Kamperman, M. Reaction Pathways in Catechol/Primary Amine Mixtures: A Window on Crosslinking Chemistry. *PLoS One* **2016**, *11* (12), e0166490. https://doi.org/10.1371/JOURNAL.PONE.0166490.

(32) Xin, Y.; Yuan, J. Schiff's Base as a Stimuli-Responsive Linker in Polymer Chemistry. https://doi.org/10.1039/c2py20290e.

(33) Choi, J. H.; Kim, S. O.; Linardy, E.; Dreaden, E. C.; Zhdanov, V. P.; Hammond, P. T.; Cho, N. J. Influence of PH and Surface Chemistry on Poly(l -Lysine) Adsorption onto Solid Supports Investigated by Quartz Crystal Microbalance with Dissipation Monitoring. *J. Phys. Chem. B* **2015**, *119* (33), 10554–10565. https://doi.org/10.1021/ACS.JPCB.5B01553/SUPPL_FILE/JP5B01553_SI_001.PDF.

(34) Liguori, A.; Hakkarainen, M. Designed from Biobased Materials for Recycling: Imine-Based Covalent Adaptable Networks. **2022**. https://doi.org/10.1002/marc.202100816.

(35) Gu, J.; Cheng, W. P.; Liu, J.; Lo, S. Y.; Smith, D.; Qu, X.; Yang, Z. PH-Triggered Reversible "Stealth" Polycationic Micelles. *Biomacromolecules* **2008**, *9* (1), 255–262. https://doi.org/10.1021/BM701084W/ASSET/IMAGES/LARGE/BM-2007-01084W_0008.JPEG.

(36) Chen, X.; Pizzi, A.; Fredon, E.; Gerardin, C.; Li, J.; Zhou, X.; Du, G. Preparation and Properties of a Novel Type of Tannin-Based Wood Adhesive. *https://doi.org/10.1080/00218464.2020.1863215* **2020**. https://doi.org/10.1080/00218464.2020.1863215.

(37) Mora, A. S.; Tayouo, R.; Boutevin, B.; David, G.; Caillol, S. A Perspective Approach on the

Amine Reactivity and the Hydrogen Bonds Effect on Epoxy-Amine Systems. *Eur. Polym. J.* **2020**, *123*, 109460. https://doi.org/10.1016/J.EURPOLYMJ.2019.109460.

(38) Li, R. J.; Gutierrez, J.; Chung, Y. L.; Frank, C. W.; Billington, S. L.; Sattely, E. S. A Lignin-Epoxy Resin Derived from Biomass as an Alternative to Formaldehyde-Based Wood Adhesives. *Green Chem.* **2018**, *20* (7), 1459–1466. https://doi.org/10.1039/C7GC03026F.

(39) Shechter, L.; Wynstra, J. Glycidyl Ether Reactions with Alcohols, Phenols, Carboxylic Acids, and Acid Anhydrides. *Ind. Eng. Chem.* **2002**, *48* (1), 86–93. https://doi.org/10.1021/IE50553A028.

(40) Stropoli, S. J.; Elrod, M. J. Assessing the Potential for the Reactions of Epoxides with Amines on Secondary Organic Aerosol Particles. *J. Phys. Chem. A* **2015**, *119* (40), 10181–10189. https://doi.org/10.1021/ACS.JPCA.5B07852/ASSET/IMAGES/MEDIUM/JP-2015-07852M_0003.GIF.

(41) Azizi, N.; Saidi, M. R. Highly Chemoselective Addition of Amines to Epoxides in Water. *Org. Lett.* **2005**, *7* (17), 3649–3651. https://doi.org/10.1021/OL051220Q/SUPPL_FILE/OL051220QSI20050706_034638.PDF.

(42) Schmidt, G.; Hamaker, B. R.; Wilker, J. J. High Strength Adhesives from Catechol Cross-Linking of Zein Protein and Plant Phenolics. *Adv. Sustain. Syst.* **2018**, *2* (3), 1700159. https://doi.org/10.1002/ADSU.201700159.

(43) Wang, Z.; Zhang, S.; Zhao, S.; Kang, H.; Wang, Z.; Xia, C.; Yu, Y.; Li, J. Facile Biomimetic Self-Coacervation of Tannic Acid and Polycation: Tough and Wide PH Range of Underwater Adhesives. *Chem. Eng. J.* **2021**, *404*, 127069. https://doi.org/10.1016/J.CEJ.2020.127069.

(44) Jenkins, C. L.; Siebert, H. M.; Wilker, J. J. Integrating Mussel Chemistry into a Bio-Based Polymer to Create Degradable Adhesives. *Macromolecules* **2017**, *50* (2), 561–568. https://doi.org/10.1021/ACS.MACROMOL.6B02213/SUPPL_FILE/MA6B02213_SI_001.PDF.

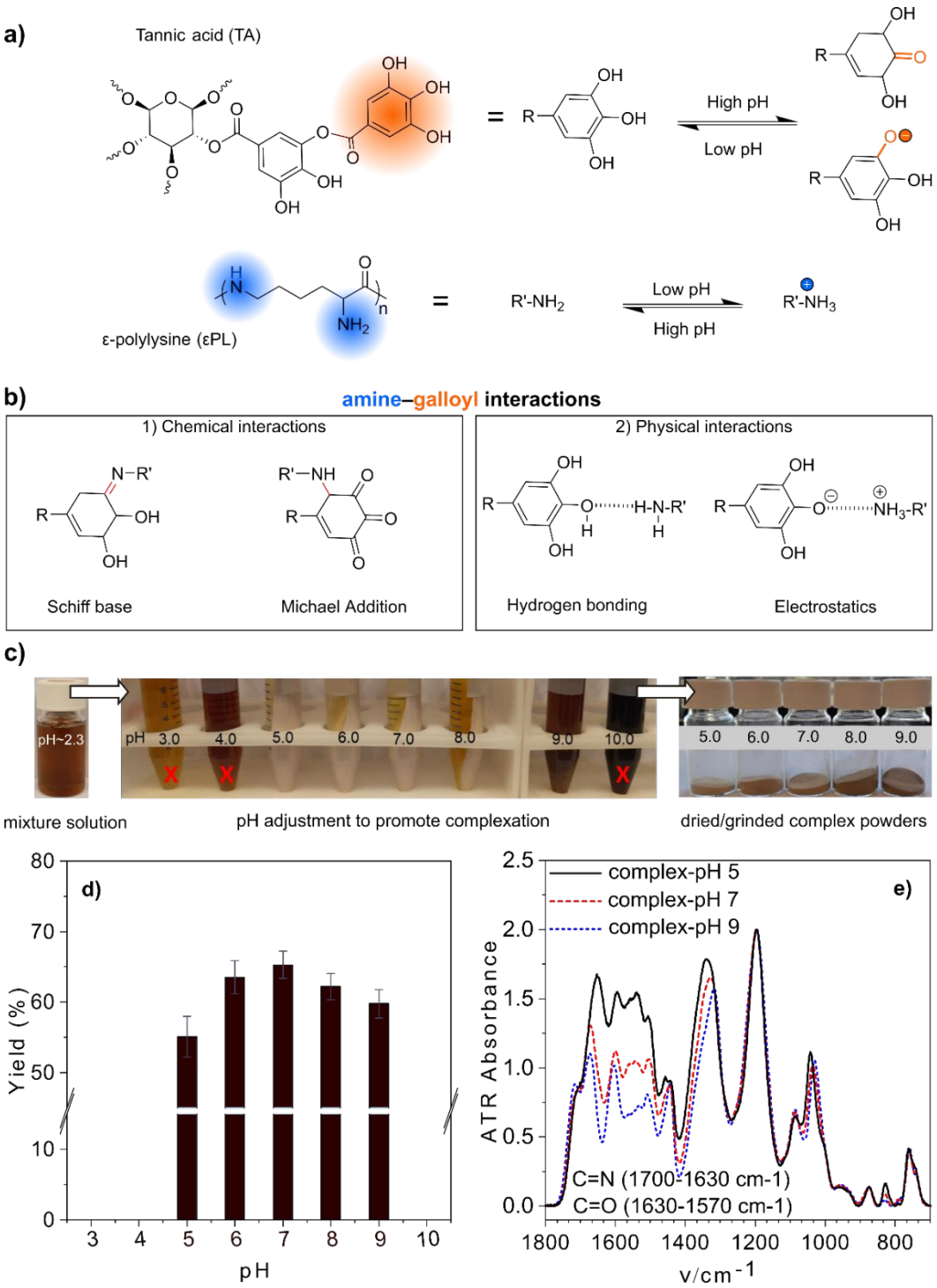

Figure 1 ε-PL–TA complexation: (a) chemical structure and pH-responsive chemistry of ε-PL and TA, (b) possible chemical and physical interactions between the amine groups of ε-PL and the galloyl groups of TA, (c) preparation of ε-PL–TA complexes at

different pH values, (d) yield of complexation at different pH, (e) ATR spectra of complexes (dried powder) prepared at pH 5, 7, and 9.

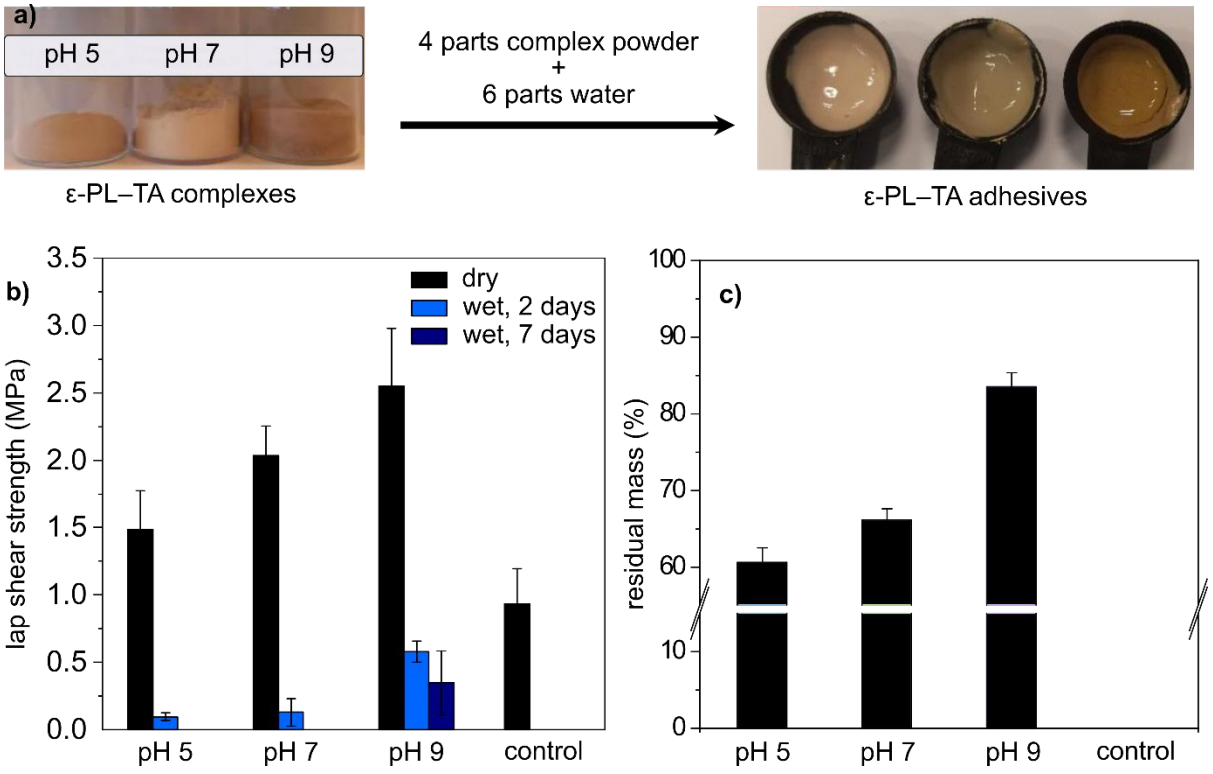

Figure 2 ε-PL–TA adhesives: a) Preparation of ε-PL–TA adhesives from dried complex powders, b) lap shear adhesion strength of ε-PL–TA adhesives (from complexes prepared at pH 5, 7, and 9) measured dry and wet after 2 & 7 days of underwater immersion, c) insoluble matter (residual mass) of ε-PL–TA adhesives after 48 h of water immersion.

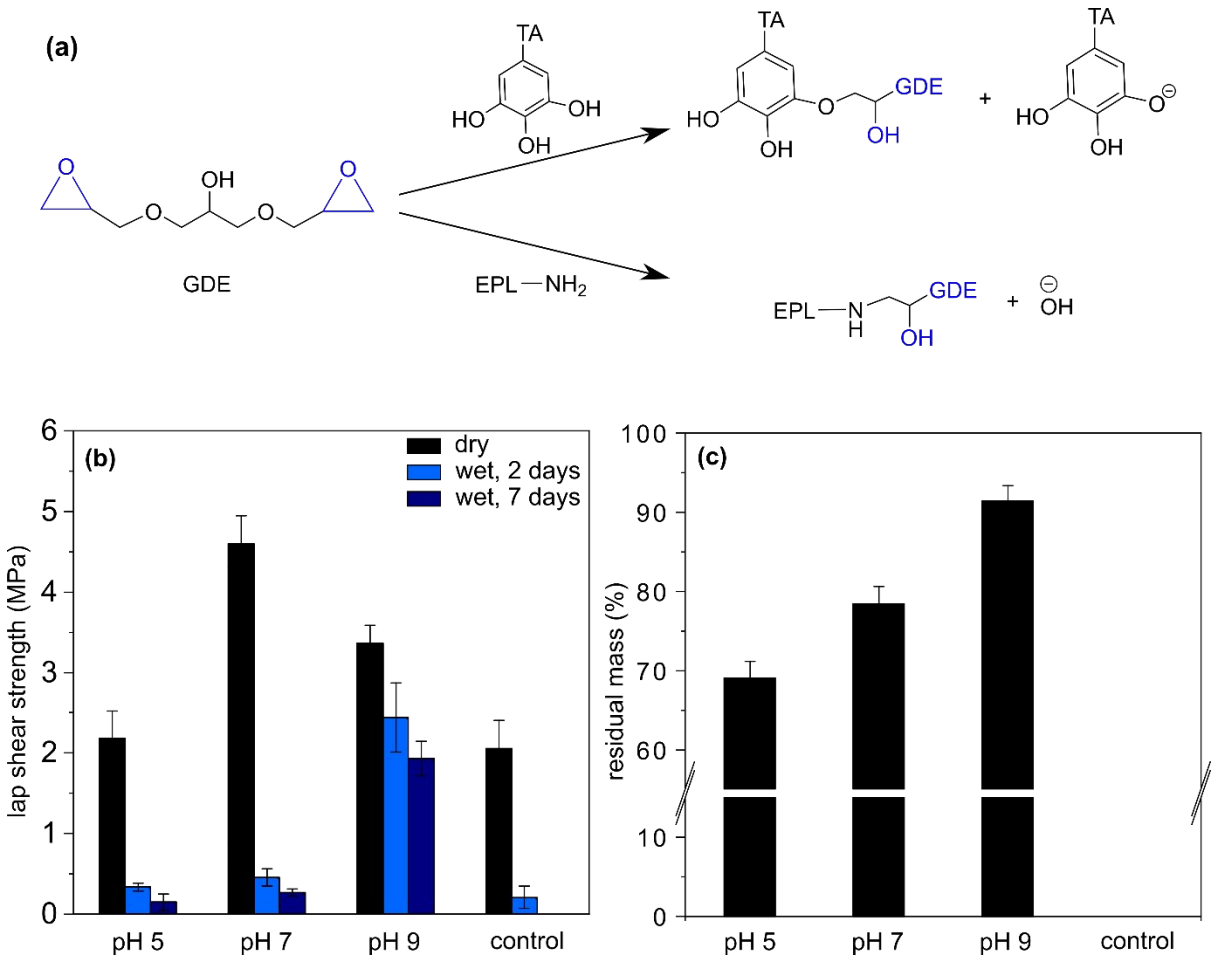

Figure 3 ε-PL–TA adhesives with GDE added as cross-linker: a) possible covalent cross-linking of GDE with ε-PL and TA, b) lap shear adhesion strength of ε-PL–TA adhesives with 5 wt.% GDE (from complexes prepared at pH 5, 7, and 9) measured dry and wet after 2 & 7 days of underwater immersion, c) insoluble matter (residual mass) of ε-PL–TA adhesives with 5 wt.% GDE after 48 h of water immersion.

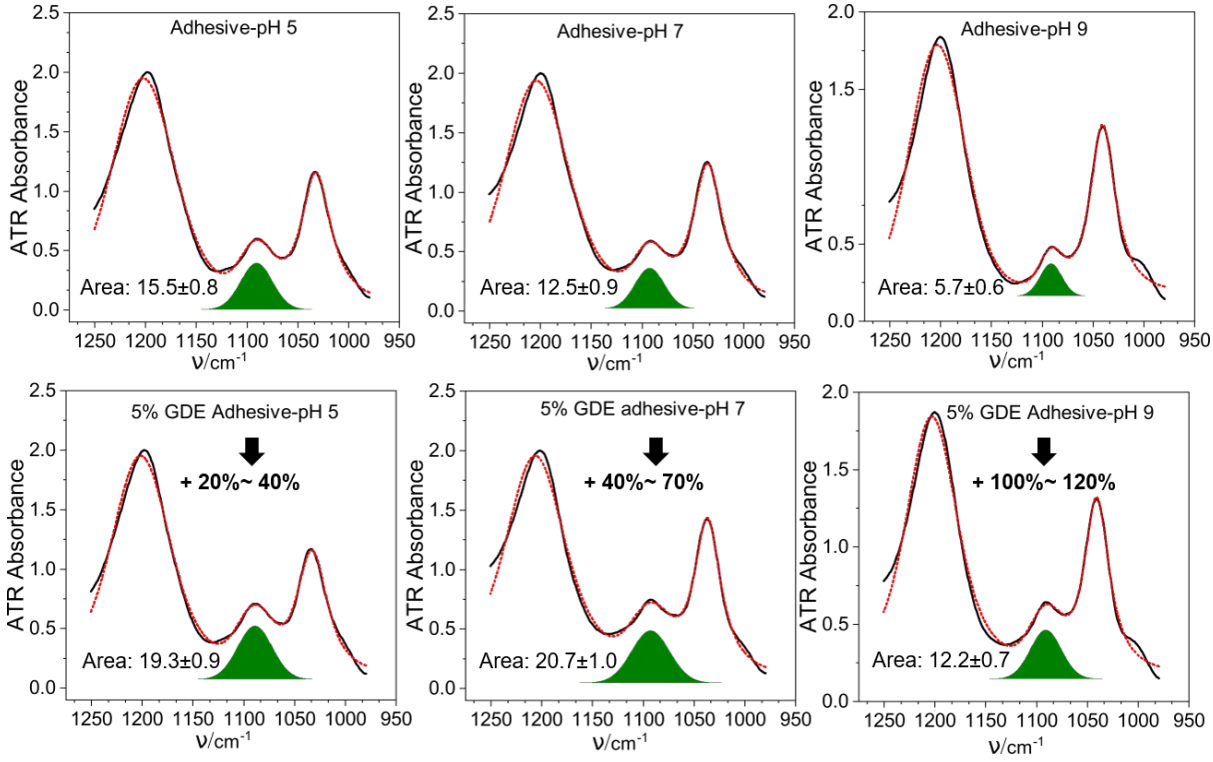

Figure 4 ATR spectra of ε-PL–TA adhesives with and without GDE

Table 1 Dry and wet lap shear adhesion strength of ε-PL–TA adhesive (from complex made at pH 9, with 5 wt.% GDE) compared with two commercial bio-based adhesives and literature.

Adhesive	Adhesion [MPa] in dry state	Adhesion in wet condition		ref
		[MPa]	Soaking time [hr]	
ε-PL–TA	3.36 ± 0.22	2.44 ± 0.42	48	
UHU Glue	1.04 ± 0.27	0.58 ± 0.23	48	
Pritt Glue	0.74 ± 0.3	-	48	
Zein-TA	7.5	3.5	72	[11]
Gelatin-TA	6.3	0.3	24	[11]
Zein-catechol	7.5 ± 0.7	0.3 ± 0.2	24	[42]
PAE-TA	1.55 ± 0.08	0.26 ± 0.01	24	[43]
PLA-catechol copolymers	2.6 ± 0.4	1.0 ± 0.3	24	[44]

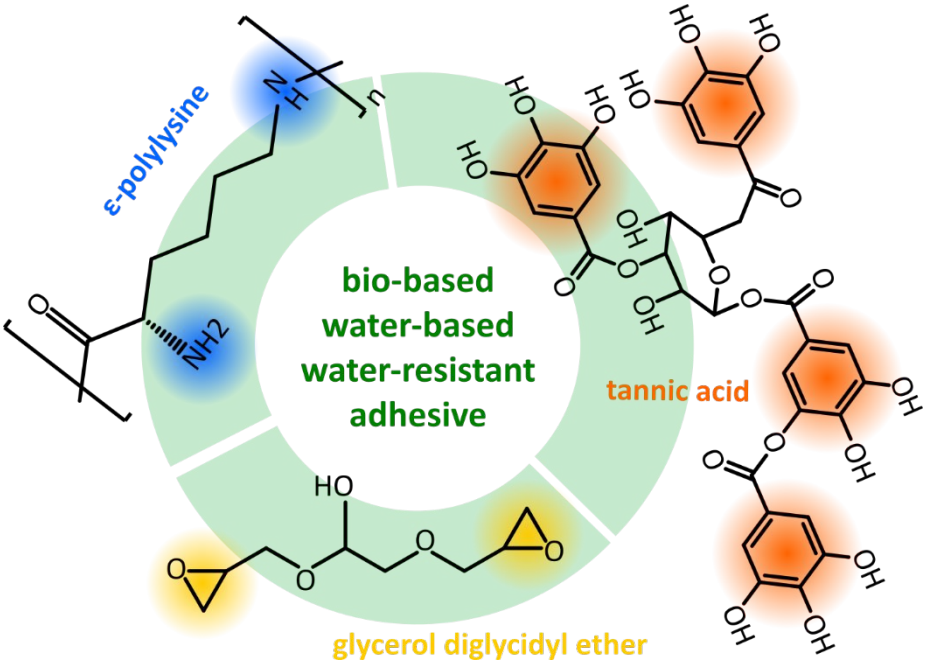

Graphical Abstract

Supporting Information

A biomimetic water-resistant adhesive based on ε-polylysine/tannic acid complexation

*Junjie Kang, Saeed Zajforoushan Moghaddam, René Wugt Larsen, Esben Thormann**

Department of Chemistry, Technical University of Denmark, 2800 Kgs. Lyngby, Denmark

S1. Characterization of ε-PL and TA: Figure S1 displays the ^{1}H-NMR and ^{13}C-NMR spectra of ε-PL used in this study, which is in accordance with previous reports.[1] The NMR measurements were carried out on a Bruker Avance, 400 MHz using D_2O as a solvent and TMS as an internal reference. The acquired data was processed with the software of Mestrenova 11.0.0.

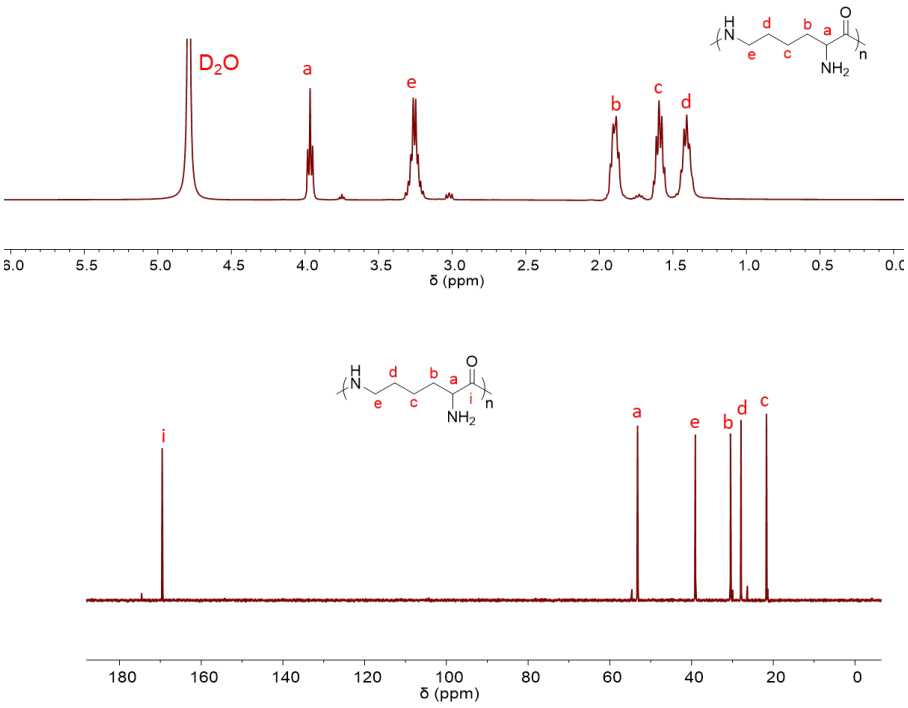

Figure S1 ^{1}H-NMR (top) and ^{13}C-NMR (bottom) spectra of ε-PL

Figure S2 depicts the FTIR spectra of TA and ε-PL. The spectra were collected using a VERTEX80v Fourier transform vacuum spectrometer from Bruker Optics GmbH Fourier. The FTIR spectrum of TA (Figure S2a) exhibited peaks at 3640-3000 cm^{-1} and 1700-1630 cm^{-1}, corresponding to the functional groups of O-H and C=O, respectively.[3] Pure ε-PL (Figure S2b) displayed peaks in the range of 3500-3000 cm^{-1} (N-H stretching) and 1650-1550 cm^{-1} (N-H bending), which can be attributed to the amine functional group (-NH_2-).[4]

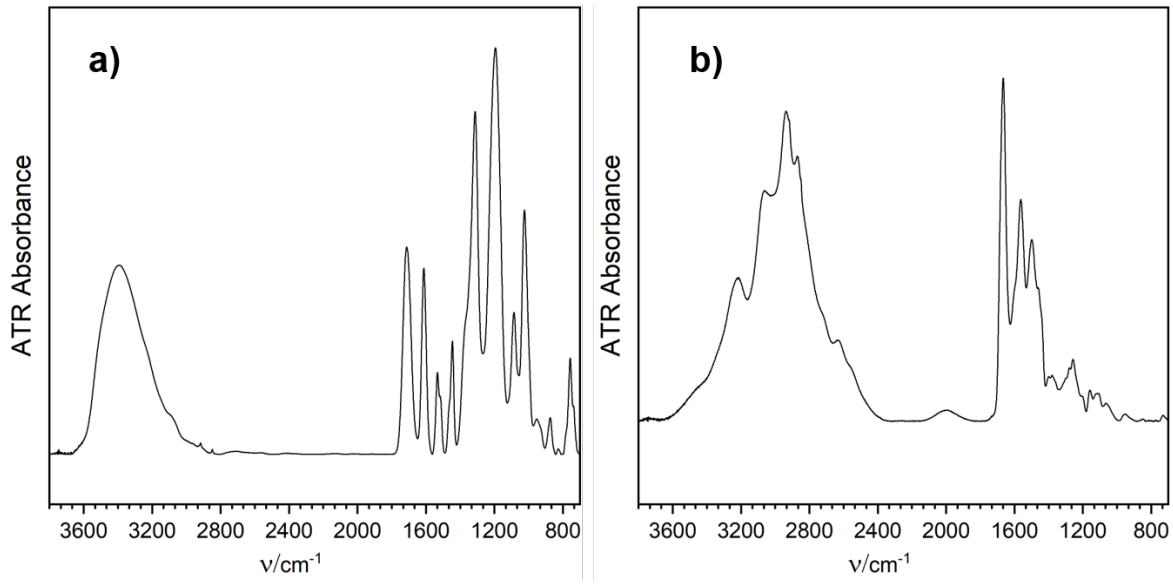

Figure S2 ATR spectra of (a) TA and (b) ε-PL.

2. Characterization of ε-PL–TA complexes: X-ray photoelectron spectroscopy (XPS) measurements were conducted using a Thermo Scientific K-Alpha X-ray photoelectron spectrometer equipped with a hemispherical analyser and an Al Ka micro-focused monochromator. Herein, the elemental content of nitrogen was used to estimate the content of ε-PL in ε-PL–TA complexes. As shown in Table S1, ε-PL–TA complexes are estimated to contain ~ 50-60% ε-PL, depending on pH of complexation.

Table S1 XPS determination for ε-PL and TA weight ratio of dry complexes prepared at pH 5, 7, and 9. (n=3)

	Elemental weight ratio (%)			Content of E-PL and TA	
	C	N	O	E-PL (wt.%)	TA (wt.%)
Polylysine ($C_6H_{12}N_2O$)	65.448	20.255	14.297	100	-
Tannic acid ($C_{76}H_{52}O_{46}$)	60.621	-	39.379	-	100
Complex-pH 5	61.245	9.9876	28.767	49.31	50.69
Complex-pH 7	62.177	11.926	25.898	58.88	41.12
Complex-pH 9	61.075	10.772	28.153	53.18	46.82

TGA 5500 analyzer (Mettler Toledo, Guyancourt, France) was used to examine the thermal stability of ε-PL–TA complexes. Samples weighing ~3-5 mg were placed into a platinum pan and heated at a rate of 10 °C min^{-1} under a nitrogen flow of 20 ml min^{-1}, within the temperature range of 25 to 800 °C. The corresponding curves and their first derivatives (DTGA) for each specimen are presented in Figure S3. At 800 °C, the residual weights of ε-PL and TA were approximately 7% and 25%, respectively. Both TA and ε-PL demonstrated two-step thermal degradation behaviors. For the ε-PL–TA complexes, a higher residual weight was observed compared to ε-PL and TA, and

a new step for thermal degradation was also detected, with pH 9 complex being in the top. These findings suggest that complexation at elevated pH appear to provide more covalent bonding between ε-PL and TA.

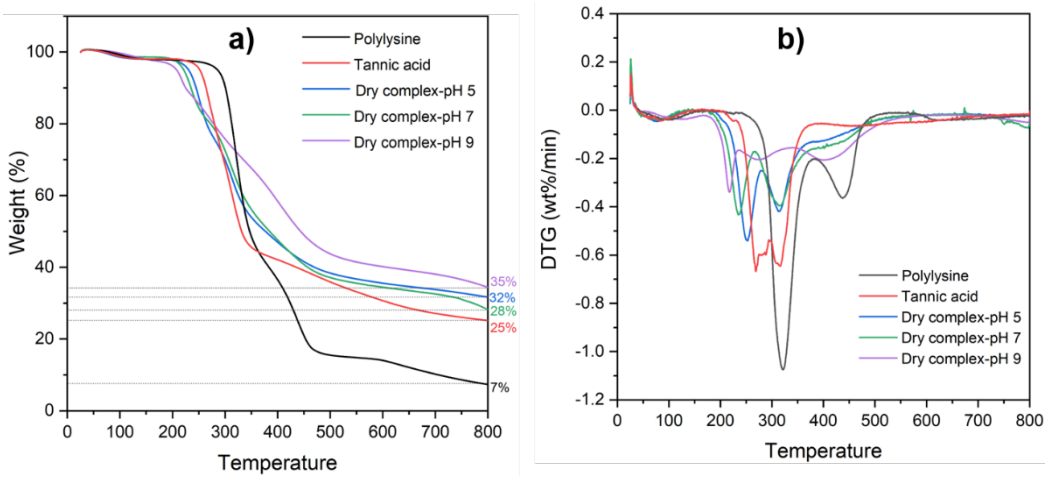

Figure S3 a) TG and b) DTG curves of E-PL, TA, and three complexes prepared at pH 5, 7, and 9.

3. ε-PL–TA adhesive: curing optimization:

Thermal curing: we found that ε-PL–TA adhesive requires thermal curing to achieve maximal performance. This was based on observation of nearly-zero dry lap shear strength of specimens that were left to dry/cure at room temperature for 48 hr. Herein, the adhesive line after drying was found to be non-uniform and cluster-like rather than cohesive film. For this reason, we investigated thermal curing as a solution. It was found that a short thermal treatment appear to produce a sort of phase transition, yielding a uniform and homogenous adhesive film.

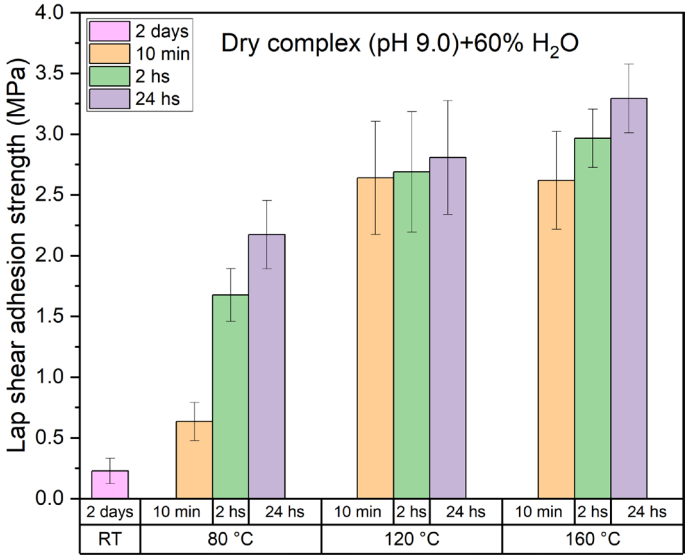

Figure S4 Lap shear adhesion strength effect of temperature and time on mechanical properties

The effect of curing temperature/duration on the adhesive properties of ε-PL–TA adhesive was then investigated. As shown in Figure S4, the lap shear strength of ε-PL–TA adhesives strongly depends on the curing temperature/time. When cured at room temperature, a poor adhesion strength ~ 0.25 MPa is found. Contrarily, curing at elevated temperatures significantly improved

the adhesive properties, depending on both curing temperature and time. Accordingly, curing at 120 °C for 10 min was selected as the optimum condition.

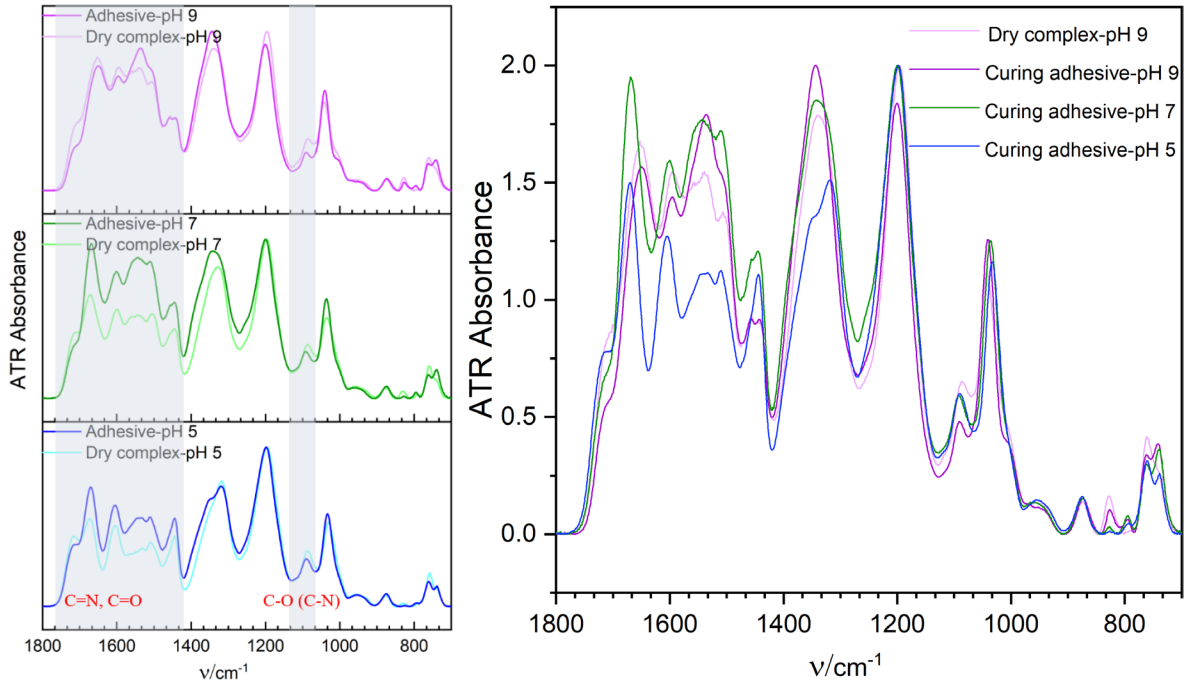

Figure S5 ATR spectra of dry ε-PL–TA complex and ε-PL–TA adhesive after thermal curing

To explore possible cross-linking reactions induced by thermal curing,[5] Fourier transform infrared (FTIR) spectroscopy was conducted (Figure S5). For this reason, for each complex, ATR spectra of complex powder and adhesive after thermal curing were first compared (left panel). The analysis was focused on two distinct regions of the spectra, before and after thermal curing:

- C=O/C=N stretching in 1800-1400 cm^{-1}
- C-O/C-N stretching in 1150-1050 cm^{-1}

The peak at 1150-1050 cm^{-1} showed a minor decrease in intensity, which may hint to decrease in C-O content due to oxidation of TA. More importantly, the peaks at 1800-1400 cm^{-1} showed a

more pronounced gain after thermal curing. Such gain can be attributed to the formation of C=O bonds due to TA oxidation, also may hint to formation of Schiff base bonds between TA and ε-PL. Notably, the effect of thermal curing herein is more pronounced for pH 5 and pH 7 complexes.

Additionally, the ATR spectra of the three adhesives (made from pH 5, 7, and 9 complexes) were compared against pH 9 complex before thermal curing. Overall, it can be seen that the complex made at pH, before and after thermal curing, shows larger absorption in 1800-1400 cm^{-1} range, which can indicate higher level of oxidation and covalent cross-linking in this sample.

Effect of pH: as discussed in the manuscript, the lap shear strength of the ε-PL–TA adhesive depends on the pH of complex preparation. Figure S6 depicts the dry lap shear strength of ε-PL–TA adhesives prepared from complexes made at different pH value.

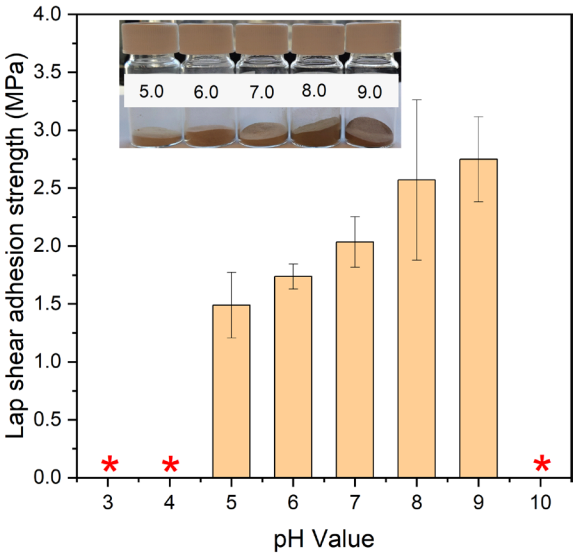

Figure S6 Lap shear adhesion strength of ε-PL–TA adhesives as a function of pH values (curing at 120 ℃ for 10 min, ε-PL 40 wt.% and TA 20 wt.%, red asterisk: no complexes formation).

Effect of TA concentration: we also investigated if the weight ratio between ε-PL and TA (when preparing the complex) has an impact on the lap shear strength of the adhesive. To do so, the concentration of TA in its initial solution was systematically varied, while keeping the mixing ratio fixed to 1:1. As shown in Figure S7, the amount of dried complex (precipitate) increased with the concentration of TA. However, no significant effect was found on the dry lap shear strength; hence, 20 wt.% TA solution was selected for the next studies.

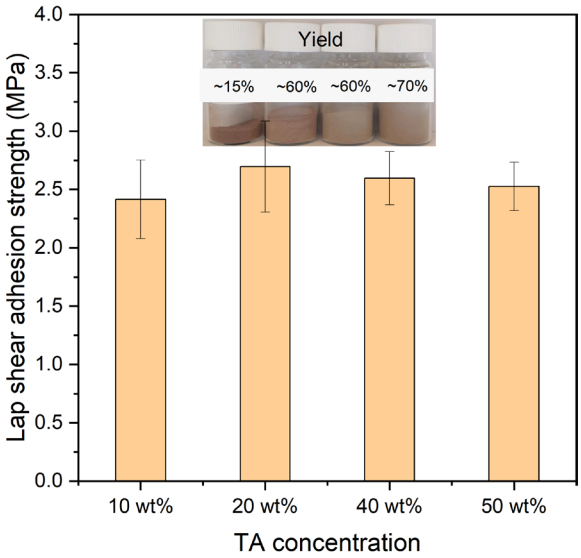

Figure S7 Lap shear adhesion strength of ε-PL–TA as a function of TA concentration; all complexes were made at pH 9, using 40 wt.% ε-PL solution, and a mixing ratio of 1:1.

4. ε-PL–TA adhesives treated by GDE: Table S2 summarizes the composition of all adhesives prepared in this study.

Table S2 formulation of ε-PL-TA adhesives with GDE treatment

Adhesive	Mass of dry complex (g)	Mass of Water (g)	Mass of GDE (g)
0% GDE	0.8		-
2.5% GDE	0.78		0.02
5% GDE	0.76	1.2	0.04
10% GDE	0.72		0.08
20% GDE	0.64		0.16

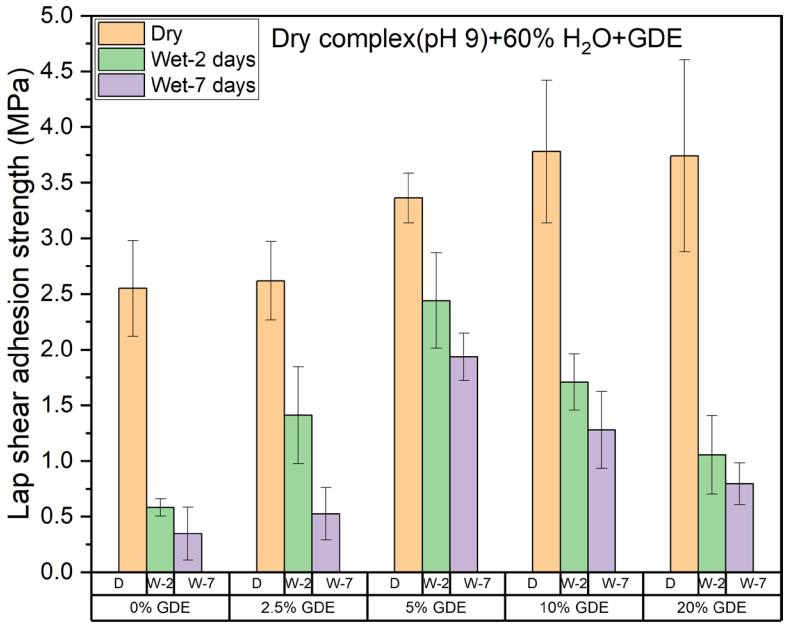

Figure S8 Dry and wet lap shear strength of ε-PL–TA adhesives (prepared from the complex made at pH 9) with different GDE content

Figure S8 depicts the effect of GDE content on the dry/wet lap shear strength of the ε-PL–TA adhesives. Overall, a rather monotonic grow in the dry lap shear strength was found, which can be attributed to both cross-linking and plasticizing abilities of GDE. However, it was found that the maximal wet lap shear strength is achieved at ~5% GDE (relative to the total dry content),

which may suggest that higher GDE content increases the soluble content of the adhesive and thus deteriorates water-resistance.

ATR peak integral analysis: To assess the extent of crosslinking for different complexes, ATR measurements were conducted on ε-PL–TA adhesives with and without GDE treatment. As discussed in the manuscript, the integral area of the peak at 1150-1050 cm^{-1} was considered a measure of GDE cross-linking (content of C-O/C-N). Here, we studied if spectra normalization affects the observed trends in general. For this reason, the data were normalized using two different ranges of the spectra, i.e., 700-1416 cm^{-1} (Figure S9) and 700-1050 cm^{-1} (Figure S10). I was found that the trends remain consistent regardless of the normalization parameters.

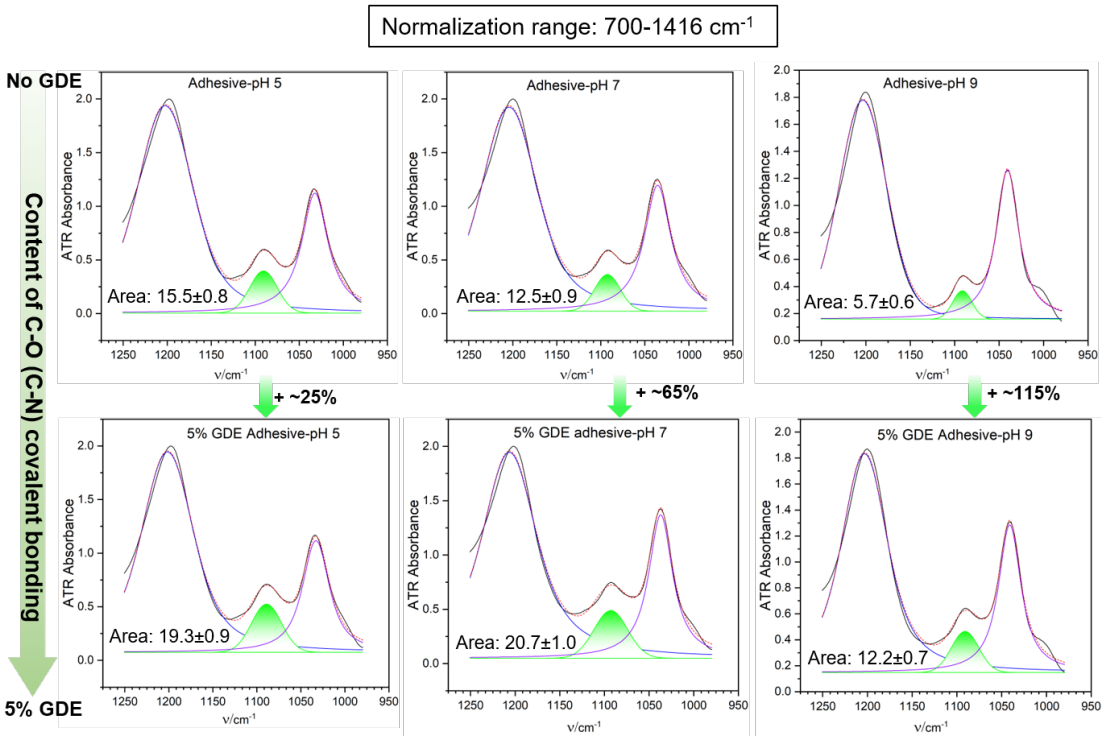

Figure S9 ATR spectra quantification based on the normalization in the range of 700-1416 cm^{-1}.

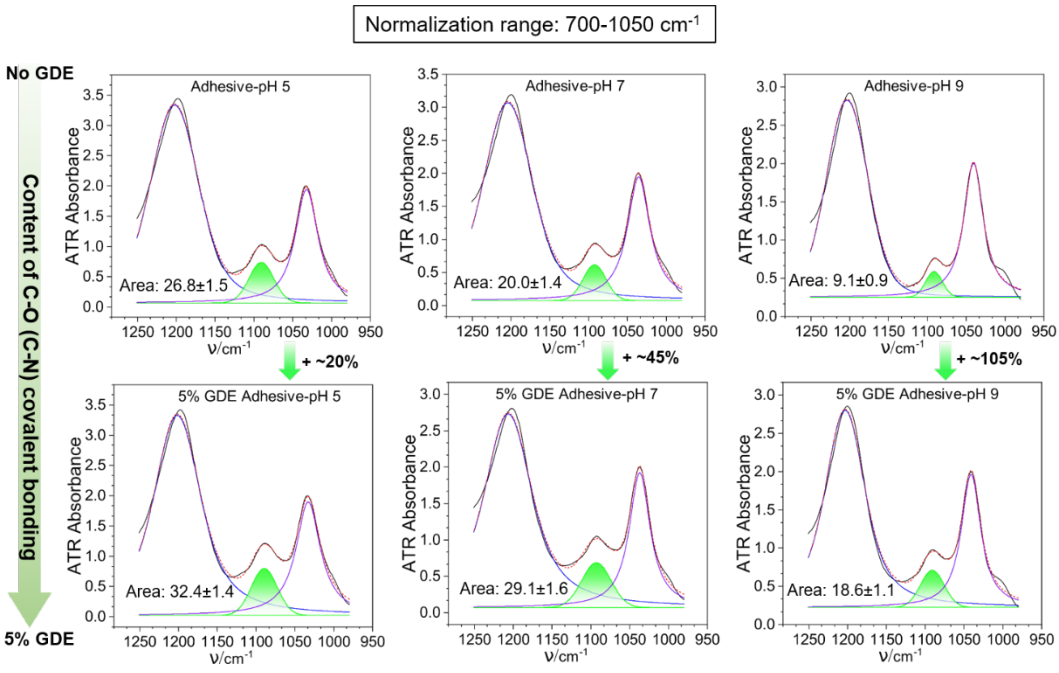

Figure S10 ATR spectra quantification based on the normalization in the range of 700-1050 cm^{-1}.

Reference

1. Tao, Y. *et al.* New chemosynthetic route to linear ε-poly-lysine. *Chem. Sci.* **6**, 6385–6391 (2015).

2. Jiang, T., Moghaddam, S. Z. & Thormann, E. A pH-responsive Polyelectrolyte Multilayer Film with Tunable Interfacial Properties. *Polymer (Guildf).* **214**, 123367 (2020).

3. Nam, S. *et al.* A reinforced thermal barrier coat of a Na–tannic acid complex from the view of thermal kinetics. *RSC Adv.* **9**, 10914–10926 (2019).

4. Rozenberg, M. & Shoham, G. FTIR spectra of solid poly-l-lysine in the stretching NH mode range. *Biophys. Chem.* **125**, 166–171 (2007).

5. Schmidt, G., Hamaker, B. R. & Wilker, J. J. High Strength Adhesives from Catechol Cross-Linking of Zein Protein and Plant Phenolics. *Adv. Sustain. Syst.* **2**, 1700159 (2018).

PAPER III

Self-coacervation of catechol-modified chitosan for biomaterial mimicking mussel adhesive properties

Junjie Kang, Saeed Zajforoushan Moghaddam, Esben Thormann*

Department of Chemistry, Technical University of Denmark, 2800 Kgs. Lyngby, Denmark

Abstract: This study presents a novel biomimetic material based on the mussel adhesive proteins (mfps). The mfps rendering mussels underwater adhesion contain amine groups, catechol groups, and undergo self-coacervation in the presence of salt. For the first time, we developed a material that mimics all three aspects in one molecule. Chitosan, a bio-based material containing amine groups, was modified with catechol (0-50%) to replicate the functionality of mfps' catechol groups. We studied the self-coacervation behavior of synthesized chitosan-catechol in the presence of NaCl (0-2 M). The phase separated material showed tunable physicomechanical properties, particularly underwater adhesion was found to be adjustable by both catechol content and amount of added salt. Moreover, an enzymatically catalyzed approach, using horseradish peroxidase and H_2O_2, was examined as a way to render the adhesive material curability. Our findings suggest that this biomimetic material has potential applications in various fields, including biomedical and environmental engineering.

Keywords: mussel-inspired materials, chitosan, self-coacervation, wet adhesion,

Introduction

The development of materials with novel functionalities such as underwater adhesion and self-healing has been greatly inspired by mussels.[1] These biomimetic studies focus on replicating the main adhesion mechanisms of mussels,[2] including catechol chemistry,[3] catechol-amine synergy,[4] and coacervation of the mussel adhesive foot proteins.[5] The first two mechanisms, which are linked to the mussel adhesive's chemistry, assist the adhesive proteins in establishing a range of physical and chemical interactions, enhancing interfacial adhesion as well as cohesive cross-linking between the proteins.[6] The third mechanism pertains more to the physical properties of the mussel adhesive, suggesting that mussel adhesive proteins, in particular mfp-3, in the coacervate form can easily spread onto underwater surfaces without being dispersed into the water.[7,8]

Various strategies have been employed in the design of mussel-inspired materials.[9]These include the functionalization of the target polymer with catechol moieties,[10–13] blending the target polymer with plant phenolics,[14–17] incorporation of polyamines as secondary cross-linkers,[18,19] and adjusting the medium parameters to promote complexation/coacervation.[20–22] However, a common requirement among these strategies is the inclusion of at least two components that possess both catechol and amine functionalities, and can undergo complexation/coacervation between them.

Mussel adhesive proteins, particularly mfp-3, undergo self-coacervation without the need for another complexing agent.[7] This occurs due to the electrostatic screening in sea water where the relatively high ionic strength shields long-range electrostatic interactions between individual proteins and allows short-range inter- and intra-chain interactions in the form of cation-pi and pi-pi interactions.[23] Drawing inspiration from this phenomenon, we hypothesized that other molecules with similar amine and catechol functionalities could also undergo self-coacervation, if short-ranged attractive interactions and long-ranged electrostatic repulsion is balanced by addition of salt.

We selected chitosan as a molecule with great potential, given its bio-based origin and amine-rich structure that could be easily functionalized with catechol moieties. We hypothesized that, by adjusting the pH and ionic strength of the medium, catechol-functionalized chitosan (Chi-C) would undergo self-coacervation or more generally self-complexation. To test our hypothesis, we synthesized Chi-C with varying catechol content and studied the physical phase transitions over a broad range of pH and ionic strengths. Our results demonstrated that the newly developed material exhibited wet adhesion capability and curability, among other potential functionalities.

Experimental Section

Materials: Chitosan (Chi, 75-85% deacetylated with low molecular weight), sodium cyanoborohydride ($NaCNBH_3$, ≥ 95%, for synthesis), 3,4-dihydroxybenzaldehyde

(DHBA, ≥ 97%), horseradish peroxidase (HRP, lyophilized powder, ~ 150 U/mg), hydrogen peroxide (H_2O_2, 30 wt% in water), and sodium chloride (NaCl) were purchased from Sigma-Aldrich and used without further purification. All solutions were prepared using ultrapure water (Arium® Pro) with a resistivity of 18.2 MΩ cm. pH adjustment was conducted using a HCl solution.

Table 1. Summary of the conditions employed for achieving various degrees of catechol conjugations.

Target Samples	Mass of DHBA added (g)	Reaction time (hours)	Reducing time (hours)	Reducing agent	pH Values	
					For reaction	For precipitate
CHIc10%	0.16	1	4	$NaCNBH_3$	4.5	6.5
CHIc20%	0.5	1				
CHIc25%	0.65	1				
CHIc30%	1.0	1				
CHIc40%	1.5	1				
CHIc50%	2.5	2				

Synthesis of catechol-substituted Chi: Chi-C with different catechol contents (10%, 20%, 25%, 34% 43%, and 54%) were synthesized according to a previously reported method.[12] Details of synthetic method and polymer characterization are provided as supporting information (S1).

Chi-C Phase separation: To prepare the Chi-C solution, a 1 mM NaCl solution at pH 3.0 was first prepared. Next, 0.5 g of dried Chi-C powder was added to obtain a 50 mL Chi-C solution at a concentration of 1 wt%. Once fully dissolved, the pH value was readjusted to 3.0 using a 1 M HCl. The solution was then transferred to 16 glass vials, each containing 2.5 mL of the solution, for further phase separation testing. Subsequently, a 2.5 mL NaCl

solution (pH 3.0) with an ionic strength from 0.2 M to 4 M was separately added to ChiC solutions. After stirring, the solution was allowed to settle and centrifuged at 6500 rpm/min for 5 minutes.

Adhesion testing: An underwater adhesion test (Instron 34SC-2, 50 N load cell) was conducted on the aluminum substrates in a 1 mM NaCl solution. The Chi-C material (0.2 g) was applied onto the bottom cylinder (diameter 20 mm) underwater, then the upper cylinder (diameter 10 mm) was lowered (vertical approach step) at a constant speed of 1 mm min^{-1} until contact was made (set point: 10 N, duration: 60 s). The upper probe was then retracted with a speed of 1 mm min^{-1}. The adhesion strength was calculated as the maximum recorded force on retraction normalized by the contact area. Data were plotted as mean ± standard deviation, calculated based on five replicates. To confirm the results, an additional independent experiment was performed.

Chi-C curing: A covalent curing strategy was employed using HRP in the presence of H_2O_2.[24] Chi-C25 coacervate was mixed with HRP and H_2O_2 in separate batches, with an optimized weight ratio of 1500: 1 (Chi-C25/HRP both in dried state) and 187.5:1 (Chi-C25/H_2O_2). Specifically, 0.5 g of Chi-C25 coacervate was mixed with 100 μL of 0.1 wt% HRP as the first part, and 0.5 g of Chi-C25 coacervate was mixed with 100 μL of 0.8 wt% H_2O_2 as the second part. These two constituents were thoroughly mixed using a spatula

to achieve a uniform mixture, after which a color change and gelation occurred within a certain amount of time.

Rheological measurements: To evaluate the gelation behavior of Chi-C25, rheological measurements were performed using a conventional rheometer (RSA II, TA Instruments, USA) with a parallel plate geometry (diameter: 20 mm, gap distance: 0.5 mm). Strain-sweep analysis was conducted at a fixed frequency of 10 Hz across a strain range of 0.01 to 100%, with data points collected within 2 minutes. The effect of HRP/H2O2 on curability was investigated by treating Chi-C25 coacervate samples with or without HRP/H2O2, and their gelation behavior was examined. Additionally, the effect of curing time on gelation was studied. Specifically, Chi-C25 coacervate samples with HRP/H2O2 treatment were cured for 15 minutes before testing, while samples without HRP/H2O2 were tested similarly. To minimize the evaporation of water from the sample edges during the measurement, a humidity cover was placed around the sample. All experiments were performed at 25 °C. To validate the findings, an additional experiment was conducted.

3. Results

Our mfp3-mimetic material has (i) catechol groups, (ii) amine groups, and (iii) self-coacervation functionality. Chitosan (Chi), in its pristine form, contains amine groups (pka ~ 6.5) that become protonated at low pH.[25] This leads to inter- and intra-chain

electrostatic repulsions that cause stretching of the molecular chains and increase the distance between them. However, increasing the ionic strength of the solution reduces the range of these electrostatic repulsions, effectively screening the long-range repulsions. This leads to a reduction in the stretching of the Chi chains and promotes their approach towards each other where short-ranged attractive forces such as hydrogen bonding and van der Waals forces can kick in. For pure chitosan though, these short-range attractive forces are not expected to promote complexation or self-coacervation.[26] By putting catechol on chitosan though, one can expect additional short-range attractive forces such as catechol-catechol (pi-pi) and catechol-amine (cation-pi), which are believed to be the source of self-coacervation in mfp3 as well. It should be noted that in this biomimetic approach, the focus is not exclusively on coacervation, but on the formation of a phase-separated condensed material that is rich in polymer and possesses desired substantivity and flowing properties.

3.1 Chi-C phase transition induced by NaCl

Initially, we conducted an investigation into the phase behavior of Chi-C polymers with varying catechol contents in response to increasing concentrations of NaCl. To achieve this, a solution of Chi-C at a concentration of 1 wt.% in NaCl 1 mM with pH adjusted to 3 was prepared. An equal volume of NaCl solution with a higher concentration was then added to the Chi-C solution. For instance, to attain a Chi-C solution with a NaCl

concentration of 100 mM, we mixed the Chi-C solution with NaCl at a concentration of 200 mM. By adopting this approach, we ensured that the concentration of NaCl in the final solution was the only variable, while the polymer concentration and total volume remained consistent across all combinations.

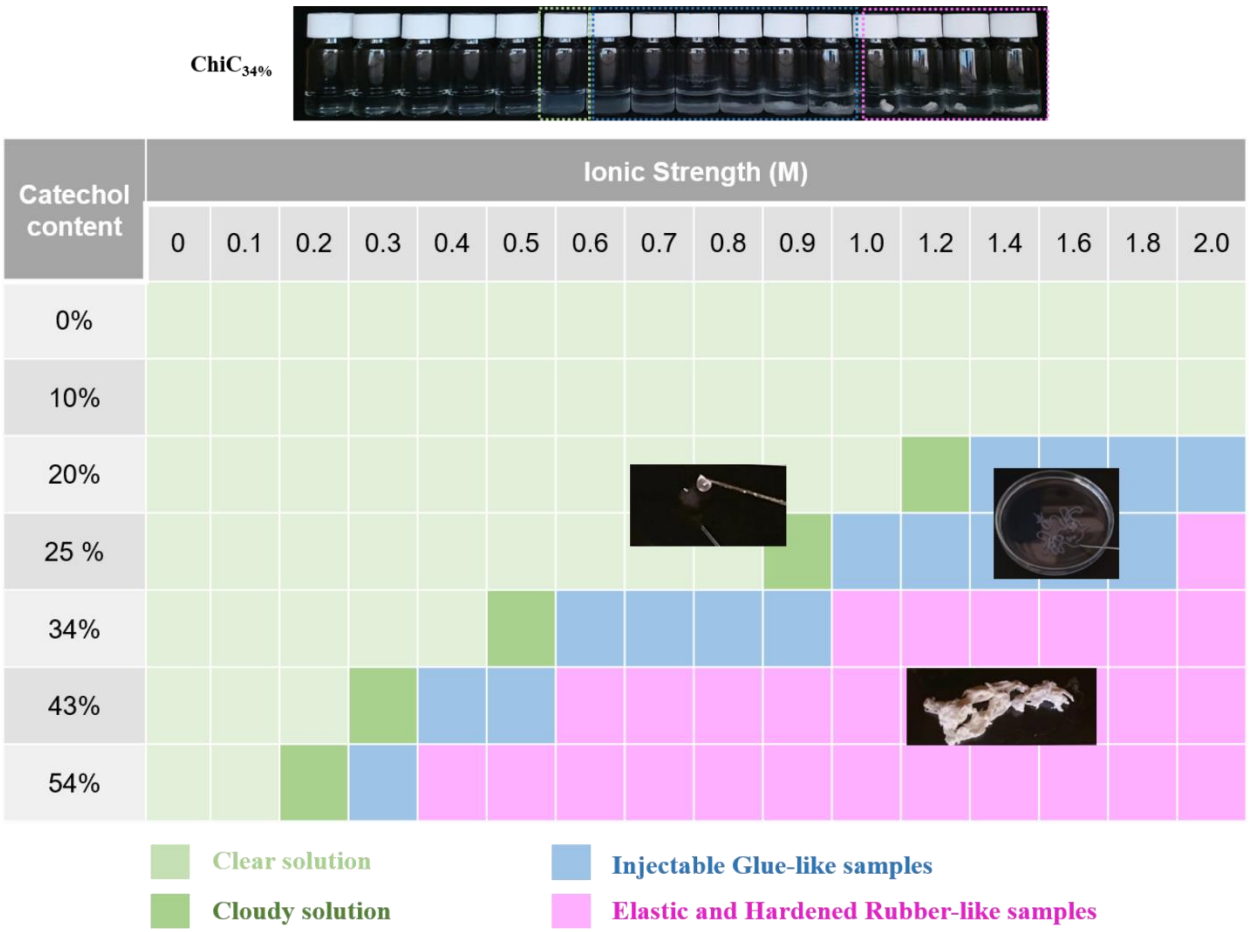

Figure 1. Phase separation of Chi-C solution at pH 3.0 effected on catechol content and ionic strength. The light green square represents a state of the clear solutions. Heavy green color means turbidity or cloudy, which can not use to test adhesion underwater. The blue squares indicate an injectable glue-like sample, but displays different properties with ionic strength increase. The pink squares display a solid-state sample, which is more like gum or rubber.

The phase diagram in Figure 1 shows the behavior of Chi-C solutions with varying NaCl concentrations and catechol contents. Different phase behaviors were observed based on the concentration of salt and catechol content of Chi-C. When the concentration of salt and catechol content were low (top left corner of the diagram: light green color), no phase separation occurred and Chi-C remained in solution. Conversely, as the concentration of salt and catechol content increased, phase separation occurred (bottom right corner of the diagram: colors in heavy green, blue, and pink). A certain minimum amount of catechol was required to initiate phase separation through the addition of salt. Notably, Chi and Chi-C10 solutions did not show any phase separation even in the presence of 2 M NaCl. Chi-C20 showed no clear phase separation up to 1 M NaCl either, but at 1.2 M NaCl, the solution turned cloudy, indicating the onset of phase separation, with precipitated material that could be collected by centrifugation. The minimum amount of salt required to initiate phase separation was observed to be dependent on the catechol content, Chi-C with higher catechol contents requiring less salt to undergo phase separation.

The precipitated material collected at the onset of phase separation (green areas) did not exhibit strong cohesive properties, and shaking could easily re-disperse it into a cloudy mixture. Increasing the salt concentration beyond the onset of phase separation significantly affected the properties of the collected precipitate. Initially, a gel-like material (blue areas) was formed, followed by a more solid and rubbery material (pink

areas) at higher salt concentrations. Both of these phases rendered proper cohesively and homogeneity, but the gel-like phase showed more favorable flow properties.

To more quantitatively compare the mechanical characteristics of the two types of precipitates, their underwater adhesion properties were examined.

3.2 Adhesion Property

Next, we explored the adhesion characteristics of Chi-C with varying catechol concentrations (20%, 25%, 34%, 43%, and 54%), which showed phase separation/precipitation when NaCl was added. We aimed to investigate how altering the catechol content and the amount of salt affected the properties of the precipitate. We focused on underwater adhesion since the design of Chi-C was inspired by mussel adhesive proteins, and we wanted to determine if this material could exhibit improved underwater adhesion. To evaluate the adhesive strength of the precipitate, we applied a specific amount of Chi-C precipitate (0.2 g) onto an aluminum substrate, submerged it underwater, pressed another aluminum substrate onto it, allowed it to dwell, and measured the maximum recorded force upon retraction using tensile mode. Figure 2 displays the adhesion strength of Chi-C precipitates with varying catechol contents prepared by adding different salt amounts. It was found that the physical properties of the precipitate significantly affected the adhesion strength. The gel-like material in the blue bars had larger adhesion properties, supposedly due to its ability to flow and form

good contact between substrates, whereas the solid rubbery material in the pink bars was harder to flow and form contact area thus rendered reduced adhesion.

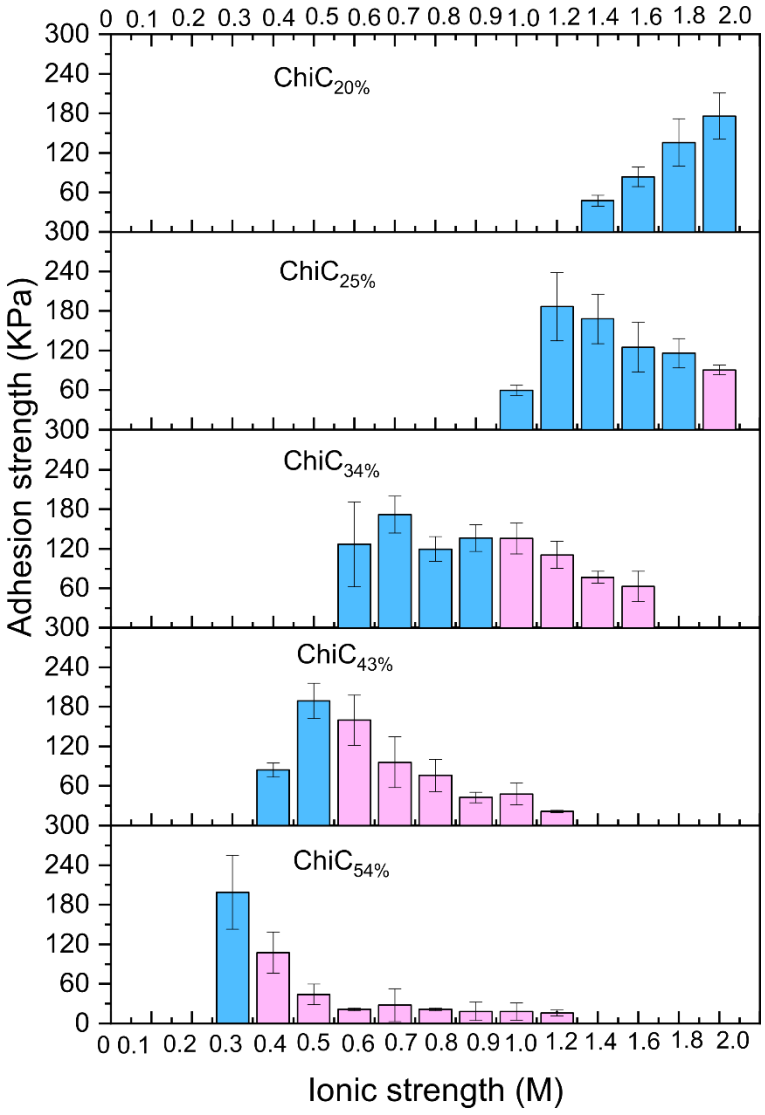

Figure 2. Adhesion strength underwater as a function of ionic strength and catechol content. Blue bars indicate an injectable glue-like precipitate. Pink bars exhibit a solid-/rubbery-like precipitate. The data plotted as the average ± standard deviations (n = 5).

Furthermore, we observed that both the catechol content and NaCl concentration affected underwater adhesion strength. For a fixed catechol content, adhesion strength increased with increasing NaCl concentration until an optimum point was reached. Further increase in NaCl concentration led to a decrease in adhesion strength, and this trend was more pronounced in the blue areas. The optimum NaCl concentration providing maximal adhesion strength decreased with increasing catechol content.

Accordingly, the physical properties of the precipitate, dictated by the NaCl concentration and catechol content, are crucial determinants of the adhesion strength of the material.

3.3 Enzymatic Curing

Up to this point, we have demonstrated the versatility of utilizing salt-induced phase separation of Chi-C to create a single-component bio-based material with adjustable physico-mechanical properties and enhanced underwater adhesion. In order to further investigate the capabilities of this material, we set out to examine its chemical curability functionality. When employed as a coating or adhesive, the applied material is typically subjected to covalent reactions which serve to cure the material and significantly enhance its mechanical properties. Specifically, when wet adhesion is necessary, such as in the case of medical tissue adhesives, it is desirable for the mechanical properties to improve

and create a stronger bond after initial contact is made. Therefore, we conducted research to investigate the possibility of utilizing Chi-C as a curable adhesive material.

The presence of catechol groups in the Chi-C material allows for a vast range of different curing strategies. Catechol oxidation can be achieved through various methods, including exposure to air, metal ions, heat, UV radiation, and enzymatic catalysis. For instance, it has been shown that UV radiation can be used to oxidize catechol and create cross-linkable curable materials. In a study by Hu et al., methacrylated Chi-C was quickly induced into an adhesive hydrogel with enhanced mechanical properties after UV radiation.[27] The resulting photo-cross-linked hydrogel exhibited more than twice the adhesion strength as high as its original strength. Other examples from literature include the use of metal ions,[28,29] enzymatic catalysis,[30,31] use of strong oxidants such as periodate[12,32] and heat oxidation[33] to create cross-linked materials with desirable properties.

The HRP-catalyzed oxidation of catechol is a process that involves the use of horseradish peroxidase (HRP) enzyme to catalyze the oxidation of catechol. This process can be combined with various oxidants to produce cross-linked polymers. Hydrogen peroxide (H2O2),[34] sodium periodate (NaIO4),[12,32] silver nitrate (AgNO3),[35] and iron(III) chloride (FeCl3)[28] are among the oxidants that have been utilized.[6] For instance, Hou et al.[36] reported alginate-dopamine conjugates became gels due to the HRP-catalyzed chemical crosslinking in the presence of H2O2. The resulting hydrogels were systematically

explored how the mechanical strength and gelation behavior were influenced by H2O2 concentrations.

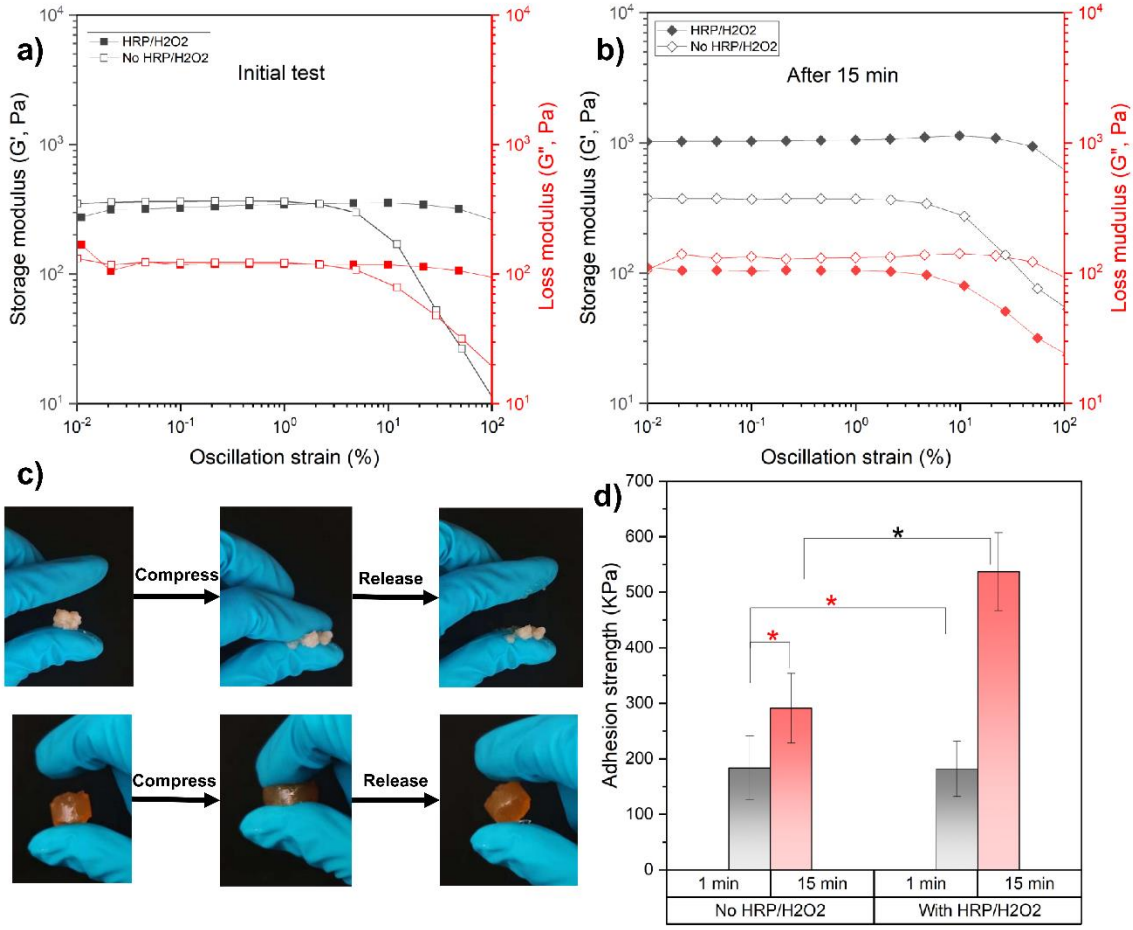

Figure 3. Mechanical properties investigation of Chi-C coacervate with and without HRP/H2O2. The rheological properties evaluated as a function of curing time **a)** in the beginning and **b)** curing after 15 minutes**. c)** Compression and resilience behaviors. **d)** Tensile adhesion strength. Statistical analysis considered significant when $p^* < 0.001$.

With the presence of nucleophilic amine groups on Chi-C, we conducted an investigation into whether a combination of HRP and H2O2 could be utilized in self-cross-linking Chi-C. We chose to test Chi-C25 due to its favorable physical properties, including maximal adhesion performance (as shown in Figure 2), ease of application to a surface, and injectability. After optimizing the Chi-C/HRP/H2O2 mixing ratios (SI), we developed a two-part adhesive chemistry. The first part involved mixing Chi-C precipitate with HRP in a ratio of 1500: 1, while in the second part, Chi-C was mixed with H2O2 in a ratio of 625:1. The two parts were hand mixed in a 1:1 ratio before being applied and tested as an underwater adhesive.

Herein, we aimed to investigate the curability of ChiC coacervate with or without HRP/H2O2 treatment using rheological techniques. The viscoelastic properties were measured in a strain-controlled oscillatory mode with a fixed frequency at 10 Hz. The storage modulus (G') and loss modulus (G") were recorded within 2 minutes during the measurement, reflecting the elastic and viscous characteristics, respectively. G' was used to evaluate the gel strength of ChiC coacervate and its resistance to deformation. The linear viscoelastic region (LVR) is generally used for evaluating elastic properties, as stress changes occur within this region without causing structural damage to the sample.[37] For example, with GDE treatment, we expected that ChiC coacervates could exhibit enhanced G' values within LVR.

Figure 3a displays the the gel evolution of ChiC coacervates influenced by HRP/H2O2 treatment. To begin, ChiC coacervate with and without HRP/H2O2 treatment was placed onto the rheometer and then examined immediately. It was found that G′ and G″ values were rather similar in the LVR (strain: 0.01%-1%), and G′ was larger than G″. These results suggest that ChiC coacervate treated by HRP/H2O2 exhibits relatively the same gel-like behavior as its original status. As the strain increased from 1% to 100%, G′ and G″ values from ChiC coacervate with HRP/H2O2 treatment remained the same tendency. In contrast, G′ and G″ values from ChiC coacervate without HRP/H2O2 treatment significantly decreased. The measurement was assumed to take 2 minutes from low strain to high, so curability could start occurring. Therefore, ChiC coacervate with HRP/H2O2 treatment exhibited a slightly stronger resistance to deformation than its original status.

To further confirm the occurrence of curability, we conducted a test (Figure 3b) to evaluate the effect of HRP/H2O2 treatment on the viscoelastic properties of ChiC after 15 minutes. We observed that ChiC coacervate without HRP/H2O2 did not exhibit significant changes in G′ and G″ values compared to the quick test. However, when treated with HRP/H2O2, ChiC coacervate showed at least two times higher G′ values, indicating that the curability of HRP/H2O2 can accelerate crosslinking and significantly improve the mechanical strength of the hydrogels.[38] Furthermore, with increasing strain from 10%-100%, we noticed a slight decrease in G′ and G″ values for ChiC coacervate

with HRP/H2O2 treatment. It is possible to speculate that prolonged curing time may lead to a decrease in gel strength and reduced resistance to deformation.

Next, we examined the gel strength and resistance to deformation of ChiC coacervate using a visual demonstration. Briefly, ChiC coacervate with or without HRP/H2O2 was cured in room temperature for 15 minutes, followed by compression-release measurements. As shown in the figure 3c, a visible change in color from white to brown was observed in the HRP/H2O2 treated ChiC, indicating the occurrence of catechol oxidative crosslinking.[39] Notably, the introduction of HRP/H2O2 enable to increase the rigidity of the gel network, resulting in higher compression strength and better resilience. These findings suggest that HRP/H2O2 curability can endow ChiC coacervate with a robust polymer network that could exhibit better wet performance.

In addition, Figure 3d displays the adhesion strength measurements of ChiC coacervate with or without HRP/H2O2 curing underwater. For a given curing time (15 minutes), we observed that HRP/H2O2 curability significantly improved adhesion strength to ~ 550 KPa, which was nearly twice as strong as that of ChiC coacervate without HRP/H2O2. In addition to HRP/H2O2, we noted that curing time also played an important role in adhesion strength. For example, compared to ChiC coacervate without HRP/H2O2, a one-minute curing did not exhibit any changes in adhesion strength. Overall, our study suggest that ChiC coacervate with HRP/H2O2 treatment can promote catechol oxidative

crosslinking and significantly improve its wet adhesion strength after 15 minutes of curability.

Conclusion

In summary, this mussel-inspired study has yielded a novel chitosan-based material with improved wet adhesive properties. Our innovative approach involves modifying chitosan with catechol and inducing phase separation by the addition of salt, resulting in a precipitate material. The material possesses crucial features, such as amine groups and catechol, similar to those present in the mussel adhesive plaque. Additionally, it undergoes phase separation, i.e., precipitation, by addition of salt, mimicking the self-coacervation of mussel adhesive proteins. Our material displays outstanding underwater adhesion strength of ~250 kPa, which can be tuned by varying the catechol content and salt concentration. Additionally, we have demonstrated that our chitosan-catechol material can be cross-linked using catechol oxidation chemistry and enzymatic approaches. In conclusion, this research opens up an exciting avenue for developing novel adhesives, coatings, and hydrogels based on this material, i.e., salt-precipitated chitosan-catechol, for a wide range of biomedical applications.

Reference

(1) Guo, Q.; Chen, J.; Wang, J.; Zeng, H.; Yu, J. Recent Progress in Synthesis and Application of Mussel-Inspired Adhesives. *Nanoscale* **2020**, *12* (3), 1307–1324. https://doi.org/10.1039/c9nr09780e.

(2) Taghizadeh, A.; Taghizadeh, M.; Yazdi, M. K.; Zarrintaj, P.; Ramsey, J. D.; Seidi, F.; Stadler, F. J.; Lee, H.; Saeb, M. R.; Mozafari, M. Mussel-Inspired Biomaterials: From Chemistry to Clinic. *Bioeng. Transl. Med.* **2022**, *7* (3), e10385. https://doi.org/10.1002/BTM2.10385.

(3) Ryu, J. H.; Hong, S.; Lee, H. Bio-Inspired Adhesive Catechol-Conjugated Chitosan for Biomedical Applications: A Mini Review. *Acta Biomater.* **2015**, *27*, 101–115. https://doi.org/10.1016/J.ACTBIO.2015.08.043.

(4) An, S.; Jeon, E. J.; Han, Y.; Jeon, J.; Lee, M. J.; Kim, S.; Shin, M.; Cho, S.-W.; An, S.; Jeon, E. J.; Han, S. Y.; Jeon, J.; Lee, M. J.; Kim, S.; Cho, S.-W.; Shin, M. PH-Universal Catechol-Amine Chemistry for Versatile Hyaluronic Acid Bioadhesives. *Small* **2022**, 2202729. https://doi.org/10.1002/SMLL.202202729.

(5) Forooshani, P. K.; Lee, B. P. Recent Approaches in Designing Bioadhesive Materials Inspired by Mussel Adhesive Protein. *J. Polym. Sci. Part A Polym. Chem.* **2017**, *55* (1), 9–33. https://doi.org/10.1002/POLA.28368.

(6) Yang, J.; Stuart, M. A. C.; Kamperman, M. Jack of All Trades: Versatile Catechol

Crosslinking Mechanisms. *Chem. Soc. Rev.* **2014**, *43* (24), 8271–8298. https://doi.org/10.1039/C4CS00185K.

(7) Wei, W.; Tan, Y.; Martinez Rodriguez, N. R.; Yu, J.; Israelachvili, J. N.; Waite, J. H. A Mussel-Derived One Component Adhesive Coacervate. *Acta Biomater.* **2014**, *10* (4), 1663–1670. https://doi.org/10.1016/j.actbio.2013.09.007.

(8) Kim, S.; Huang, J.; Lee, Y.; Dutta, S.; Young Yoo, H.; Mee Jung, Y.; Jho, Y.; Zeng, H.; Hwang, D. S. Complexation and Coacervation of Like-Charged Polyelectrolytes Inspired by Mussels. *Proc. Natl. Acad. Sci. U. S. A.* **2016**, *113* (7), E847–E853. https://doi.org/10.1073/PNAS.1521521113/SUPPL_FILE/PNAS.201521521SI.PDF.

(9) Narayanan, A.; Dhinojwala, A.; Joy, A. Design Principles for Creating Synthetic Underwater Adhesives. *Chem. Soc. Rev.* **2021**, *50* (23), 13321–13345. https://doi.org/10.1039/D1CS00316J.

(10) S. Desai, M.; Chen, M.; Hing Julio Hong, F.; Hun Lee, J.; Wu, Y.; Lee, S.-W. Catechol-Functionalized Elastin-like Polypeptides as Tissue Adhesives. *Biomacromolecules* **2020**, *21* (7), 2938–2948. https://doi.org/10.1021/acs.biomac.0c00740.

(11) Xu, R.; Ma, S.; Wu, Y.; Lee, H.; Zhou, F.; Liu, W. Adaptive Control in Lubrication, Adhesion, and Hemostasis by Chitosan-Catechol-PNIPAM. *Biomater. Sci.* **2019**, *7*

(9), 3599–3608. https://doi.org/10.1039/c9bm00697d.

(12) Yavvari, P. S.; Srivastava, A. Robust, Self-Healing Hydrogels Synthesised from Catechol Rich Polymers. *J. Mater. Chem. B* **2015**, *3* (5), 899–910. https://doi.org/10.1039/c4tb01307g.

(13) Hyun Ryu, J.; Lee, Y.; Ho Kong, W.; Gyoung Kim, T.; Gwan Park, T.; Lee, H. Catechol-Functionalized Chitosan/Pluronic Hydrogels for Tissue Adhesives and Hemostatic Materials. *Biomacromolecules* **2011**, *12* (7), 2653–2659. https://doi.org/10.1021/bm200464x.

(14) Kim, K.; Shin, M.; Koh, M.-Y.; Ryu, J. H.; Lee, M. S.; Hong, S.; Lee, H. TAPE: A Medical Adhesive Inspired by a Ubiquitous Compound in Plants. *Adv. Funct. Mater.* **2015**, *25* (16), 2402–2410. https://doi.org/10.1002/adfm.201500034.

(15) ZajforoushanMoghaddam, S.; Qie, R.; Thormann, E. Making Protein-Based Adhesives Water Resistant: Role of Protein Water Solubility, Galloyl Modification, and Complexation. *ACS Appl. Polym. Mater.* **2021**, *0* (0). https://doi.org/10.1021/acsapm.1c01089.

(16) Wang, Z.; Zhang, S.; Zhao, S.; Kang, H.; Wang, Z.; Xia, C.; Yu, Y.; Li, J. Facile Biomimetic Self-Coacervation of Tannic Acid and Polycation: Tough and Wide PH Range of Underwater Adhesives. *Chem. Eng. J.* **2021**, *404*, 127069. https://doi.org/10.1016/J.CEJ.2020.127069.

(17) Lee, D.; Hwang, H.; Kim, J.-S.; Park, J.; Youn, D.; Kim, D.; Hahn, J.; Seo, M.; Lee, H. VATA: A Poly(Vinyl Alcohol)-and Tannic Acid-Based Nontoxic Underwater Adhesive. *Cite This ACS Appl. Mater. Interfaces* **2020**, *12*. https://doi.org/10.1021/acsami.0c02037.

(18) Wang, Z.; Zhao, S.; Song, R.; Zhang, W.; Zhang, S.; Li, J. The Synergy between Natural Polyphenol-Inspired Catechol Moieties and Plant Protein-Derived Bio-Adhesive Enhances the Wet Bonding Strength. *Sci. Reports 2017 71* **2017**, *7* (1), 1–10. https://doi.org/10.1038/s41598-017-10007-8.

(19) Zhao, Q.; Mu, S.; Long, Y.; Zhou, J.; Chen, W.; Astruc, D.; Gaidau, C.; Gu, H.; Zhao, Q.; Mu, S.; Long, Y.; Zhou, J.; Chen, W.; Gu, H.; Astruc, D.; Gaidau, C. Tannin-Tethered Gelatin Hydrogels with Considerable Self-Healing and Adhesive Performances. *Macromol. Mater. Eng.* **2019**, *304* (4), 1800664. https://doi.org/10.1002/MAME.201800664.

(20) Narayanan, A.; Menefee, J. R.; Liu, Q.; Dhinojwala, A.; Joy, A. Lower Critical Solution Temperature-Driven Self-Coacervation of Nonionic Polyester Underwater Adhesives. *ACS Nano* **2020**, *14* (7), 8359–8367. https://doi.org/10.1021/acsnano.0c02396.

(21) Wang, X.; Lee, J.; Wang, Y.-W.; Huang, Q. Composition and Rheological Properties of β-Lactoglobulin/Pectin Coacervates: Effects of Salt Concentration

and Initial Protein/Polysaccharide Ratio. *Biomacromolecules* **2007**, *8* (3), 992–997. https://doi.org/10.1021/bm060902d.

(22) Shao, H.; Stewart, R. J. Biomimetic Underwater Adhesives with Environmentally Triggered Setting Mechanisms. *Adv. Mater.* **2010**, *22* (6), 729–733. https://doi.org/10.1002/adma.200902380.

(23) Waite, J. H. Mussel Adhesion – Essential Footwork. *J. Exp. Biol.* **2017**, *220* (4), 517–530. https://doi.org/10.1242/JEB.134056.

(24) Wang, R.; Li, J.; Chen, W.; Xu, T.; Yun, S.; Xu, Z.; Xu, Z.; Sato, T.; Chi, B.; Xu, H. A Biomimetic Mussel-Inspired ε-Poly- <scp>l</Scp> -Lysine Hydrogel with Robust Tissue-Anchor and Anti-Infection Capacity. *Adv. Funct. Mater.* **2017**, *27* (8), 1604894. https://doi.org/10.1002/adfm.201604894.

(25) Wang, Q. Z.; Chen, X. G.; Liu, N.; Wang, S. X.; Liu, C. S.; Meng, X. H.; Liu, C. G. Protonation Constants of Chitosan with Different Molecular Weight and Degree of Deacetylation. *Carbohydr. Polym.* **2006**, *65* (2), 194–201. https://doi.org/10.1016/J.CARBPOL.2006.01.001.

(26) Tanaka, K.; Nishida, K.; Gabrys, B. J.; Lawrence, M. J.; Kanaya, T. Critical Dissolution Ionic Strength of Aqueous Solution of Chitosan Hydrochloride Salt. *Sen'i Gakkaishi* **2014**, *70* (9), 225–231. https://doi.org/10.2115/FIBER.70.225.

(27) Hu, Y.; Xu, Y.; Wang, B.; Chen, Y.; Huang, C. Facile Preparation and

Characterization of Photopolymerized Adhesive Hydrogels Based on Methacrylated Catechol-Chitosan. *J. Mater. Sci.* **2022**, *57* (44), 20974–20986. https://doi.org/10.1007/S10853-022-07942-X/FIGURES/7.

(28) Yang, B.; Lim, C.; Hwang, D. S.; Cha, H. J. Switch of Surface Adhesion to Cohesion by Dopa-Fe3+ Complexation, in Response to Microenvironment at the Mussel Plaque/Substrate Interface. *Chem. Mater.* **2016**, *28* (21), 7982–7989. https://doi.org/10.1021/ACS.CHEMMATER.6B03676/ASSET/IMAGES/LARGE/CM-2016-03676M_0007.JPEG.

(29) Birkedal, H.; Chen, Y. Mussel Inspired Self-Healing Materials: Coordination Chemistry of Polyphenols. *Adv. Inorg. Chem.* **2020**, *76*, 269–298. https://doi.org/10.1016/BS.ADIOCH.2020.03.006.

(30) Wang, R.; Li, J.; Chen, W.; Xu, T.; Yun, S.; Xu, Z.; Xu, Z.; Sato, T.; Chi, B.; Xu, H. A Biomimetic Mussel-Inspired ε-Poly-l-Lysine Hydrogel with Robust Tissue-Anchor and Anti-Infection Capacity. *Adv. Funct. Mater.* **2017**, *27* (8), 1604894. https://doi.org/10.1002/ADFM.201604894.

(31) Choi, S.; Ahn, H.; Kim, S. H. Tyrosinase-Mediated Hydrogel Crosslinking for Tissue Engineering. *J. Appl. Polym. Sci.* **2022**, *139* (14), 51887. https://doi.org/10.1002/APP.51887.

(32) Matos-Pérez, C. R.; White, J. D.; Wilker, J. J. Polymer Composition and Substrate

Influences on the Adhesive Bonding of a Biomimetic, Cross-Linking Polymer. *J. Am. Chem. Soc.* **2012**, *134* (22), 9498–9505. https://doi.org/10.1021/ja303369p.

(33) Burke, S. A.; Ritter-Jones, M.; Lee, B. P.; Messersmith, P. B. Thermal Gelation and Tissue Adhesion of Biomimetic Hydrogels. *Biomed. Mater.* **2007**, *2* (4), 203. https://doi.org/10.1088/1748-6041/2/4/001.

(34) Liu, S.; Wu, Y.; Du, G.; Yang, H.; Ni, K.; Su, H.; Ran, X.; Zhou, X.; Gao, W.; Yang, L. H2O2-Mediated Tannin Bio-Based Wood Adhesive Inspired by Starfish Structure and Phenol-Amine Synergy. *Ind. Crops Prod.* **2022**, *188*, 115714. https://doi.org/10.1016/J.INDCROP.2022.115714.

(35) Zhang, L.; Wu, J.; Wang, Y.; Long, Y.; Zhao, N.; Xu, J. Combination of Bioinspiration: A General Route to Superhydrophobic Particles. *J. Am. Chem. Soc.* **2012**, *134* (24), 9879–9881. https://doi.org/10.1021/JA303037J/SUPPL_FILE/JA303037J_SI_001.PDF.

(36) Hou, J.; Li, C.; Guan, Y.; Zhang, Y.; Zhu, X. X. Enzymatically Crosslinked Alginate Hydrogels with Improved Adhesion Properties. *Polym. Chem.* **2015**, *6* (12), 2204–2213. https://doi.org/10.1039/C4PY01757A.

(37) Hasanvand, E.; Rafe, A. Rheological and Structural Properties of Rice Bran Protein-Flaxseed (Linum Usitatissimum L.) Gum Complex Coacervates. *Food Hydrocoll.* **2018**, *83*, 296–307. https://doi.org/10.1016/J.FOODHYD.2018.05.019.

(38) Huang, W.; Cheng, S.; Wang, X.; Zhang, Y.; Chen, L.; Zhang, L. Noncompressible Hemostasis and Bone Regeneration Induced by an Absorbable Bioadhesive Self-Healing Hydrogel. *Adv. Funct. Mater.* **2021**, 2009189. https://doi.org/10.1002/adfm.202009189.

(39) Kim, J.; Kim, S.; Son, D.; Shin, M. Phenol–Hyaluronic Acid Conjugates: Correlation of Oxidative Crosslinking Pathway and Adhesiveness. *Polymers (Basel).* **2021**, *13* (18), 3130. https://doi.org/10.3390/POLYM13183130/S1.

Supporting information for

Chitosan-catechol self-coacervation for mimicking the mussel adhesive properties

Junjie Kang, Saeed Zajforoushan Moghaddam, Esben Thormann*

Department of Chemistry, Technical University of Denmark, 2800 Kgs. Lyngby, Denmark

S1. Synthesis/characterization of chitosan-catechol:

In a volumetric flask, 2 g of chitosan was dissolved in 40 mL of water containing 0.8 mL of glacial acetic acid. The mixture was stirred overnight, and the pH was then adjusted to 4.5 using 1 M HCl. The resulting solution was clear and pale yellow in color. DHBA was dissolved in a water/methanol mixture (2:1 volume ratio, pH adjusted to 4.5) in various concentrations (see Table S1). The pH of the mixture was kept constant at 4.5 during the synthesis process.

Next, a reductive amination reaction was conducted. 2.0 g solid $NaCNBH_3$ was dissolved in water with a pH of 4.5 and added dropwise. After 4 hours, the pH was adjusted to 6.5 by adding 2 M NaOH dropwise under vigorous stirring to obtain precipitated Chi-C. The excess water was removed, and 50 ml 1 wt. % HCl solution was added to the reaction flask. The mixture was stirred to re-dissolve Chi-C. The solution was then dialyzed against HCl solution (pH 3-3.5) for 48 hours (in the beginning, four exchanges every 2h) using a regenerated cellulose dialysis membrane (MWCO: 3.5 KDa). The solution was lastly dialyzed against water for 4 hr, followed by freeze-drying for two days. Around 1.8 g dried Chi-C product was obtained and stored in a desiccator at a temperature of -20℃ covered by aluminum foil for further use. Reactions mixtures and solutions were preserved from light during the entire synthesis and dialysis process.

To confirm/quantify the catechol substitution, Chi-C products were dissolved in acetate buffer (pH 3) at a concentration of 1 wt%. The solutions were then diluted to 0.1 mg/mL for UV-Vis testing. The absorbance was recorded over a range of 200 to 800 nm using a NanoDrop 2000/2000c Spectrophotometer (Thermo Fisher Scientific; Wilmington, USA). The absorbance peak at 280 nm (Figure S1), confirms catechol grafting.

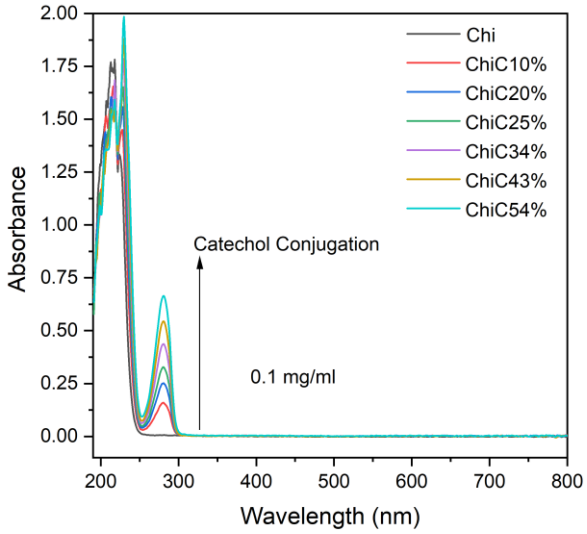

Figure S1. UV-Vis spectra of Chi-C solutions at 0.1 mg/mL

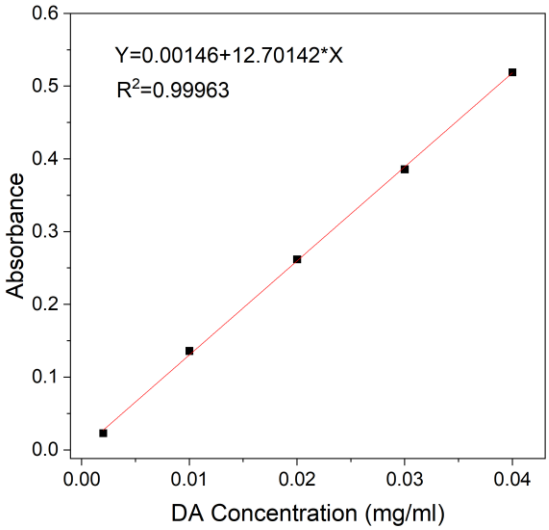

Figure S2. UV-Vis standard curve using dopamine solutions

The degree of catechol conjugation was determined using a standard calibration curve (Figure S2). The absorbance intensity at 280 nm was measured for dopamine (DA) solutions of varying concentrations (0.002, 0.01, 0.02, 0.03, and 0.04 mg/mL).

Table S1. Regent compositions of Chi-C synthesis and catechol content determinations

Sample No.	Chi (g)	DHBA (g)	Reaction time (h)	Catechol content (%): UV-Vis test			Average	St. Dev.
1	2	0.25	1	12.50391239	10.77381	10.53789	11.2	1.1
2	2	0.5	1	19.73888056	18.71655	20.60393	19.7	0.9
3	2	0.65	1	25.7155934	25.47967	24.45734	25.2	0.6
4	2	1.0	1	34.28745787	34.13018	34.13018	34.2	0.1
5	2	1.5	1	42.70204042	43.0166	43.88165	43.2	0.6
6	2	2.5	2	51.90303255	54.81275	54.97003	53.9	1.7

S2. Preparation/Characterization of Chi-C precipitates

Figure S3 shows the phase separation of Chi-C solutions for different catechol/salt combinations.

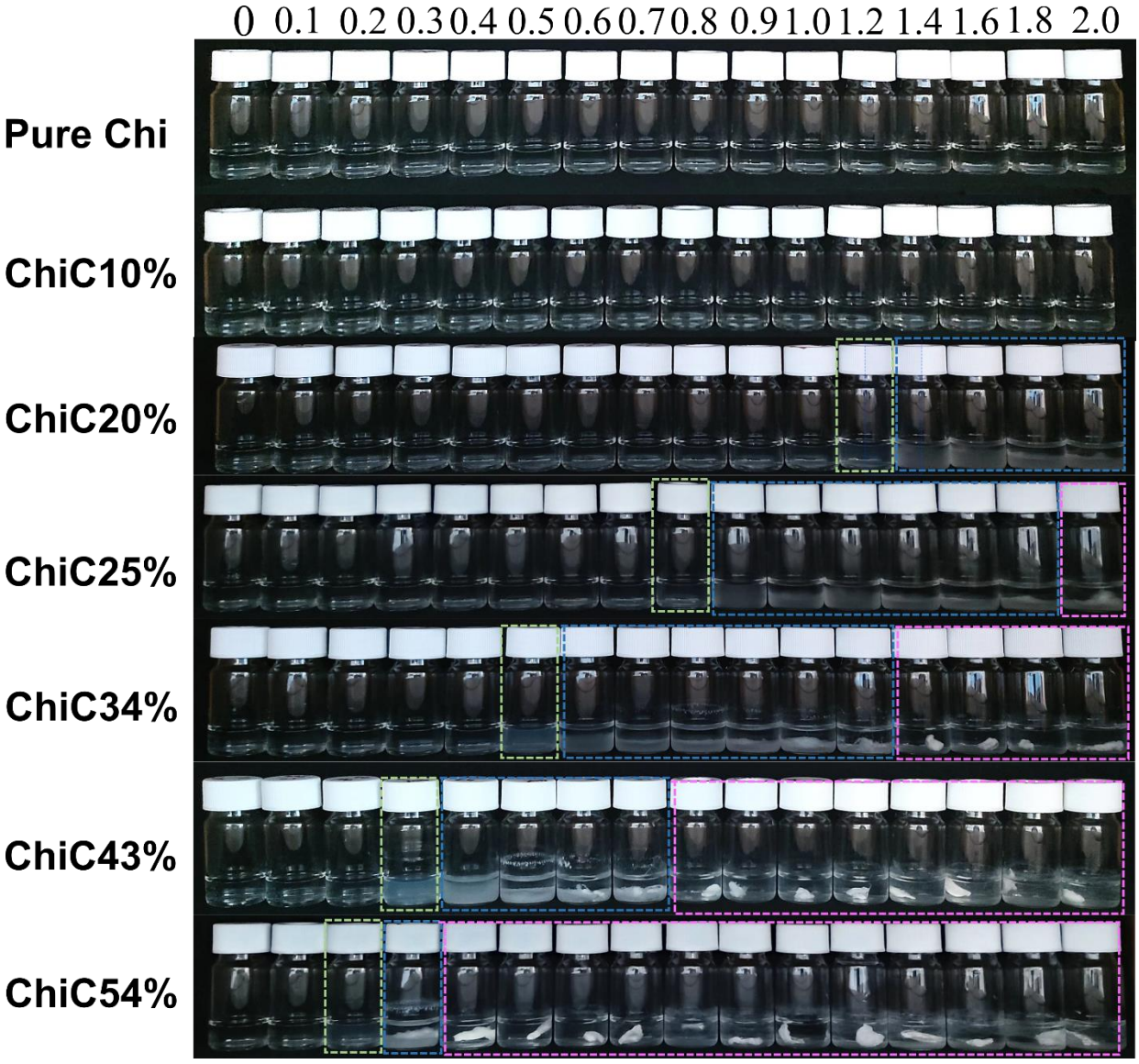

Figure S3. Chi-C solutions at different ionic strength (M) and catechol contents; green: cloudy state, blue: injectable gel-like precipitate, pink: solid gummy-like precipitate

The Chi-C coacervate, which was prepared with a 25% catechol content and an ionic strength of 1.2 M, was selected as the sample for determining water content and as the wet adhesive for curability measurements. The amount of dried polymers was used to optimize both ratios of Chi-C/HRP and Chi-C/H2O2.

To weigh the wet adhesive, the mass of the bare glass slide was measured firstly. Then, a certain amount of wet adhesive was added onto the glass slide, and the total weight of the wet specimen was recorded in the first column of Table S2. The specie was then transferred into a vacuum oven at 30 ℃ and weighed again after three days when it was completely dried. The specific data are shown in **Table S2**, and the water content was calculated using the fololowing equation:

$$Water\ content\ (\%) = \frac{Dry\ specie - glass\ slide}{Wet\ specie - glass\ slide} * 100\%$$

Table S2. The water content of Chi-C adhesive determinations

Wet species (g)	Glass slide	Dry species	Water content (%)	Average (%)	S.D
5.3143	4.8719	4.93877	84.88471971	**85.62**	**0.84**
5.64245	4.88879	5.00142	85.05559536		
5.31797	4.83411	4.90279	85.8058116		
5.30721	4.81346	4.87895	86.73620253		

There are two possible outcomes during phase separation: coacervation and precipitation. In coacervation, the polymers are concentrated on the top solution, which appears as liquid droplets. The phenomenon is different from precipitation, where a solid is formed

and droplets are no longer observed.[1] In this study, Chi-C25 solutions with 1.2 M or 2.0 M of ionic strength were used, which yielded a gel-like or rubber-like material, respectively. Figure S4 shows that a large amount of liquid droplets occurred in sample with a gel-like property (Figure S4a), while they were almost disappeared or disintegrated in the rubber-like sample (Figure S4b). These results suggest that samples with gel-like or rubber-like property underwent different phase separation processes. The gel-like samples were likely formed through coacervation, while precipitation occurred in the rubber-like material.

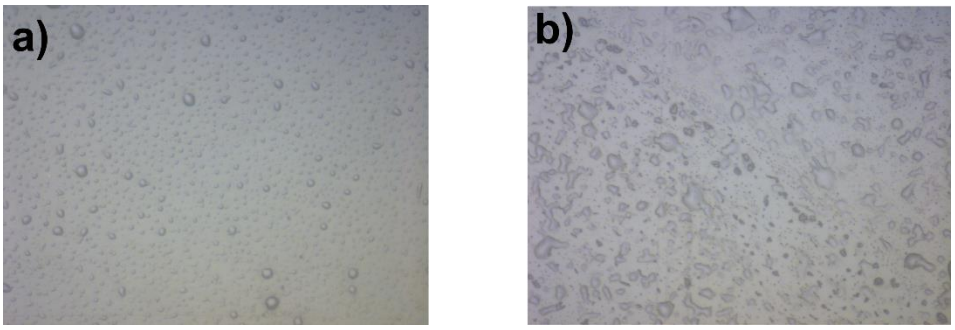

Figure S4. Microscopic observation of top solution in samples with properties of: a) gel-like and b) rubber-like.

As an additional investigation, Chi-C self-coacervation was partly studied at pH 5 as well. Chitosan, by increasing pH to 5, is expected to become less charged, which can affect the phase diagram compared to that obtained for pH 3. As shown in Figure S5, it was observed that cloudiness appeared earlier at pH 5 than at pH 3.0. For instance, Chi-C25 solution exhibited the start of phase separation at 0.4 M of ionic strength at pH 5, while at pH 3.0, it was delayed until 0.9 M. The smaller amount of salt required to initiate phase

separation at pH 5 suggests a less charged network or a more complex crosslinking in the Chi-C solution.

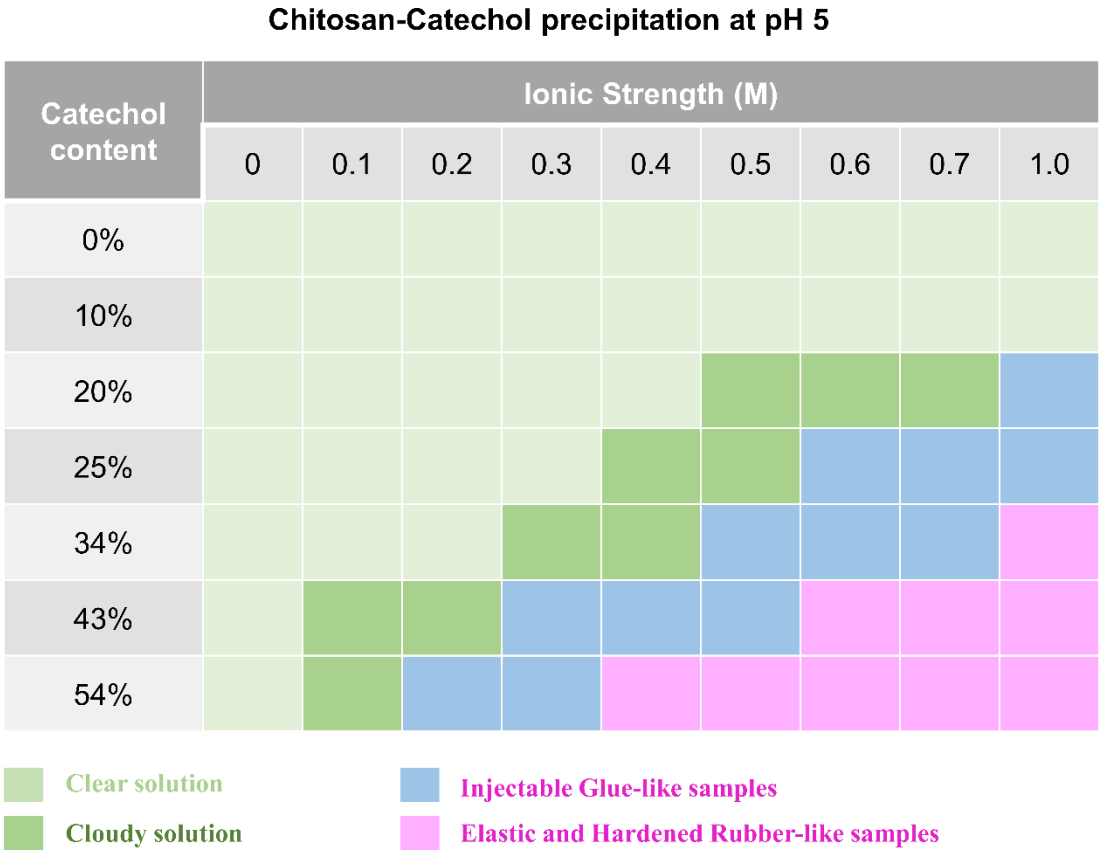

Figure S5. Phase diagram of Chi-C solutions at pH 5

S3. Optimization of enzymatic curing

In this section, the optimal ratio of HRP and H_2O_2 for achieving a gelation time of a few minutes was found (Table S3). Chi-C25% coacervate was chosen due to its favorable physical properties to be used as an adhesive. On this basis, the following recipe was used for making the two-component adhesive:

- Part A: Chi-C25% coacervate mixed with X
- Part B: Chi-C25% coacervate mixed with Y

Table S3. Curing Chi-C25% coacervate adhesive; varying ratios of HRP and H_2O_2

Chi-C/HRP (Weight ratio)	**Chi-C/H2O2 (Weight ratio)**	Description
1500	**50**	Gelation time ~ 0.5-1 hr
	500	
	625	Gelation time ~ 10-15 minutes
	1250	Gelation time ~1-5 minutes
	3000	
	5000	
	6250	
150	**625**	For the optimized H_2O_2 concentration, increase HRP concentration allowed tuning the gelation time from ~30 min to ~30 sec.
375		
937.5		
1875		
3750		
9375		
150	**6250**	For the lowest fixed H_2O_2 concentration, increasing HRP did not affect the gelling rate. All of samples showed a gelation time ~30 min.
375		
937.5		
1875		
3750		
9375		

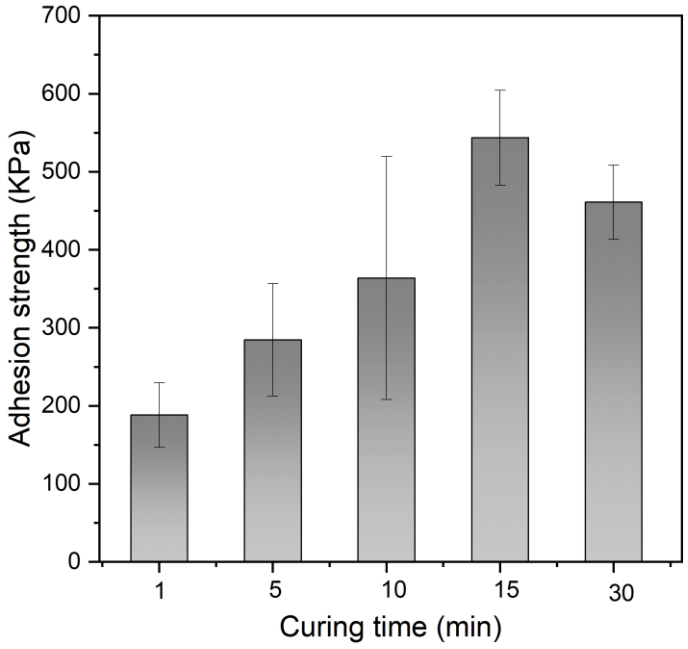

Figure S6. Underwater adhesion of the optimized two-component Chi-C25% adhesive vs. time

The gelation time of ~ 15 min was also confirmed by additional underwater adhesion data (aluminum substrates), as shown in Figure S6. Herein, it was found that adhesion strength grows with time and reaches a value of ~ 400-600 kPa after 10-30 min of curing.

Reference

(1) Perro, A.; Giraud, L.; Coudon, N.; Shanmugathasan, S.; Lapeyre, V.; Goudeau, B.; Douliez, J.-P.; Ravaine, V. Self-Coacervation of Ampholyte Polymer Chains as an Efficient Encapsulation Strategy. *J. Colloid Interface Sci.* **2019**, *548*, 275–283. https://doi.org/10.1016/j.jcis.2019.04.033.

(2) Wang, R.; Li, J.; Chen, W.; Xu, T.; Yun, S.; Xu, Z.; Xu, Z.; Sato, T.; Chi, B.; Xu, H. A Biomimetic Mussel-Inspired ε-Poly- <scp>l</Scp> -Lysine Hydrogel with Robust Tissue-Anchor and Anti-Infection Capacity. *Adv. Funct. Mater.* **2017**, *27* (8), 1604894. https://doi.org/10.1002/adfm.201604894.

(3) Hou, J.; Li, C.; Guan, Y.; Zhang, Y.; Zhu, X. X. Enzymatically Crosslinked Alginate Hydrogels with Improved Adhesion Properties. *Polym. Chem.* **2015**, *6* (12), 2204–2213. https://doi.org/10.1039/C4PY01757A.

(4) Jin, R.; Hiemstra, C.; Zhong, Z.; Feijen, J. Enzyme-Mediated Fast in Situ Formation of Hydrogels from Dextran–Tyramine Conjugates. *Biomaterials* **2007**, *28* (18), 2791–2800. https://doi.org/10.1016/J.BIOMATERIALS.2007.02.032.